Studies on Properties of Endohedral Fullerenes and Development of Fullerene Derivatives for Organic Photovoltaic Devices

Yuta Morinaka

Institute for Chemical Research

Kyoto University

2013

Table of Contents

General Introduction

Fullerenes are spherical carbon clusters that have a hollow cavity. Their unique structures with three-dimensional π-system have attracted a great deal of attention from scientists and a wide range of studies on fullerenes have been reported.[1]

There are basically three methodologies to control the properties of fullerenes (Figure 1). The first is ‘‘internal modification’’, that is, introduction of atom(s) or molecule(s) inside the fullerene cage represented as **1**.[2] The “internal modification” is attractive since it provides opportunity to elucidate interactions, such as charge transfer or weak van der Waals interaction, between guest species and the fullerene π-systems. The interactions can alter the electronic properties of fullerenes from inside with the spherical π-system intact. However, the research on the ‘‘internal modification’’ of fullerenes have been hampered by severe limitation in their production. For example, introduction of metal atoms inside the cage has

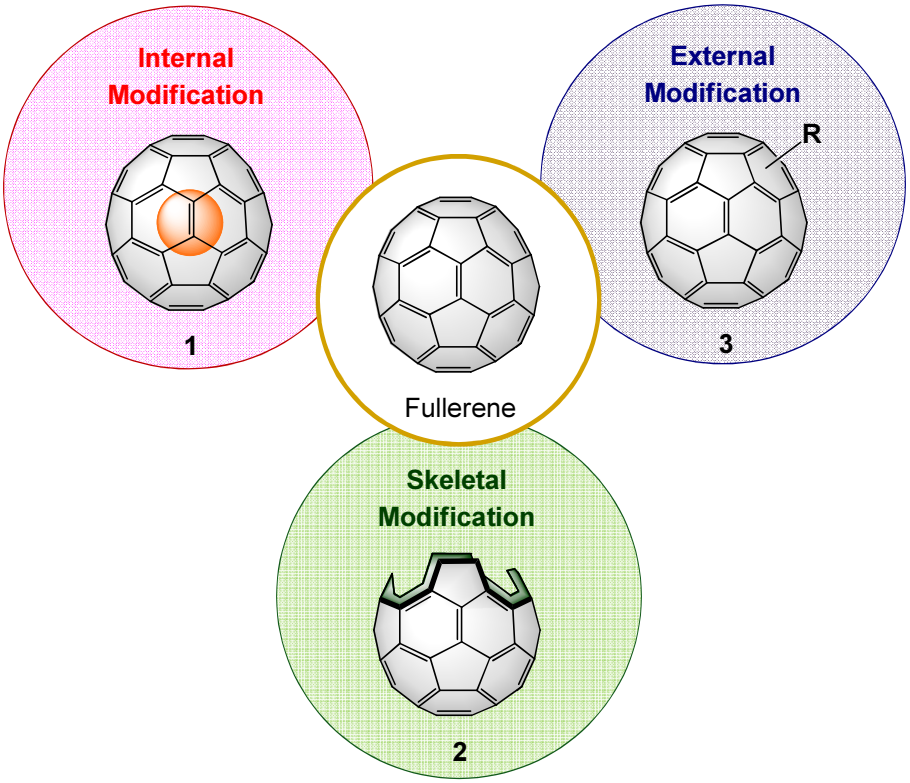

Figure 1. Modification of fullerene.

been depending on rather low yielding physical methods using arc discharge technique, providing endohedral fullerenes only in mg scale.[2] In such a situation, development of the technique to transform σ-framework of fullerenes, ‘‘skeletal modification’’, has led to creation of open-cage fullerene derivatives, represented like **2**, which would be used for the rational synthesis of endohedral fullerenes.[1] Although the ‘‘skeletal modification’’ has a potential to modify fullerene π-systems directly, the applications of this method has been limited mainly to the science of endohedral fullerenes. The third method to control the properties of fullerenes is ‘‘external modification’’, that is, installation of organic groups on the outer surface of fullerenes by chemical reactions to give **3**.[1] Today, the chemical reactivity of the outer surface of the fullerenes have been mostly disclosed.[1] Thus, the chemists can provide various functional materials that directly contribute to the development of applied science such as organic solar cells. The author describes the progress in the fullerene chemistry with a focus on internal, skeletal, and external modifications in the following sections.

Internal and Skeletal Modifications of Fullerenes

Since the early 1990s, huge efforts have been devoted to insert atom(s) or molecule(s) into fullerenes. For example, arc-discharge of metal oxide/graphite composite rods gave the fullerenes encapsulating metal(s), so called endohedral metallofullerenes, with concomitant formation of a large amount of empty fullerenes having various cage sizes (C_{60}, C_{70}, C_{76}, C_{78}, C_{80}, and C_{82}, etc.).[2] This method mainly produces endofullerenes with larger carbon cages than C_{60}. It has been very difficult to obtain C_{60} and C_{70} encapsulating metals in spite of their abundant formation under the arc-discharge conditions. As an another approach, ion beam implantation into C_{60} gave endohedral C_{60} such as Li@C_{60} and N@C_{60}.[2] Heating C_{60} powder under noble gas (He, Ne, Ar, Kr, and Xe) atmosphere at such a high temperature/pressure as 650 ºC/3000 atm afforded endohedral C_{60} encapsulating a noble gas atom at an occupation level of ca. 0.1%.[2,3] Although laborious purification is required, a number of endohedral metallofullerenes and other endohedral fullerenes have been isolated in μg- to mg-quantities by the use of recycling HPLC.[2]

As the endohedral fullerenes have become available, the effects of inner atom(s) or molecule(s) on the properties of fullerenes have been explored. For example, the chemical

reactivity of endohedral metallofullerenes such as La@C_{82} is different from that of the empty fullerenes; La@C_{82} thermally reacts with disilirane **4**, which is thermally unreactive to C_{60}, to give adduct La@**5** (Scheme 1).[2,4] Electron transfer from the inside metal to the outer fullerene cage drastically alters the electronic properties and chemical reactivities of the fullerene π-system. Thus, endohedral metallofullerenes have potential to be applied in molecular electronics,[5] medical science,[6] solar cells,[7] and so on.

Scheme 1. Reaction of La@C_{82} with disilirane **4**

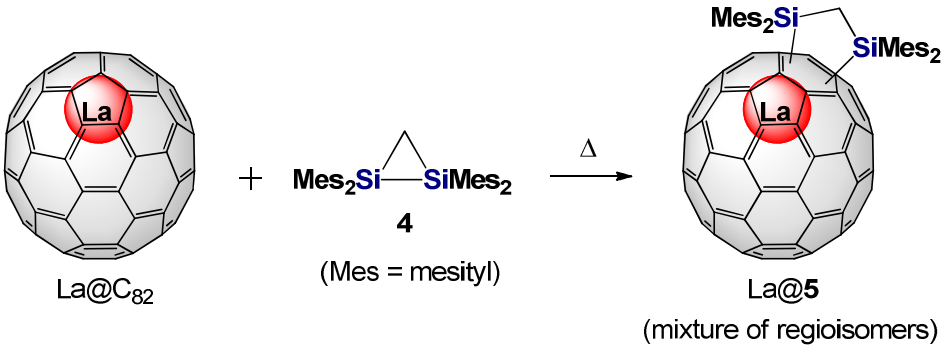

On the other hand, the van der Waals interaction between C_{60} and an encapsulated noble-gas atom has been studied by the use of ^{13}C NMR spectroscopy. The carbon signals of endohedral fullerenes tend to shift to downfield relative to that of empty C_{60}. The differences in the chemical shifts $\Delta\delta$ for Xe@C_{60}, Kr@C_{60}, and Ar@C_{60} relative to C_{60} were reported as $\Delta\delta$ = 0.95 ppm,[8] 0.39 ppm,[9] and 0.17 ppm,[10] respectively, suggesting that the van der Waals interaction decreases as the inner guests become smaller (Figure 2). The key of these studies was the enrichment of endohedral fullerenes by the use of HPLC.[8-11] Actually, there are no reports on enrichment of He@C_{60} and Ne@C_{60} from empty C_{60}, probably because of the much weaker interactions which afford the HPLC profiles similar to that of empty C_{60}, making the purification more difficult. The studies on the interaction of He@C_{60} and Ne@C_{60} have been limited only to the computational method, where estimation of the encapsulation energy highly depends on the level of theory owing to the difficulty in estimation of weak van der Waals interactions.[12]

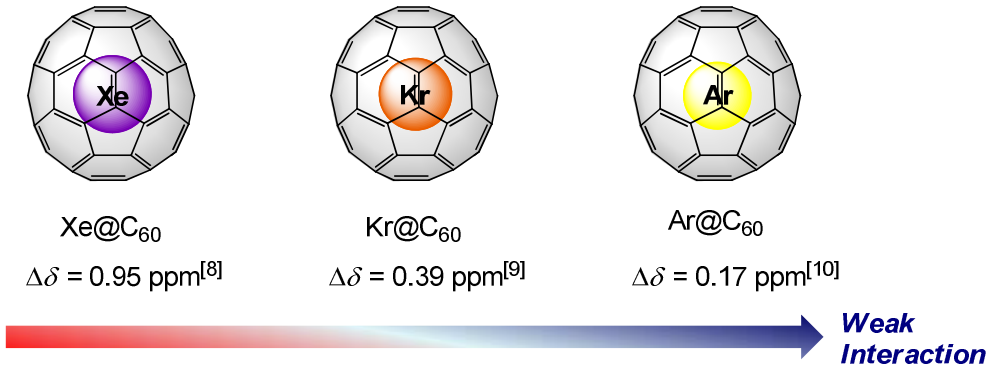

Figure 2. Differences in ^{13}C chemical shift of endohedral C_{60} compared with C_{60}.

To overcome the low efficiency in production of endohedral fullerenes, rational synthetic methodology using organic reactions, so called ‘‘molecular surgery’’,[13] should be appropriate. This method includes (1) creating an opening that is large enough to introduce small guest(s), (2) incorporating atom(s) or molecule(s) into the cavity through the opening, and (3) closing the opening with retention of the encapsulated species.

As shown in Figure 3, there is a variety of open-cage C_{60} derivatives capable of encapsulating an atom or a molecule in their cavities. In 2001, Rubin et al. synthesized open-cage C_{60} derivative **6** having a 14-membered-ring opening[14] and succeeded in encapsulation of a ^3He atom and a H_2 molecule inside **6** at occupation levels of 1.5% and 5%, respectively, for the first time.[15] In 2004, Iwamatsu et al. found that a molecule of water is spontaneously encapsulated inside the cavity of open-cage C_{60} derivative **7** with a 20-membered-ring opening.[16] Moreover, compound **7** showed the capability of encapsulating other molecules such as CO,[17] NH_3,[18] and CH_4.[19] In 2007, Gan et al. also reported the encapsulation of a molecule of water into open-cage C_{60} derivative **8** with a 19-membered-ring opening, and succeeded in characterization with X-ray crystallography.[20] However, the complete restoration of the opening of these derivatives seems to be an unrealistic challenge due to their complicated structures of the openings.

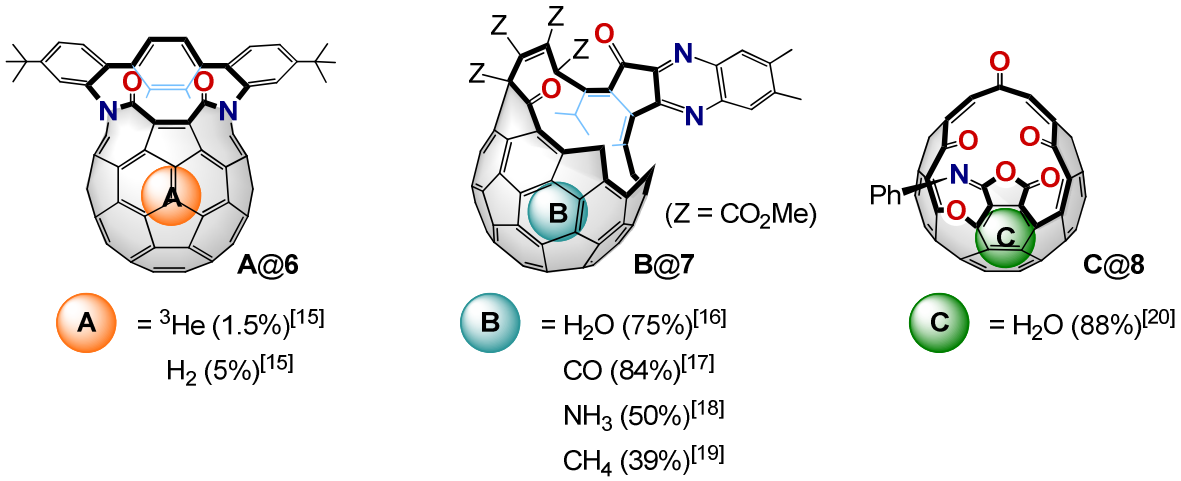

Figure 3. Insertion of an atom or a molecule into open-cage C_{60} derivatives at various occupation levels.

On the other hand, Komatsu et al. established quantitative encapsulation of a hydrogen molecule into open-cage C_{60} derivative **9**[21] in 2003,[22] and the methodology that allows complete restoration of the opening of **9** encapsulating a molecule of hydrogen in 2005.[23] By closing the opening of H_2@**9** at occupation level of 100% in four steps, H_2@C_{60} was synthesized without the significant loss of inner hydrogen molecule (Scheme 2).[23] This is the first example of ''molecular surgery'' by the rational organic synthesis. Moreover, this technique was applied to C_{70} derivative **10**[24] and succeeded in the macroscopic synthesis of endohedral C_{70} encapsulating one and two molecules of hydrogen, i.e. H_2@C_{70} and $(H_2)_2$@C_{70}, at the ratio of 97 : 3.[25]

Scheme 2. Synthesis of C_{60} and C_{70} encapsulating molecule(s) of hydrogen

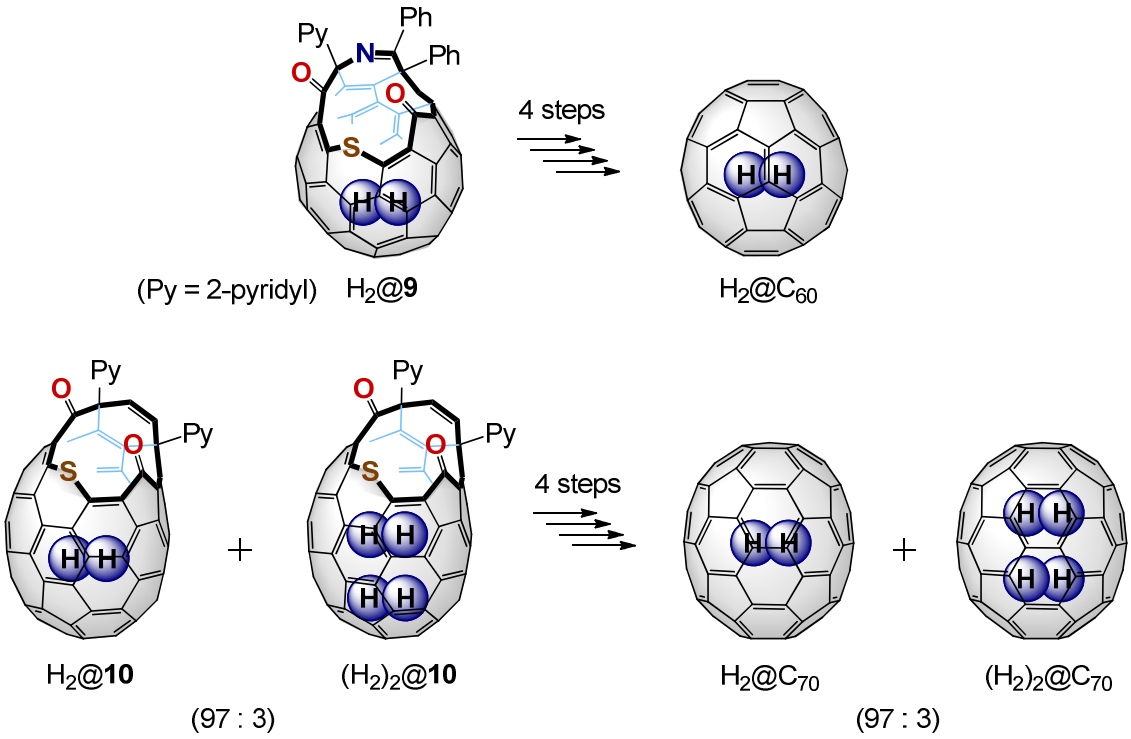

The interaction between the inner molecule of hydrogen and outer fullerene cage was found to be weaker than that of Xe@C_{60},[8] Kr@C_{60},[9] and Ar@C_{60}.[10] That is, from the ^{13}C NMR spectra, small $\Delta\delta$ values for H_2@C_{60} and H_2@C_{70} relative to empty C_{60} and C_{70} were observed as $\Delta\delta$ = 0.08 ppm,[23] and 0.02-0.07 ppm,[25] respectively. The smaller $\Delta\delta$ value of H_2@C_{70} compared to that of H_2@C_{60} reflects the larger space inside C_{70}. Although the ^{13}C NMR signals of $(H_2)_2$@C_{70} were not observed due to the limited amount, the clear signal of inner two molecules of hydrogen was observed in the ^{1}H NMR spectrum. Because the inner hydrogen molecule can be used as a powerful NMR probe to follow chemical reactions taking place at the exterior of the cage,[23,26] the author decided to utilize these signals for the investigation of the interaction between C_{70} and molecular hydrogen for H_2@C_{70} and $(H_2)_2$@C_{70}.

The author also considered that the molecular surgical technique to synthesize H_2@C_{60} and H_2@C_{70} has a potential to provide other endohedral fullerenes such as He@C_{60} and He@C_{70} with the weakest van der Waals interactions. If the production of these endohedral

fullerenes becomes reality, the understanding on the van der Waals interaction between two neutral species would be accelerated.

In addition, the cyclic voltammetry revealed that the LUMO levels of **9** and **10** are different from those of pristine C_{60} and C_{70}, respectively.[21,24] These results strongly suggest that the transformation of σ-framework of fullerenes would become a new approach to adjust the LUMO levels of fullerene derivatives suitable for organic photovoltaic devices. The detailed background is described in the next section.

External Modification of Fullerenes

The ‘‘external modification’’ of fullerenes can easily control properties of fullerenes such as solubilities, electron reduction potentials, packing structures in solid state, and so on.[1] With the development of synthetic chemistry on the outer surface of fullerenes, functionalized fullerenes have been reported for various applications such as organic field-effect transistors,[27] gene delivery,[28] polymer solar cells (PSCs),[29] and so on. Among them, the utilization of fullerenes as n-type acceptor materials for PSCs is one of the most prospective subjects for commercial application.[29]

The typical device structure of PSC is shown in Figure 4. The core of the device is the active layer composed of a mixture of a donor polymer and an acceptor fullerene with bulk-heterojunction (BHJ) structure,[30] where the large interfacial area induces the efficient

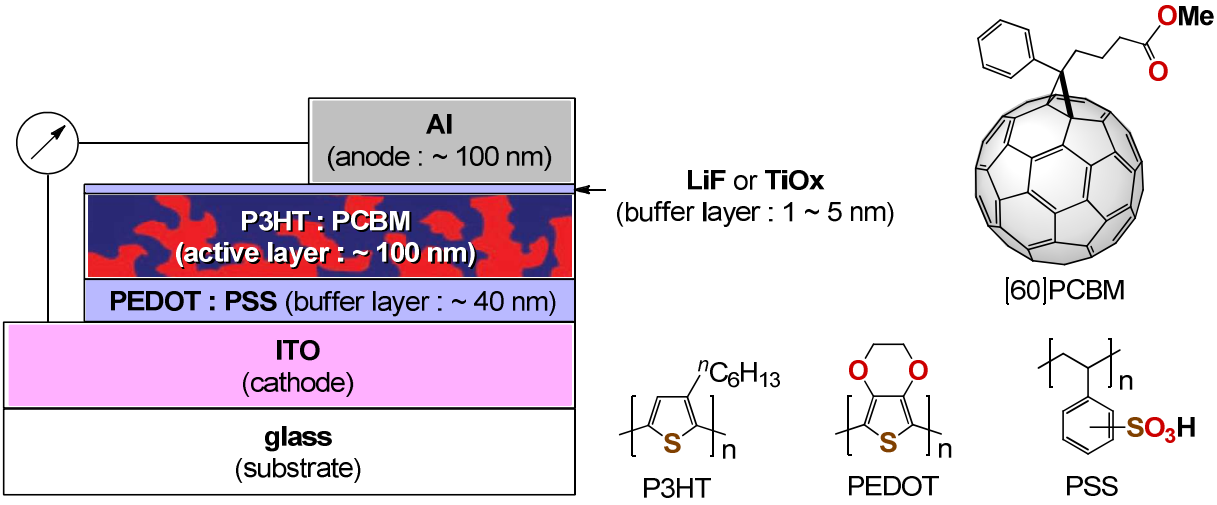

Figure 4. Typical architecture of PSC and chemical structures of composing materials.

charge separation. The representative donor and acceptor materials are poly-3-hexylthiophene (P3HT)[31] and [6,6]-phenyl-C_{61}-butyric acid methyl ester ([60]PCBM),[32] achieving the power conversion efficiency (PCE) of 5.0 ~ 6.5%.[33]

As shown in Figure 5a, under the illumination of AM1.5G (100 mW cm^{-2}) spectral conditions, the PCE is defined by the following equation: PCE (%) = V_{oc} (V) × J_{sc} (mA cm^{-2}) × FF, where V_{oc} is the open-circuit voltage, J_{sc} is the short-circuit current density, and FF is the fill factor: the ratio $(P_{max})/(V_{oc} \times J_{sc})$.[29a] Thus, the improvement of these three factors leads to the increase in PCE. As shown in Figure 5b, it is well-known that the V_{oc} tends to be proportional to the energy difference between the $LUMO_{(A)}$ and the $HOMO_{(D)}$, indicating the significance of controlling the electronic structure of the donor and the acceptor materials.[34] On the other hand, to improve the J_{sc} and the FF, it is required to achieve efficient harvest of sunlight, effective generation of holes and electrons on the interface of donor and acceptor materials, and high carrier mobility by formation of interpenetrated network of donor and acceptor materials in the active layer.

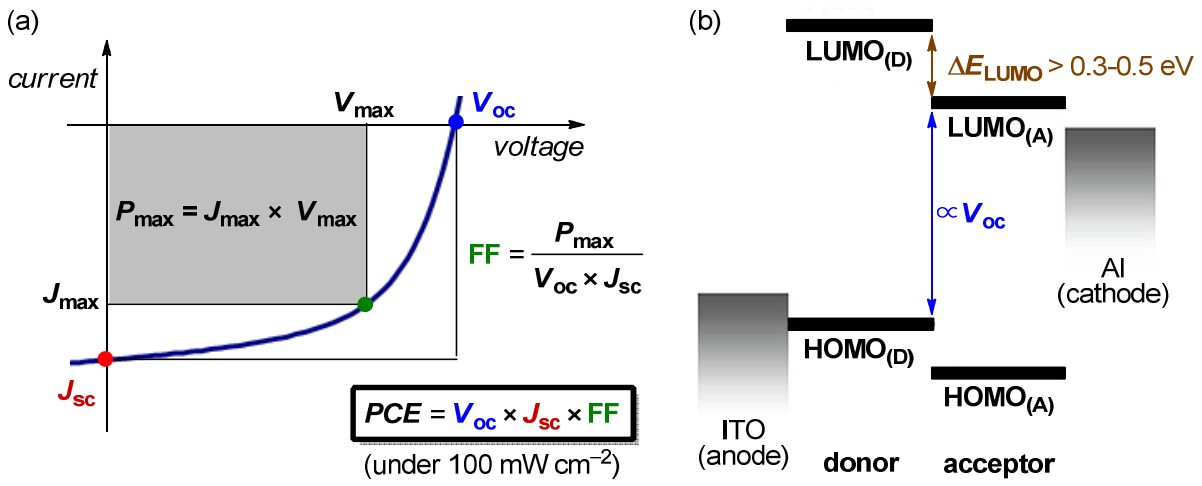

Figure 5. (a) Current density-voltage (*J*-*V*) curve under AM1.5G (100 mW cm^{-2}) illumination. (b) Energy levels diagram.

In 2006, Scharber et al. proposed guidelines for the design of donor polymers to achieve PCE of 10%.[35] As shown in Figure 5b, the energy difference between the LUMOs of the donor and acceptor materials, i.e. ΔE_{LUMO}, should be larger than 0.3-0.5 eV for efficient charge separation.[29a,35] Thus, the ideal LUMO level and bandgap energy of donor polymers

were discussed with respect to PCBM. According to this strategy, ‘‘low-bandgap polymers’’ such as PCPDTBT[36] and PTB7[37] were synthesized and the BHJ solar cells using them established high PCE values in a combination with [70]PCBM (Figure 6).[38]

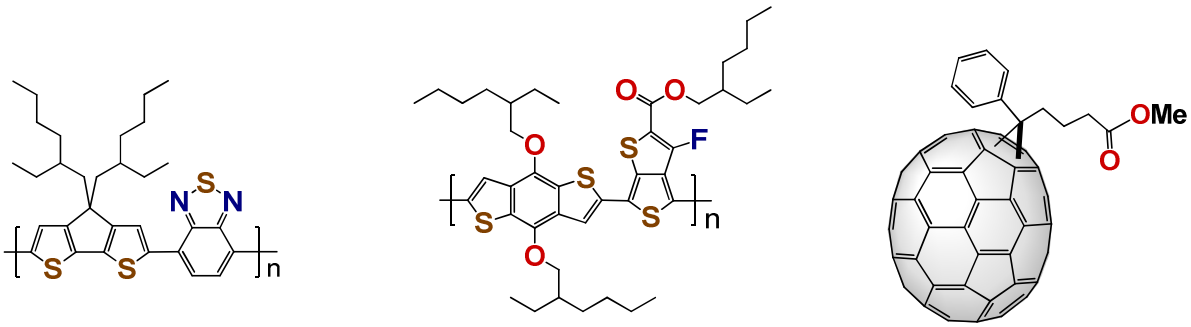

PCPDTBT (PCE = 5.5% in 2007[36]) PTB7 (PCE = 7.4% in 2010[37a], 9.2% in 2012[37b]) [70]PCBM

Figure 6. Structure of typical low-bandgap polymers and [70]PCBM.

In contrast to the rapid progress in the development of the donor polymers, the repertoire of n-type fullerene derivatives has been severely limited. In fact, [60]PCBM and [70]PCBM, which were synthesized with the traditional addition reaction, have occupied the position as the standard materials since the first report by Wudl et al. in 1995.[32]

To develop the new n-type materials, the fullerene derivatives with higher LUMO level than that of PCBM have been designed and synthesized to improve V_{oc} so far (Figure 5b). In 2007, Hummelen et al. installed electron-donating substituent(s) on the phenyl ring of [60]PCBM.[39] But they found that the effect of the electron-donating groups onto the LUMO level was quite limited due to the ‘‘remote’’ structural modification of fullerene π-system. In 2008, Blom et al. reported bis-[60]PCBM, which is the bisadduct analogue of [60]PCBM (Scheme 3) with higher LUMO level than that of PCBM, indicated from the measurement of cyclic voltammetry.[40] Indeed, the P3HT:bis-[60]PCBM device achieved higher V_{oc} (0.73 V) and PCE (4.5%) than those of P3HT:[60]PCBM device (V_{oc} = 0.58 V and PCE = 3.8%) without the significant loss of J_{sc} and FF. Following this success, the related family of bisadducts has been reported; indene-based bisadduct (ICBA),[41] dihydronaphthyl-based bisadduct (NCBA),[42] and thieno-*o*-quinodimethane-based bisadduct (TOQC)[43] were

synthesized by the traditional Diels-Alder reactions (Scheme 3). The devices using these bisadducts showed the better PCE than that using [60]PCBM when paired with P3HT. However, these bisadducts cannot be used in a combination with low-bandgap polymers presumably because the two addends on the C_{60} cage hamper the efficient carrier transportation.[44] Moreover, these bisadducts are mixtures of regioisomers with the different LUMO levels which are difficult to be separated. Thus, establishment of the methodology for tuning the LUMO levels of fullerenes has been still important to realize a better donor/acceptor pair with higher PCE.

Scheme 3. Synthesis of bisadducts for PSCs by the traditional addition reactions

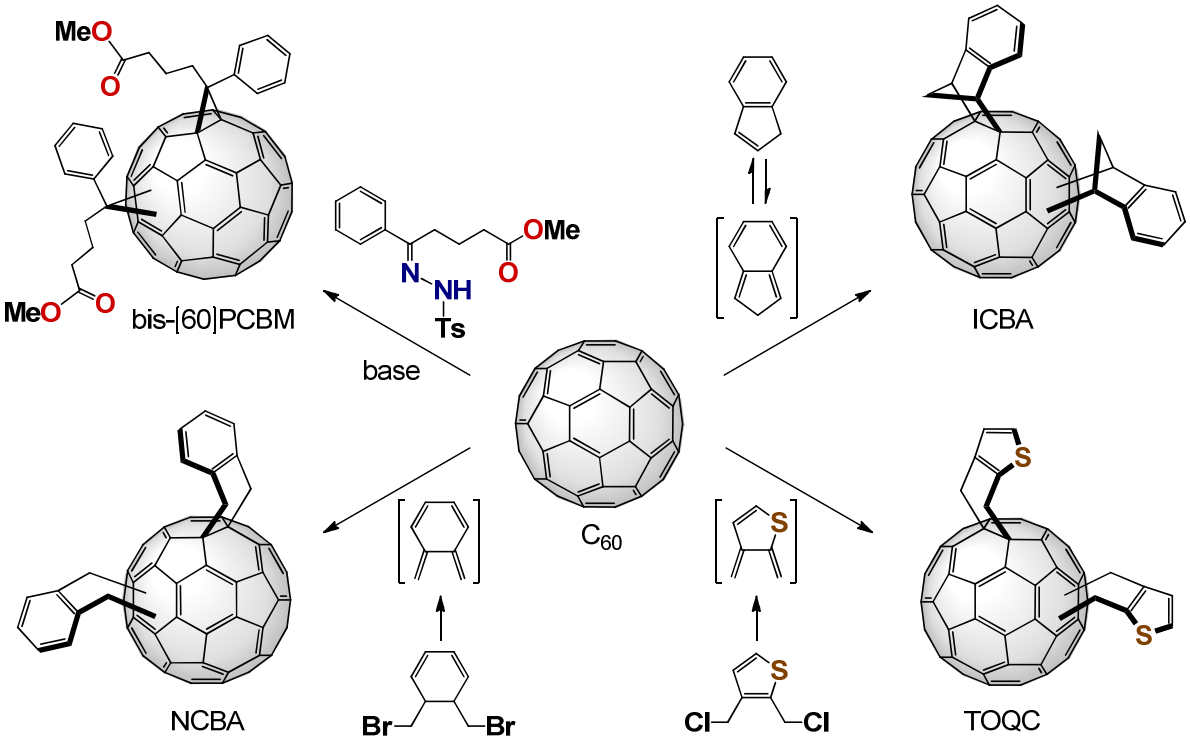

In addition to the control of electronic properties of fullerenes, morphology control is critical for improving the device performance, in particular J_{sc} and FF. In the single crystal obtained from chlorobenzene solution, [60]PCBM molecules are closely packed to form a three-dimensional network, which is suitable for the electron transport (Figure 7).[45] Because similar pass for electron transport might be expected if only a small structural modification is

applied to [60]PCBM, most studies on the morphology control have been focused on the structural modification of [60]PCBM.

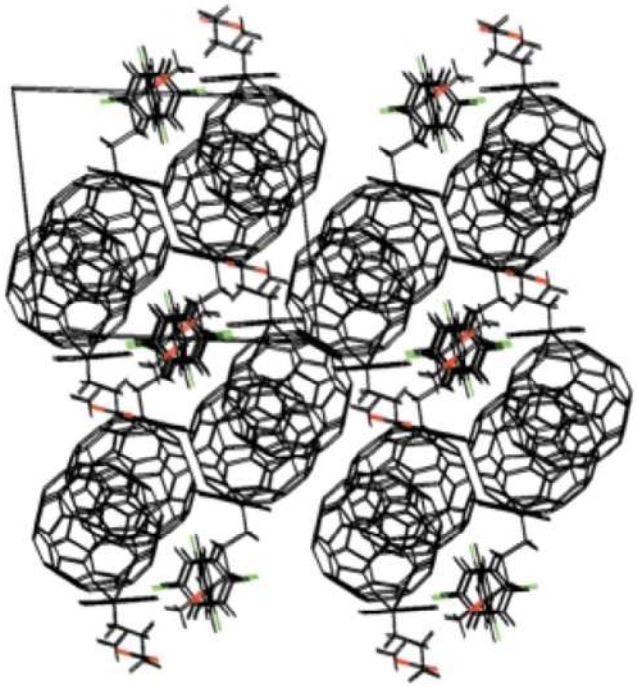

Figure 7. Packing structure of [60]PCBM in the single crystal containing chlorobenzene.[45]

As shown in Figure 8, several groups synthesized a series of [60]PCBM analogues **11** and **12** with various alkyl chains, denoted by ‘‘a’’ or ‘‘b’’, to investigate their photovoltaic properties.[46] Although these modifications are quite simple, not only J_{sc} and FF but also V_{oc} irregularly changed with the slight change of alkyl-chain length. As a result, the significant increase in device performance compared to that of P3HT:[60]PCBM standard cell has not been accomplished despite a number of experiments. The [6,6]-thienyl-C_{61}-butyric acid methyl ester ([60]ThCBM), in which the phenyl group of [60]PCBM is replaced by a thienyl group, was also designed for the purpose of improving miscibility with P3HT.[47] However, the clear difference compared to P3HT:[60]PCBM was not observed; electron transport properties, AFM images of active layer, and photovoltaic performance were almost the same. The author considered that the structural modification of the addend of PCBM is an improper approach to achieve definitive improvements.

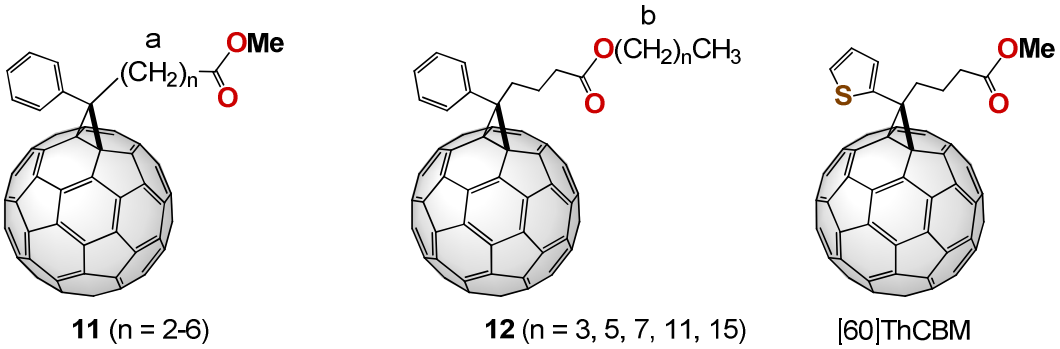

Figure 8. Structural modifications of [60]PCBM for morphology control.

As an another approach, the photovoltaic performances of penta(organo)[60]fullerene **13** and **14**, which were synthesized by the regioselective penta-addition of aryl copper reagents to C_{60}, were reported by Rubin[48] and Nakamura,[49] respectively (Figure 9). These fullerenes with 50π-electron have a higher LUMO level than that of PCBM, and form ordered structures in the solid state through polar columnar assemblies, implying a possibility of good charge transportation in active layers. However, the PCEs of P3HT:pentaadduct device were around 1% due to the low J_{sc} values of 2.0-2.5 mA cm^{-2}. The plausible reason for these results is that the pentaadduct with high crystallinity hampers the interpenetration with P3HT, resulting in formation of excessively phase-separated morphology[49] relative to the morphology of P3HT:PCBM active layer.[33,50]

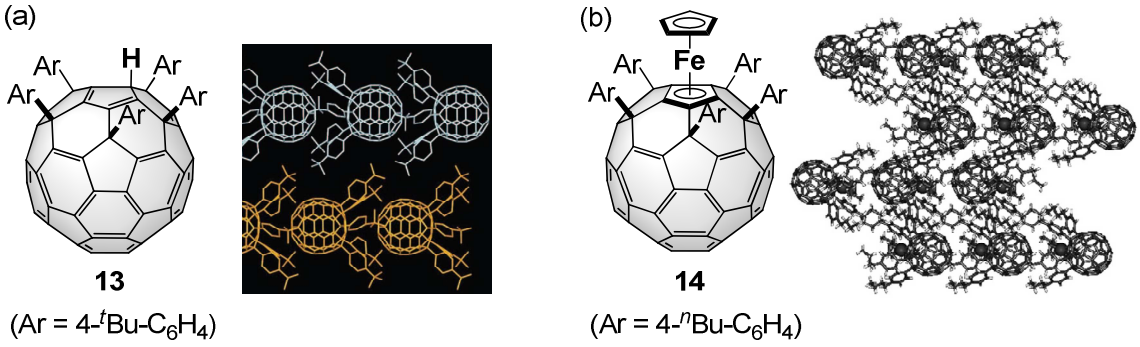

Figure 9. Packing sturucture of penta(organo)[60]fullerenes in the crystal reported by (a) Rubin[48] and (b) Nakamura.[49]

Recently, Nakamura et al. reported the BHJ solar cell composed of P3HT and bis(dimethylphenylsilylmethyl)[60]fullerene (SIMEF) with the PCE of 3.6%.[51] The SIMEF was synthesized through the DMF-assisted monoaddition of silylmethyl Grignard reagent to give **15** and the following alkylation reaction (Scheme 4).[52] The SIMEF showed phase transition from amorphous to crystal at 149 ºC, resulting in the formation of the ordered structure (Figure 10).[53] The device using the active layer of P3HT:SIMEF showed the high J_{sc} (9.0 mA cm^{-2}) and FF (0.62) comparable with those of P3HT:[60]PCBM (J_{sc} = 8.9 mA cm^{-2}, FF = 0.61), suggesting the good electron transport of SIMEF in the active layer.[51]

Scheme 4. Synthesis of SIMEF

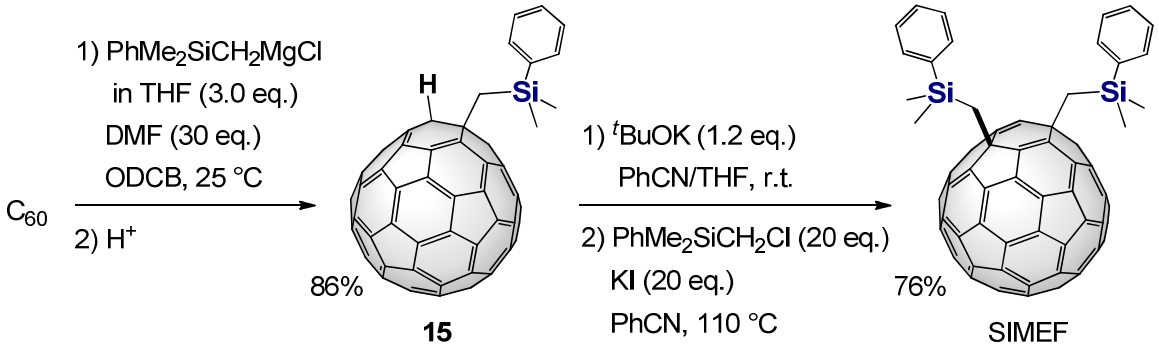

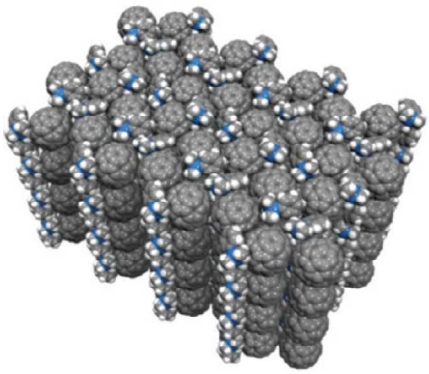

Figure 10. Packing stuructures of SIMEF at crystalline states.[53]

As has been described above, most studies on fullerenes for the acceptor materials of PSCs have been based on the ‘‘external modification’’. Although this methodology has

produced a variety of fullerene derivatives bearing organic groups, [60]PCBM and [70]PCBM still occupy the dominant position as the n-type materials. To realize new n-type materials that can replace PCBM, development of new design concept and synthetic strategy of the acceptor materials is important.

Survey of This Thesis

The fullerene functionalization includes ‘‘internal modification’’, ‘‘skeletal modification’’, and ‘‘external modification’’. In this thesis, the author has investigated the weak interaction of endohedral fullerenes to develop the science of ‘‘internal modification’’. Furthermore, the author has proposed new strategies of providing acceptor fullerenes for PSCs by developing the ‘‘skeletal modification’’, that is an unexplored approach against the traditional ‘‘external modification’’.

Chapter 1 describes a [4+2] cycloaddition reaction of $H_2@C_{70}$ and $(H_2)_2@C_{70}$ with 9,10-dimethylanthracene (DMA) to investigate the difference in chemical reactivity by utilizing the ^{1}H NMR signals of inner hydrogen molecule(s) of $(H_2)_n@C_{70}$ and $(H_2)_n@$**16** (n = 1, 2) (Scheme 5).[25] By comparison of the equilibrium constants of the reaction of $(H_2)_n@C_{70}$ (n = 1, 2) and DMA, it was found that the encapsulated two hydrogen molecules of $(H_2)_2@C_{70}$ ‘‘apparently’’ decrease the reactivity of C_{70} framework toward DMA, indicating that more interaction is present between two molecules of hydrogen and C_{70}.

Scheme 5. Reaction of $(H_2)_n@C_{70}$ (n = 1, 2) with DMA

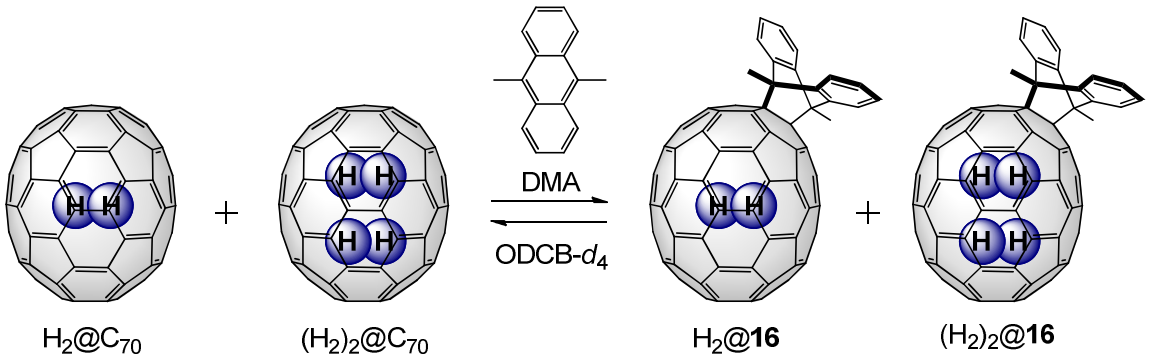

Chapter 2 describes the rational synthesis of He@C_{60} and He@C_{70} at occupation levels of 30% by the molecular surgery method (Figure 11).[54] In the ^{13}C NMR measurements, the signals of He@C_{60} and He@C_{70} were slightly shifted to downfield as compared to those of empty C_{60} and C_{70} in the range $\Delta\delta$ = 0.02-0.03 ppm. Although the interactions of He@C_{60} and He@C_{70} are quite small, the separations from an empty counterpart were possible by the use of recycling HPLC equipped with Cosmosil Buckyprep columns.

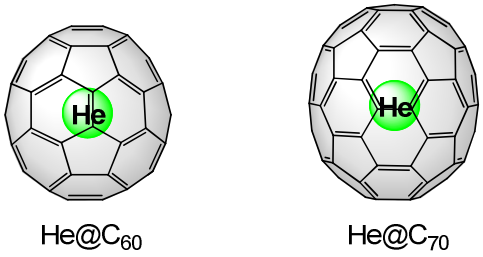

Figure 11. Structures of He@C_{60} and He@C_{70}.

In Chapter 3, the X-ray diffraction study of He@C_{60} is demonstrated as the direct evidence of the fact that a single atom of helium is encapsulated inside C_{60}.[55] Moreover, the chapter describes the generation of C_{60} and C_{70} encapsulating both helium and nitrogen atoms (HeN@C_{60} and HeN@C_{70}) by combining two individual insertion methodologies, ‘‘molecular surgery’’ and ‘‘nitrogen radio-frequency (RF) plasma’’[2,56] techniques (Figure 12). The electron spin state of the nitrogen atoms of HeN@C_{60} and HeN@C_{70} was found to be retained in spite of the existence of the closely packed helium atom.

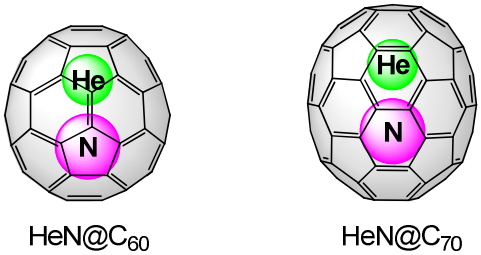

Figure 12. Structures of HeN@C_{60} and HeN@C_{70}.

Here, the studies on ‘‘molecular surgery’’ have provided not only the production of endohedral fullerenes but also the reactions to transform the σ-framework of fullerenes. The open-cage C_{60} derivatives with distinct LUMO levels prompted the author to investigate the photovoltaic performance of them with expectation of high V_{oc} values in BHJ solar cells.

Hence, Chapter 4 describes the synthesis and properties of highly soluble open-cage C_{60} derivatives **17**-**19** with various LUMO levels (Figure 13).[57] Indeed, the photovoltaic characteristics of open-cage C_{60} derivatives are discussed through the fabrication of BHJ solar cells composed of P3HT as a donor and **17**-**19** as acceptors.[58]

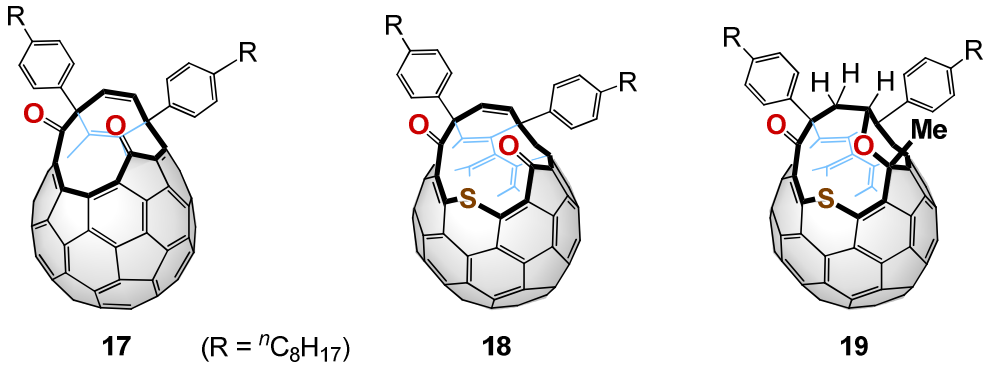

Figure 13. Structures of open-cage C_{60} derivatives.

As mentioned above, efforts to produce novel acceptor materials for BHJ solar cells have largely focused on the modification of monomeric fullerene derivatives. There are only limited reports on the synthesis of dimeric fullerenes and less reports on their photovoltaic properties.[59] In addition, the device performance of dimers in a combination with low-bandgap polymers has not been discussed so far. Thus, the author considered that the dimerization of a PCBM analogue would lead to understanding of the importance of molecular arrangements as well as the design rules for acceptor materials.

Hence, Chapter 5 describes the synthesis, properties, and photovoltaic performance of dumbbell-shaped fullerene derivatives, in which two C_{60} moieties are connected at *para*- and *meta*-position (PDB and MDB) on the central phenyl group (Figure 14).[60] It is demonstrated that PDB is the unique acceptor which shows PCE comparable to that of [60]PCBM not only in P3HT system but also in PTB7 (*vide supra*) system.

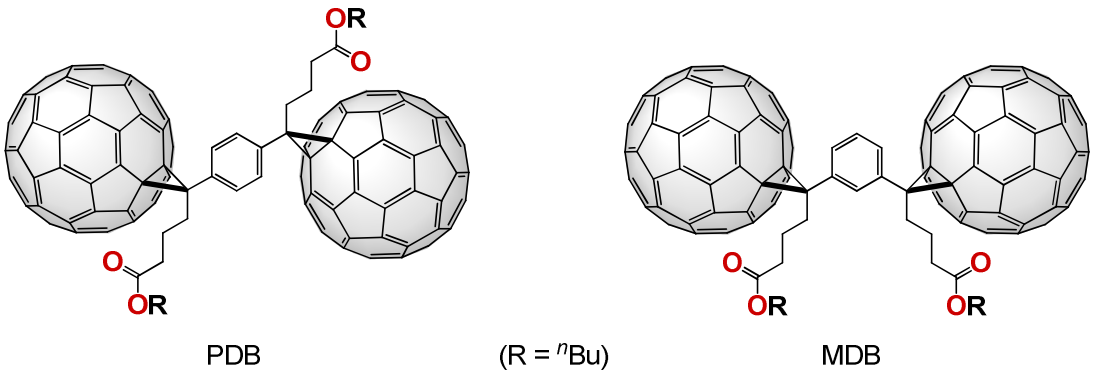

Figure 14. Structures of PDB and MDB.

References

(1) (a) Hirsch, A.; Brettreich, M. *Fullerenes: Chemistry and Reactions*; Wiley-VCH, Weinheim, **2005**. (b) Akasaka, T.; Wudl, F.; Nagase, S. *Chemistry of Nanocarbons*; Wiley-Blackwell, Oxford, **2010**. (c) Martín, N. *Chem. Commun*. **2006**, 2093. (d) Sánchez, L.; Otero, R.; Gallego, J. M.; Miranda, R.; Martín, N. *Chem. Rev*. **2009**, *109*, 2081. (e) Itami, K. *Chem. Rec*. **2011**, *11*, 226. (d) Vougioukalakis, G. C.; Roubelakis, M. M.; Orfanopoulos, M. *Chem. Soc. Rev*. **2010**, *39*, 817.

(2) (a) Akasaka, T.; Nagase, S. *Endofullerenes*: *A New Family of Carbon Clusters*; Kluwer Academic, Dordrecht, **2002**. (b) Lu, X.; Feng, L.; Akasaka, T.; Nagase, S. *Chem. Soc. Rev*. **2012**, *41*, 7723.

(3) (a) Saunders, M.; Cross, R. J.; Jiménez-Vázquez, H. A.; Shimshi, R.; Khong, A. *Science* **1996**, *271*, 1693. (b) Saunders, M.; Jiménez-Vázquez, H. A.; Cross, R. J.; Mroczkowski, S.; Freedberg, D. I.; Anet, F. A. L. *Nature* **1994**, *367*, 256.

(4) Akasaka, T.; Kato, T.; Kobayashi, K.; Nagase, S.; Yamamoto, K.; Funasaka, H.; Takahashi, T. *Nature* **1995**, *374*, 600.

(5) (a) Sato, S.; Seki, S.; Honsho, Y.; Wang, L.; Nikawa, H.; Luo, G.; Lu, J.; Haranaka, M.; Tsuchiya, T.; Nagase, S.; Akasaka, T. *J. Am. Chem. Soc*. **2011**, *133*, 2766. (b) Kobayashi, S.; Mori, S.; Iida, S.; Ando, H.; Takenobu, T.; Taguchi, Y.; Fujiwara, A.; Taninaka, A.; Shinohara, H.; Iwasa, Y. *J. Am. Chem. Soc*. **2003**, *125*, 8116.

(6) (a) Dorn, H. C.; Fatouros, P. P. *Nanosci*. *Nanotechnol*. *Lett*. **2010**, *2*, 65. (b) Kato, H.; Kanazawa, Y.; Okumura, M.; Taninaka, A.; Yokawa, T.; Shinohara, H. *J*. *Am*. *Chem*. *Soc*. **2003**, *125*, 4391.

(7) (a) Ross, R. B.; Cardona, C. M.; Guldi, D. M.; Sankaranarayanan, S. G.; Reese, M. O.; Kopidakis, N.; Peet, J.; Walker, B.; Bazan, G. C.; Keuren, E. V.; Holloway, B. C.; Drees, M. *Nature Mater*. **2009**, *8*, 208. (b) Ross, R. B.; Cardona, C. M.; Swain, F. B.; Guldi, D. M.; Sankaranarayanan, S. G.; Keuren, E. V.; Holloway, B. C.; Drees, M. *Adv*. *Funct*. *Mater*. **2009**, *19*, 2332. (c) Liedtke, M.; Sperlich, A.; Kraus, H.; Baumann, A.; Deibel, C.; Wirix, M. J. M.; Loos, J.; Cardona, C. M.; Dyakonov, V. *J*. *Am*. *Chem*. *Soc*. **2011**, *133*, 9088.

(8) Syamala, M. S.; Cross, R. J.; Saunders, M. *J*. *Am*. *Chem*. *Soc*. **2002**, *124*, 6216.

(9) Yamamoto, K.; Saunders, M.; Khong, A.; Cross, R. J.; Grayson, M.; Gross, M. L.; Benedetto, A. F.; Weisman, R. B. *J*. *Am*. *Chem*. *Soc*. **1999**, *121*, 1591.

(10) Takeda, A.; Yokoyama, Y.; Ito, S.; Miyazaki, T.; Shimotani, H.; Yakigaya, K.; Kakiuchi, T.; Sawa, H.; Takagi, H.; Kitazawa, K.; Dragoe, N. *Chem*. *Commun*. **2006**, 912.

(11) (a) Lee, H. M.; Olmstead, M. M.; Suetsuna, T.; Shimotani, H.; Dragoe, N.; Cross, R. J.; Kitazawa, K.; Balch, A. L. *Chem*. *Commun*. **2002**, 1352. (b) DiCamillo, B. A.; Hettich, R. L.; Guiochon, G.; Compton, R. N.; Saunders, M.; Jiménez-Vázquez, H. A.; Khong, A.; Cross, R. J. *J*. *Phys*. *Chem*. **1996**, *100*, 9197.

(12) (a) Son, M.-S.; Sung, Y. K. *Chem*. *Phys*. *Lett*. **1995**, *245*, 113. (b) Bühl, M.; Patchkovskii, S.; Thiel, W. *Chem*. *Phys*. *Lett*. **1997**, *275*, 14. (c) Albert, V. V.; Sabin, J. R.; Harris, F. E. *Int*. *J*. *Quant*. *Chem*. **2007**, *107*, 3061. (d) Hesselmann, A.; Korona, T. *Phys*. *Chem*. *Chem*. *Phys*. **2011**, *13*, 732. (e) Varandas, A. J. C. *Int*. *J*. *Quant*. *Chem*. **2011**, *111*, 416.

(13) Rubin, Y. *Chem*. *Eur*. *J*. **1997**, *3*, 1009.

(14) Schick, G.; Jarrosson, T.; Rubin, Y. *Angew*. *Chem*. *Int*. *Ed*. **1999**, *38*, 2360.

(15) Rubin, Y.; Jarrosson, T.; Wang, G.-W.; Bartberger, M. D.; Houk, K. N.; Schick, G.; Saunders, M.; Cross, R. J. *Angew*. *Chem*. *Int*. *Ed*. **2001**, *40*, 1543.

(16) Iwamatsu, S.; Uozaki, T.; Kobayashi, K. Re, S.; Nagase, S.; Murata, S. *J*. *Am*. *Chem*. *Soc*. **2004**, *126*, 2668.

(17) Iwamatsu, S.; Stanisky, C. M.; Cross, R. J.; Saunders, M.; Mizorogi, N.; Nagase, S.;

Murata, S. *Angew*. *Chem*. *Int*. *Ed*. **2006**, *45*, 5337.

(18) Whitener, K. E. Jr.; Frunzi, M.; Iwamatsu, S.; Murata, S.; Cross, R. J.; Saunders, M. *J*. *Am*. *Chem*. *Soc*. **2008**, *130*, 13996.

(19) Whitener, K. E. Jr.; Cross, R. J.; Saunders, M.; Iwamatsu, S.; Murata, S.; Mizorogi, N.; Nagase, S. *J*. *Am*. *Chem*. *Soc*. **2009**, *131*, 6338.

(20) Xiao, Z.; Yao, J.; Yang, D.; Wang, F.; Huang, S.; Gan, L.; Jia, Z.; Jiang, Z.; Yang, X.; Zheng, B.; Yuan, G.; Zhang, S.; Wang, Z. *J*. *Am*. *Chem*. *Soc*. **2007**, *129*, 16149.

(21) Murata, Y.; Murata, M.; Komatsu, K. *Chem*. *Eur*. *J*. **2003**, *9*, 1600.

(22) Murata, Y.; Murata, M.; Komatsu, K. *J*. *Am*. *Chem*. *Soc*. **2003**, *125*, 7152.

(23) (a) Komatsu, K.; Murata, M.; Murata, Y. *Science* **2005**, *307*, 238. (b) Murata, M.; Murata, Y.; Komatsu, K. *J*. *Am*. *Chem*. *Soc*. **2006**, *128*, 8024.

(24) Murata, Y.; Maeda, S.; Murata, M.; Komatsu, K. *J*. *Am*. *Chem*. *Soc*. **2008**, *130*, 6702.

(25) Murata, M.; Maeda, S.; Morinaka, Y.; Murata, Y.; Komatsu, K. *J*. *Am*. *Chem*. *Soc*. **2008**, *130*, 15800.

(26) (a) Matsuo, Y.; Isobe, H.; Tanaka, T.; Murata, Y.; Murata, M.; Komatsu, K.; Nakamura, E. *J. Am. Chem. Soc.* **2005**, *127*, 17148. (b) Murata, M.; Ochi, Y.; Kitagawa, T.; Komatsu, K.; Murata, Y. *Chem*. *Asian J*. **2008**, *3*, 1336. (c) Murata, M.; Ochi, Y.; Tanabe, F.; Komatsu, K.; Murata, Y. *Angew*. *Chem*. *Int*. *Ed*. **2008**, *47*, 2039.

(27) (a) Anthopoulos, T. D.; Tanase, C.; Setayesh, S.; Meijer, E. J.; Hummelen, J. C.; Blom, P. W. M.; Leeuw, D. M. *Adv*. *Mater*. **2004**, *16*, 2174. (b) Wöbkenberg, P. H.; Ball, J.; Bradley, D. D. C.; Anthopoulos, T. D.; Kooistra, F.; Hummelen, J. C.; Leeuw, D. M. *Appl*. *Phys*. *Lett*. **2008**, *92*, 143310.

(28) (a) Nakamura, E.; Isobe, H.; Tomita, N.; Sawamura, M.; Jinno, S.; Okayama, H. *Angew*. *Chem*. *Int*. *Ed*. **2000**, *39*, 4254. (b) Isobe, H.; Nakanishi, W.; Tomita, N.; Jinno, S.; Okayama, H.; Nakamura, E. *Chem*. *Asian J*. **2006**, *1-2*, 167. (c) Klumpp, C.; Lacerda, L.; Chaloin, O.; Ros, T. D.; Kostarelos, K.; Prato, M.; Bianco, A. *Chem*. *Commun*. **2007**, 3762. (d) Maeda-Mamiya, R.; Noiri, E.; Isobe, H.; Nakanishi, W.; Okamoto, K.; Doi, K.; Sugaya, T.; Izumi, T.; Homma, T.; Nakamura, E. *Proc*. *Natl*. *Acad*. *Sci*. *U*. *S*. *A*. **2010**, *107*, 5339. (e) Sigwalt, D.; Holler, M.; Iehl, J.; Nierengarten, J.-F.; Nothisen, M.; Morin, E.; Remy, J.-S. *Chem*. *Commun*. **2011**, *47*, 4640.

(29) (a) Po, R.; Maggini, M.; Camaioni, N. *J*. *Phys*. *Chem*. *C* **2010**, *114*, 695. (b) Krebs, F.

C.; Fyenbo, J.; Jørgensen, M. *J. Mater. Chem.* **2010**, *20*, 8994. (c) Li, C.-Z.; Yip, H.-L.; Jen, A. K.-Y. *J. Mater. Chem.* **2012**, *22*, 4161. (d) Liang, Y.; Yu, L. *Acc. Chem. Res.* **2010**, *43*, 1227. (e) Heremans, P.; Cheyns, D.; Pand, B. P. *Acc. Chem. Res.* **2009**, *42*, 1740.

(30) Yu, G.; Gao, J.; Hummelen, J. C.; Wudl, F.; Heeger, A. J. *Science* **1995**, *270*, 1789.

(31) (a) Chen, T.-A.; Rieke, R. D. *J. Am. Chem. Soc.* **1992**, *114*, 10087. (b) McCullough, R. D.; Lowe, R. D. *J. Chem. Soc., Chem. Commun.* **1992**, 70. (c) Chen, T.-A.; Wu, X.; Rieke, R. D. *J. Am. Chem. Soc.* **1995**, *117*, 233. (d) Wang, T.; Takita, R.; Kikuzaki, Y.; Ozawa, F. *J. Am. Chem. Soc.* **2010**, *132*, 11420.

(32) Hummelen, J. C.; Knight, B. W.; LePeq, F.; Wudl, F. *J. Org. Chem.* **1995**, *60*, 532.

(33) (a) Ma, W.; Yang, C.; Gong, X.; Lee, K.; Heeger, A. J. *Adv. Funct. Mater.* **2005**, *15*, 1617. (b) Reyes-Reyes, M.; Kim, K.; Carroll, D. L. *Appl. Phys. Lett.* **2005**, *87*, 083506. (c) Lee, S.-H.; Kim, D.-H.; Kim, J.-H.; Lee, G.-S.; Park, J.-G. *J. Phys. Chem. C* **2009**, *113*, 21915.

(34) (a) Vandewal, K.; Tvingstedt, K.; Gadisa, A.; Inganäs, O.; Manca, J. V. *Nat. Mater.* **2009**, *8*, 904. (b) Brabec, C. J.; Cravino, A.; Meissner, D.; Sariciftci, N. S.; Fromherz, T.; Rispens, M. T.; Sanchez, L.; Hummelen, J. C. *Adv. Funct. Mater.* **2001**, *11*, 374.

(35) Scharber, M. C.; Mühlbacher, D.; Koppe, M.; Denk, P.; Waldauf, C.; Heeger, A. J.; Brabec, C. J. *Adv. Mater.* **2006**, *18*, 789.

(36) Peet, J.; Kim, J. Y.; Coates, N. E.; Ma, W. L.; Moses, D.; Heeger, A. J.; Bazan, G. C. *Nature Mater.* **2007**, *6*, 497.

(37) (a) Liang, Y.; Xu, Z.; Xia, J.; Tsai, S.-T.; Wu, Y.; Li, G.; Ray, C.; Yu, L. *Adv. Mater.* **2010**, *22*, E135. (b) He, Z.; Zhong, C.; Su, S.; Xu, M.; Wu, H.; Cao, Y. *Nature Photon.* **2012**, *6*, 591.

(38) Wienk, M. M.; Kroon, J. M.; Verhees, W. J. H.; Knol, J.; Hummelen, J. C.; Hal, P. A.; Janssen, R. A. J. *Angew. Chem. Int. Ed.* **2003**, *42*, 3371.

(39) Kooistra, F. B.; Knol, J.; Kastenberg, F.; Popescu, L. M.; Verhees, W. J. H.; Kroon, J. M.; Hummelen, J. C. *Org. Lett.* **2007**, *9*, 551.

(40) Lenes, M.; Wetzelaer, G.-J. A. H.; Kooistra, F. B.; Veenstra, S. C.; Hummelen, J. C.; Blom, P. W. M. *Adv. Mater.* **2008**, *20*, 2116.

(41) (a) He, Y.; Chen, H.-Y.; Hou, J.; Li, Y. *J. Am. Chem. Soc.* **2010**, *132*, 1377. (b) Zhao,

G.; He, Y.; Li, Y. *Adv*. *Mater*. **2010**, *22*, 4355.

(42) (a) Meng, X.; Zhang, W.; Tan, Z.; Du, C.; Li, C.; Bo, Z.; Li, Y.; Yang, X.; Zhen, M.; Jiang, F.; Zheng, J.; Wang, T.; Jiang, L.; Shu, C.; Wang, C. *Chem*. *Commun*. **2012**, *48*, 425. (b) Kim, K.-H.; Kang, H.; Nam, S. Y.; Jung, J.; Kim, P. S.; Cho, C.-H.; Lee, C.; Yoon, S. C.; Kim, B. J. *Chem*. *Mater*. **2011**, *23*, 5090.

(43) Zhang, C.; Chen, S.; Xiao, Z.; Zuo, Q.; Ding, L. *Org*. *Lett*. **2012**, *14*, 1508.

(44) (a) Miller, N. C.; Sweetman, S.; Hoke, E. T.; Gysel, R.; Miller, C. E.; Bartelt, J. A.; Xie, X.; Toney, M. F.; McGehee, M. D. *Nano Lett*. **2012**, *12*, 1566. (b) Guo, X.; Zhang, M.; Huo, L.; Cui, C.; Wu, Y.; Hou, J.; Li, Y. *Maclomolecules* **2012**, *45*, 6930. (c) He, Y.; You, J.; Dou, L.; Chen, C.-C.; Richard, E.; Cha, K. C.; Wu, Y.; Li, G.; Yang, Y. *Chem*. *Commun*. **2012**, *48*, 7616. (d) He, Y.; Peng, B.; Zhao, G.; Zou, Y.; Li, Y. *J*. *Phys*. *Chem*. *C* **2011**, *115*, 4340.

(45) Rispens, M. T.; Meetsma, A.; Rittberger, R.; Brabec, C. J.; Sariciftci, N. S.; Hummelen, J. C. *Chem*. *Commun*. **2003**, 2116.

(46) (a) Zhao, G.; He, Y; Xu, Z.; Hou, J.; Zhang, M.; Min, J.; Chen, H.-Y.; Ye, M.; Hong, Z.; Yang, Y.; Li, Y. *Adv*. *Funct*. *Mater*. **2010**, *20*, 1480. (b) Zheng, L.; Zhou, Q.; Deng, X.; Yuan, M.; Yu, G.; Cao, Y. *J*. *Phys*. *Chem*. *B* **2004**, *108*, 11921. (c) Troshin, P. A.; Hoppe, H.; Renz, J.; Egginger, M.; Mayorova, J. Y.; Goryachev, A. E.; Peregudov, A. S.; Lyubovskaya, R. N.; Gobsch, G.; Sariciftci, N. S.; Razumov, V. F. *Adv*. *Funct*. *Mater*. **2009**, *19*, 779.

(47) (a) Popescu, L. M.; Hof, P. van't; Sieval, A. B.; Jonkman, H. T.; Hummelen, J. C. *Appl*. *Phys*. *Lett*. **2006**, *89*, 213507. (b) Zhao, H.; Guo, X.; Tian, H.; Li, C.; Xie, Z.; Geng, Y.; Wang, F. *J*. *Mater*. *Chem*. **2010**, *20*, 3092. (c) Choi, J. H.; Son, K.-I.; Kim, T.; Ohkubo, K.; Fukuzumi, S. *J*. *Mater*. *Chem*. **2010**, *20*, 475.

(48) Kennedy, R. D.; Ayzner, A. L.; Wanger, D. D.; Day, C. T.; Halim, M.; Khan, S. I.; Tolbert, S. H.; Schwartz, B. J.; Rubin, Y. *J*. *Am*. *Chem*. *Soc*. **2008**, *130*, 17290.

(49) Niinomi, T.; Matsuo, Y.; Hashiguchi, M.; Sato, Y.; Nakamura, E. *J*. *Mater*. *Chem*. **2009**, *19*, 5804.

(50) (a) Li, G.; Shrotriya, V.; Yao, Y.; Yang. Y. *J*. *Appl*. *Phys*. **2005**, *98*, 043704. (b) Yang, X.; Loos, J.; Veenstra, S. C.; Verhees, W. J. H.; Wienk, M. M.; Kroon, J. M.; Michels, M. A. J.; Janssen, R. A. J. *Nano Lett*. **2005**, *5*, 579.

(51) Matsuo, Y.; Oyama, H.; Soga, I.; Okamoto, T.; Tanaka, H.; Saeki, A.; Seki, S.; Nakamura, E. *Chem*. *Asian J*. **2013**, *8*, 121.

(52) Matsuo, Y.; Iwashita, A.; Abe, Y.; Li, C.-Z.; Matsuo, K.; Hashiguchi, M.; Nakamura, E. *J*. *Am*. *Chem*. *Soc*. **2008**, *130*, 15429.

(53) Matsuo, Y.; Sato, Y.; Niinomi, T.; Soga, I.; Tanaka, H.; Nakamura, E. *J*. *Am*. *Chem*. *Soc*. **2009**, *131*, 16048.

(54) Morinaka, Y.; Tanabe, F.; Murata, M.; Murata, Y.; Komatsu, K. *Chem*. *Commun*. **2010**, *46*, 4532.

(55) Morinaka, Y.; Sato, S.; Wakamiya, A.; Nikawa, H.; Mizorogi, N.; Tanabe, F.; Murata, M.; Komatsu, K.; Furukawa, K.; Kato, T.; Nagase, S.; Akasaka, T.; Murata, Y. *Nat*. *Commun*. **2013**, accepted.

(56) (a) Huang, H.; Ata, M.; Ramm, M. *Chem*. *Commun*. **2002**, 2076. (b) Ata, M.; Huang, H.; Akasaka, T. *J*. *Phys*. *Chem*. *B* **2004**, *108*, 4640.

(57) Murata, M.; Morinaka, Y.; Kurotobi, K.; Komatsu, K.; Murata, Y. *Chem*. *Lett*. **2010**, *39*, 298.

(58) Murata, M.; Morinaka, Y.; Murata, Y.; Yoshikawa, O.; Sagawa, T.; Yoshikawa, S. *Chem*. *Commun*. **2011**, *47*, 7335.

(59) (a) Delgado, J. L.; Espíldora, E.; Liedtke, M.; Sperlich, A.; Rauh, D.; Baumann, A.; Deibel, C.; Dyakonov, V.; Marín, N. *Chem*. *Eur*. *J*. **2009**, *15*, 13474. (b) Liu, J.; Guo, X.; Qin, Y.; Liang, S.; Guo, Z.-X.; Li, Y. *J*. *Mater*. *Chem*. **2012**, *22*, 1758. (c) Ge, J.; Liu, J.; Guo, X.; Qin, Y.; Luo, H.; Guo, Z.-X.; Li, Y. *Chem*. *Phys*. *Lett*. **2012**, *535*, 100.

(60) Morinaka, Y.; Nobori, M.; Murata, M.; Wakamiya, A.; Sagawa, T.; Yoshikawa, S.; Murata, Y. submitted.

Chapter 1

[4+2] Cycloaddition Reaction of Fullerene C_{70} Encapsulating Two Molecules of H_2

Abstract: The [4+2] cycloaddition reaction of $H_2@C_{70}$ and $(H_2)_2@C_{70}$ with 9,10-dimethylanthracene (DMA) was conducted to investigate the interaction between inner hydrogen molecule(s) and outer C_{70} cage. In the ^1H NMR spectra of the reaction mixture, the distinguished signals of inner hydrogen molecules of $(H_2)_n@C_{70}$ (n = 1, 2) and DMA monoadducts were observed at such a high field in the range δ –21 ~ –24 ppm. The equilibrium constant $K_{eq}(H_2)_2$ for the addition of DMA to $(H_2)_2@C_{70}$ was smaller than $K_{eq}(H_2)$ for that to $H_2@C_{70}$, suggesting the decrease in chemical reactivity of $(H_2)_2@C_{70}$ compared with that of $H_2@C_{70}$. Theoretical calculations also showed that more van der Waals interaction is present between two molecules of hydrogen and C_{70} cage.

Introduction

As mentioned in General Introduction, Komatsu et al. developed the rational synthetic methodology of endohedral fullerenes,[1] so-called ‘‘molecular surgery’’,[2] and succeeded in the synthesis of endohedral C_{70} encapsulating one and two molecules of hydrogen, i.e. $H_2@C_{70}$ and $(H_2)_2@C_{70}$ (Figure 1).[3] To investigate the effect of the inner hydrogen molecule(s) on chemical reactivity of the outer C_{70} cage, the author decided to conduct the Diels-Alder reaction of $H_2@C_{70}$ and $(H_2)_2@C_{70}$ with 9,10-dimethylanthracene (DMA); the addition of DMA to fullerenes is known to occur reversibly at room temperature (Scheme 1).[4]

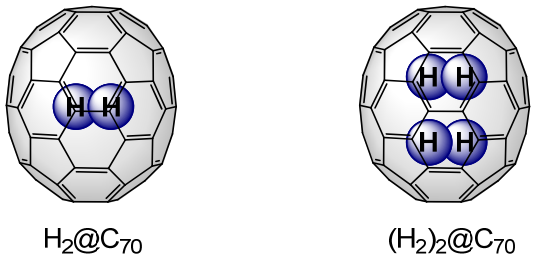

Figure 1. Structures of $H_2@C_{60}$ and $(H_2)_2@C_{70}$.[3]

Scheme 1. Diels-Alder reaction of C_{60} with DMA

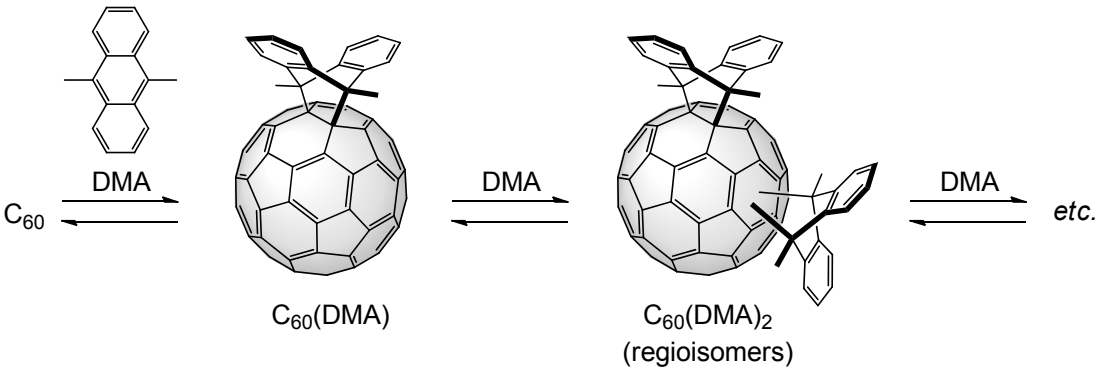

As a related study, Saunders et al. conducted the reaction of $^3He@C_{60}$[5] and $^{129}Xe@C_{60}$[5a,6] with DMA; the inner ^3He and ^{129}Xe atoms were utilized as NMR probes[5,6] to determine the equilibrium constant K_{eq} for the addition of DMA to $^3He@C_{60}$ and $^{129}Xe@C_{60}$ (Figure 2).[7,8] As a result, they found that the K_{eq} for the reaction of the DMA-monoadduct

with DMA giving the bisadducts is smaller for ^{129}Xe than for ^{3}He, indicating that the reactivity of ^{129}Xe@C_{60} was lower than that of ^{3}He@C_{60}.[7,8] In addition, it was revealed that the equilibrium constants for the reaction of ^{3}He@C_{60} and H_2@C_{60}[1] with DMA were almost the same ($K_{eq}(^{3}He)/ K_{eq}(H_2) = 1.05 \pm 0.10$),[9] which are also the same as that of empty C_{60}[2] ($\Delta H(^{3}He) = -22.9$ kcal mol^{-1}, $\Delta S(^{3}He) = 61.2$ cal mol^{-1} K^{-1})[9] within experimental error. Although the interaction between the encapsulated H_2 and C_{70} cage is quite minute for H_2@C_{70} as shown by the small differences in chemical shifts of ^{13}C NMR compared with those of empty C_{70},[3b] there is still a possibility that a difference in chemical reactivity of the outer cage becomes appreciable when two molecules of H_2 are encapsulated inside the cage. In this chapter, the reaction, thermodynamic parameters, and interaction of H_2@C_{70} and $(H_2)_2$@C_{70} are described.

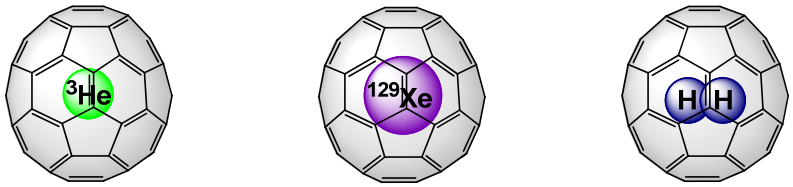

Figure 2. Structures of ^{3}He@C_{60}, ^{129}Xe@C_{60}, and H_2@C_{60}.

Results and Discussion

A solution of a mixture of H_2@C_{70}, $(H_2)_2$@C_{70}, and C_{70} (molar ratio, 70 : 2 : 28; total concentration, 13.8 mM) and DMA (6.11 mM) in ODCB-d_4 was prepared (Scheme 2).[7] As shown in Figure 3, appearance of new singlet signals at δ = 2.9 and 2.4 ppm as well as multiplets in the aromatic region suggested the formation of the monoadducts, H_2@**1**, $(H_2)_2$@**1**, and **1**, respectively. However, it is very difficult to determine the ratio of them owing to the severe overlaps. On the other hand, the spectrum of very high magnetic field showed clear distributions of the starting material (H_2@C_{70} and $(H_2)_2$@C_{70}) and products (H_2@**1** and $(H_2)_2$@**1**), owing to the strongly shielded signals of encapsulated H_2 molecules.[1,3,10] The NMR spectrum exhibited new signals for the encapsulated H_2 of

monoadducts H_2@**1** and $(H_2)_2$@**1** at δ = −22.22 and −21.80 ppm, respectively, in addition to the H_2 signals of unreacted H_2@C_{70} and $(H_2)_2$@C_{70} (δ = −23.97 and −23.80 ppm, respectively). The equilibrium constant $K_{eq}(H_2)$ and free-energy difference $\Delta G(H_2)$ for the addition of DMA to H_2@C_{70}, together with $K_{eq}(H_2)_2$ and $\Delta G(H_2)_2$ for that to $(H_2)_2$@C_{70} at 30, 40, and 50 °C were determined based on the intensity of the NMR signals of the encapsulated H_2 and the concentration of unreacted DMA. The equations is:

$$K_{eq}(H_2)_n = \frac{[(H_2)_n@\mathbf{1}]}{[(H_2)_n@C_{70}] \times [DMA]} \quad (n = 1, 2) \quad (1)$$

The relative intensities of the NMR signals, estimated concentrations of free DMA, equilibrium constants, and free-energy differences are summarized in Table 1. The $K_{eq}(H_2)_2$ value is smaller than the $K_{eq}(H_2)$ value by more than 15% at each temperature, demonstrating the ‘‘*apparently*’’ decreased reactivity of $(H_2)_2$@C_{70} toward DMA.

Scheme 2. Diels-Alder reaction of $(H_2)_n$@C_{70} (n = 1, 2) with DMA

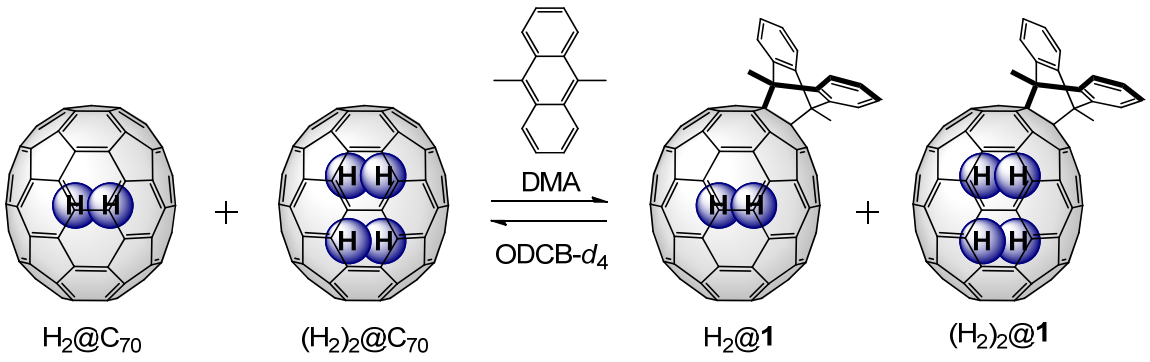

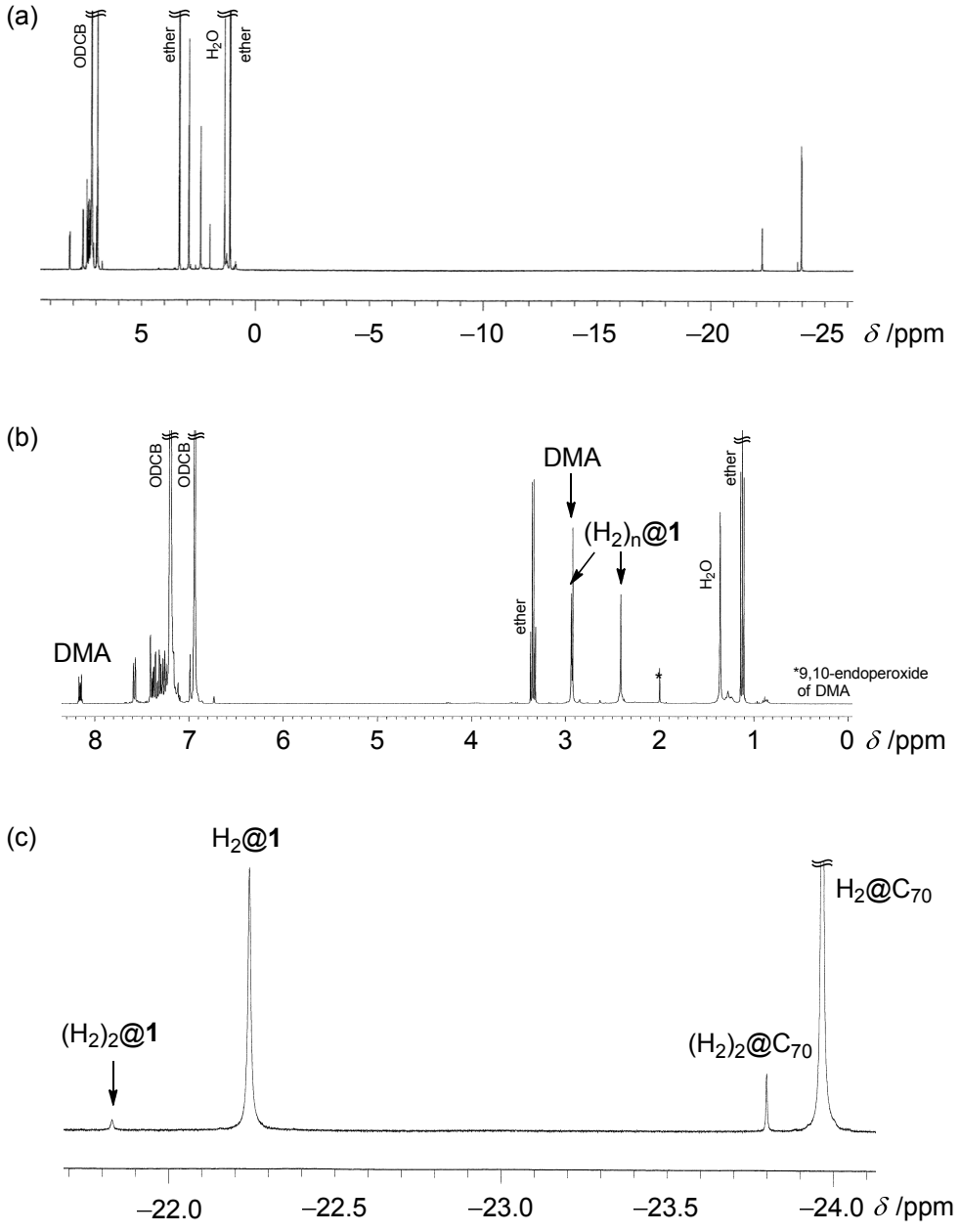

Figure 3. (a) The ^{1}H NMR (400 MHz, ODCB-d_4) of the reaction mixture of $(H_2)_n@C_{70}$ (n = 0 (28%), 1 (70%), 2 (2%)) and DMA at 30 °C, and the expanded spectra in the regions of (b) 8.5 ~ 0 ppm and (c) –21.5 ~ –24.0 ppm.

Table 1. Relative intensities of the NMR signals, estimated concentrations of free DMA, equilibrium constants, and free-energy differences at 30, 40, and 50 °C

T (°C)	30	40	50
$H_2@C_{70}$	65.04	69.21	75.45
$H_2@$**1**	31.00	26.92	20.74
$(H_2)_2@C_{70}$	2.846	2.938	3.081
$(H_2)_2@$**1**	1.103	0.926	0.716
free DMA (mM)	1.309	2.199	3.111
$K_{eq}(H_2)$ (M^{-1})	364	177	88.4
$K_{eq}(H_2)_2$ (M^{-1})	296	143	74.7
$\Delta G(H_2)$ (kcal mol^{-1})	–3.55	–3.22	–2.88
$\Delta G(H_2)_2$ (kcal mol^{-1})	–3.43	–3.09	–2.77

Next, the van't Hoff equation gives:

$$\ln K_{eq}(H_2)_n = -\frac{\Delta H(H_2)_n}{RT} + \frac{\Delta S(H_2)_n}{R} \quad (n = 1, 2) \qquad (2)$$

As shown in Figure 4, the van't Hoff plot of ln $K_{eq}(H_2)$ or ln $K_{eq}(H_2)_2$ versus $1/T$ gave excellent linear fits and provided $\Delta H(H_2)$ and $\Delta H(H_2)_2$ as −13.8 ± 0.1 and −13.4 ± 0.2 kcal mol^{-1}, respectively, and $\Delta S(H_2)$ and $\Delta S(H_2)_2$ as −33.7 ± 0.3 and −32.9 ± 0.6 cal mol^{-1} K^{-1}, respectively.

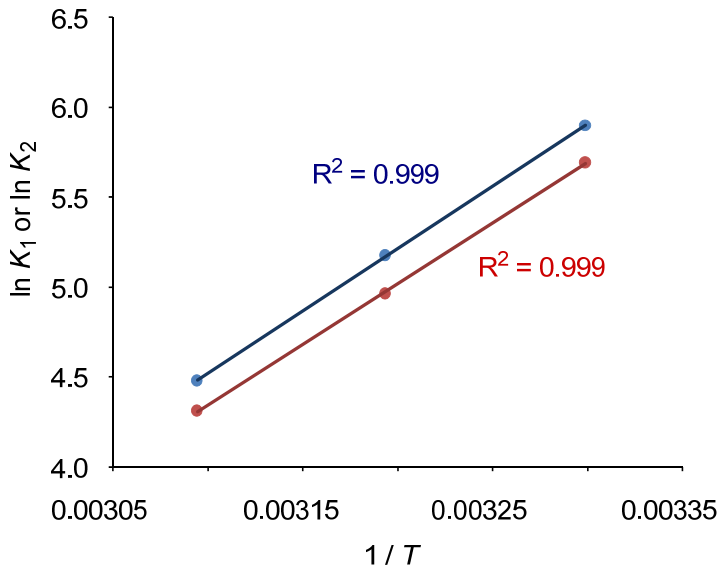

Figure 4. The van't Hoff plots of ln $K_{eq}(H_2)$ vs. T^{-1} (blue) and ln $K_{eq}(H_2)_2$ vs. T^{-1} (red).

To elucidate the difference in chemical reactivity between $H_2@C_{70}$ and $(H_2)_2@C_{70}$, theoretical calculations using the M06-2X[11] functional with the 6-31G(d,p) basis set were conducted.[12] First, the optimized structure of $(H_2)_2@C_{70}$ was compared with that of $H_2@C_{70}$ because structural distortion is usually associated with an increase in chemical reactivity.[13] It was shown that the long axis of the C_{70} cage of $(H_2)_2@C_{70}$ is elongated by 0.011 Å, while the short axis is shortened by 0.006 Å, as compared to those of $H_2@C_{70}$ (Figure 5). As described above, Saunders et al. reported the decreased reactivity of $^{129}Xe@C_{60}$ to the addition of DMA as compared to that of $^{3}He@C_{60}$.[7,8] The encapsulated Xe atom was suggested to have substantial interaction with C_{60} and push the π-electron density outwards from the C_{60} cage.[8] Considering the fact that the total size of two molecules of hydrogen is comparable to that of one Xe atom (van der Waals diameter of Xe, 4.32 Å; those of H_2, 2.40 Å for short axis and 4.06 Å for long axis, respectively),[14] the possibility of such effect of the two molecules of hydrogen on the C_{70} cage would be considerable. It is worth noting that the energy levels of the frontier orbitals of $H_2@C_{70}$ and $(H_2)_2@C_{70}$ are almost identical (HOMO –7.10 eV and LUMO –2.77 eV for $H_2@C_{70}$, and HOMO –7.11 eV and LUMO –2.78 eV for $(H_2)_2@C_{70}$, respectively).

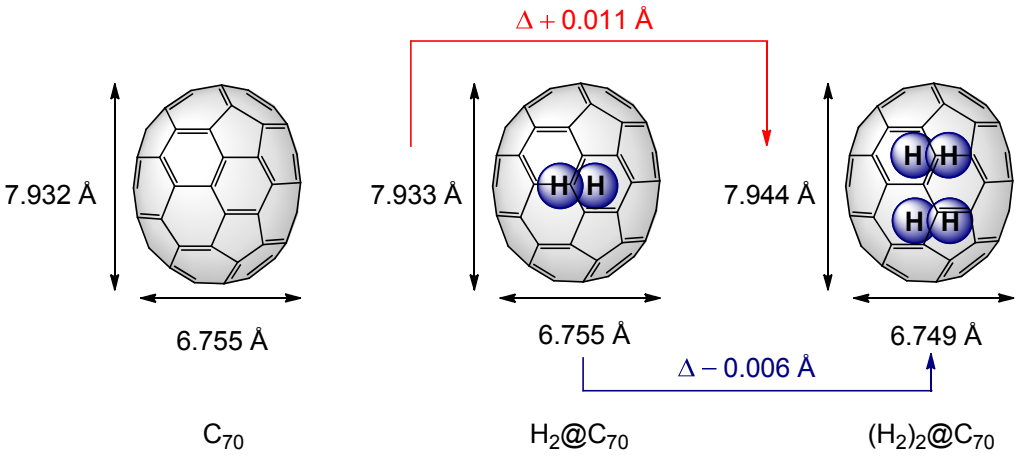

Figure 5. The optimized structures of C_{70}, $H_2@C_{70}$, and $(H_2)_2@C_{70}$. Geometries were fully optimized at the M06-2X level using 6-31G(d,p) basis set.

Next, using the optimized structures at the M06-2X method, the stabilization energies were studied by the single-point calculations at M06-2X, MPWB1K,[15] and MP2[16] methods, respectively, to obtain insight into the interaction between the inner molecule(s) of hydrogen and the C_{70} cage. The stabilization energies of model compounds $(H_2)_n@$**1'** (n = 1, 2) (the structures are shown in Figure 6) were also calculated by the same methods. It should be mentioned that the representative DFT functional B3LYP is not suitable to estimate the stabilization energies of endohedral fullerenes.[17] The 6-31G(d,p) basis set was applied to all calculations and the results are summarized in Table 2. At the M06-2X and the MPWB1K levels, the encapsulation of two molecules of H_2 into C_{70} is shown to be more exothermic than that of one molecule of H_2 after basis set superposition error (BSSE) correction, indicating that more attractive interaction is present between two molecules of H_2 and the C_{70} cage. These results are in good agreement with the related theoretical studies on $H_2@C_{70}$ and $(H_2)_2@C_{70}$.[18] On the other hand, calculations at MP2 level showed the decreased stabilization energy of $(H_2)_2@C_{70}$ or $(H_2)_2@$**1'** relative to that of $H_2@C_{70}$ or $H_2@$**1'**. This would be ascribed to the use of 6-31G(d,p) basis set which would cause large superposition error; it was reported that the calculations at MP2 level using TQZP basis set produced the trend in the increased stabilization for the encapsulation of two molecules of hydrogen.[18a] Moreover, the stabilization energies of $(H_2)_n@$**1'** (n = 1, 2) were smaller than those of $(H_2)_n@C_{70}$ (n = 1, 2), indicating that the interaction between the inner molecule(s) of

hydrogen and the outer C_{70} cage becomes weaker as the scission of π-system of the C_{70} cage. For example, as shown in Figure 6, the energy difference between $(H_2)_2@C_{70}$ and $(H_2)_2@$**1'** ($\Delta\Delta E_2$ = 0.21 kcal mol^{-1}) is larger than that between $H_2@C_{70}$ and $H_2@$**1**' ($\Delta\Delta E_1$ = 0.06 kcal mol^{-1}) at the M06-2X level and this trend is reproduced at both the MPWB1K and the MP2 levels. Hence, it would be also reasonable to conclude that $(H_2)_2@C_{70}$ tends to retain its 70π-electron system and thus resulted in the smaller $K_{eq}(H_2)_2$ value than the $K_{eq}(H_2)$ value.

Table 2. Stabilization energies (kcal mol^{-1}) after BSSE correction; single-point calculations (6-31G(d,p) basis set) on the M06-2X/6-31G(d,p) optimized structures

Method	$H_2@C_{70}$	$(H_2)_2@C_{70}$	$H_2@$**1'**	$(H_2)_2@$**1'**
M06-2X	–5.94	–12.74	–5.88	–12.53
MPWB1K	–3.85	–7.53	–3.68	–7.16
MP2	–1.83	–1.42	–1.70	–1.12

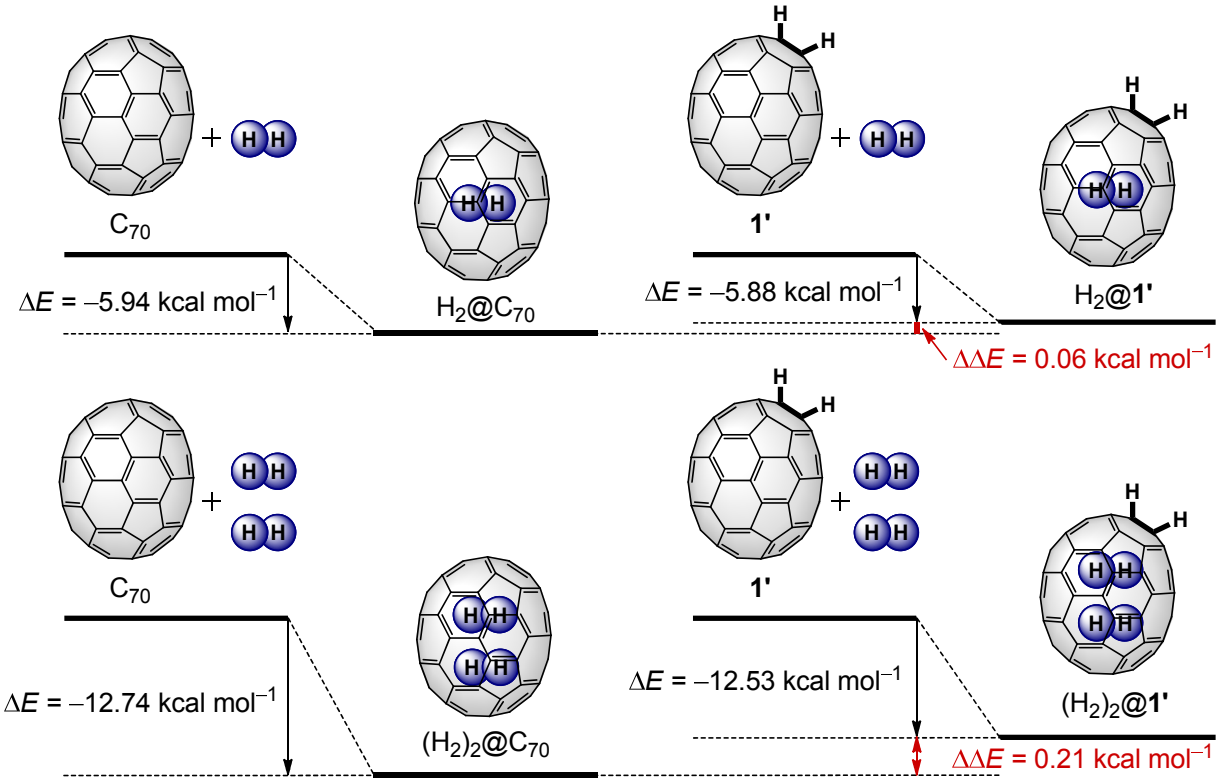

Figure 6. The stabilization energies at M06-2X/6-31G(d,p) level after BSSE correction.

Conclusion

In summary, the Diels-Alder reaction of $H_2@C_{70}$ and $(H_2)_2@C_{70}$ with 9,10-dimethylanthracene (DMA) was conducted for the purpose of investigation of the chemical reactivity of the C_{70} cages. In the ^{1}H NMR measurements, the inner hydrogen molecules act as a powerful NMR probe to give clear information of relative ratio of the species in the system. The equilibrium constants $K_{eq}(H_2)_n$ for the addition of DMA to $(H_2)_n@C_{70}$ (n = 1, 2) were influenced by the number of hydrogen molecule(s) inside C_{70} and $K_{eq}(H_2)_2$ was found to be smaller than $K_{eq}(H_2)$ by 15 ~ 19%, suggesting the decrease in chemical reactivity of $(H_2)_2@C_{70}$. To obtain more information about the interaction between the inner hydrogen molecule(s) and the outer C_{70} cage, theoretical calculations were performed. As a result, the stabilization energy of $(H_2)_2@C_{70}$ was larger than that of $H_2@C_{70}$, indicating that more interaction is present between two molecules of hydrogen and C_{70} cage.

Experimental Section

General. The ^{1}H and ^{13}C NMR measurements were carried out on a JEOL AL-400 instrument and the chemical shifts are reported in ppm with reference to tetramethylsilane, or residual protons and carbons of *o*-dichlorobenzene-d_4 (ODCB-d_4) (δ 7.20 ppm in ^{1}H NMR, δ 132.35 ppm in ^{13}C NMR). ODCB-d_4 and 9,10-dimethylanthracene (DMA) were purchased from Aldrich Co. $H_2@C_{70}$ and $(H_2)_2@C_{70}$ were prepared by following the literature.[3]

Computational Method. All calculations were conducted with Gaussian 09 packages. The structures were fully optimized with the M06-2X functional and 6-31G(d,p) basis set without any symmetry assumptions. To estimate the stabilization energies after BSSE correction, single-point calculations were conducted at M06-2X, MPWB1K, and MP2 (second-order Møller-Plesset perturbation theory) levels, respectively, using 6-31G(d) basis set.

The Diels-Alder reaction of a mixture of $H_2@C_{70}$, $(H_2)_2@C_{70}$, and C_{70} with DMA. A mixture of $H_2@C_{70}$, $(H_2)_2@C_{70}$, and C_{70} (molar ratio of 70 : 2 : 28) (8.19 mg, 9.73 mmol

(calculated with an averaged molecular weight as 842.2)), and DMA (0.887 mg, 4.30 mmol) were dissolved in ODCB-d_4 (943 mg, 0.704 mL). The solution was transferred into an NMR tube and the tube was sealed under argon. Before the acquisition of the variable-temperature NMR, the sample solution was kept for one hour in the NMR probe to reach the equilibrium. The NMR spectra were taken at 30, 40, and 50 ºC with a JEOL AL-400 instrument using 5.0 μs pulse width, 6.554 s acquisition time, 15 s pulse delay, and 131,072 data points for a 40-ppm spectral width. The reversibility of the system was confirmed by measuring the NMR at 30 ºC again after the all measurements, and no formation of precipitation was observed during all experiments.

The concentrations of free DMA was determined based on the initial concentration of DMA (6.11 mM) subtracted by the amounts consumed for the formation of **1**, H_2@**1**, and $(H_2)_2$@**1** as well as the amount of 9,10-endoperoxide of DMA formed during the sample preparation by photochemical oxidation. The ratio of free DMA, monoadducts, and 9,10-endoperoxide in the system are shown below. The signals used for estimation of the ratio are δ 8.17 ppm for free DMA, δ 2.41 ppm for three monoadducts H_2@**1**, $(H_2)_2$@**1**, and empty **1**, and δ 2.00 ppm for the 9,10-endoperoxide, respectively. Only one isomer of the monoadduct of C_{70} with DMA was observed, and the amounts of bisadducts, probably corresponding to the signals between at δ –18.78 and –20.99 ppm, were negligible (< 1%). The ratios of [H_2@C_{70}]/[H_2@**1**] and [$(H_2)_2$@C_{70}]/[$(H_2)_2$@**1**] were determined by the integrated peak areas for the encapsulated H_2 molecule(s) at –23.97 and –22.24 for [H_2@C_{70}]/[H_2@**1**], and –23.80 and –21.83 for [$(H_2)_2$@C_{70}]/[$(H_2)_2$@**1**], respectively.

H_2@**1**: ^{13}C NMR (100 MHz, ODCB-d_4) δ 159.44, 156.06, 151.25, 151.20, 150.70, 150.55, 150.50, 150.11, 149.75, 149.64, 149.18, 149.07, 148.97, 148.53, 147.32, 147.23, 147.03, 146.78, 146.16, 146.13, 145.57, 143.12, 143.09, 143.08, 143.03, 142.99, 142.76, 141.29, 139.63, 137.78, 133.45, (the signals at the range of δ 132.4 ~ 126.8 were overlapped with the signals of ODCB-d_4), 122.97, 122.34, 71.19, 71.17, 70.18, 49.34, 48.45.

References

(1) (a) Murata, Y.; Murata, M.; Komatsu, K. *Chem*. *Eur*. *J*. **2003**, *9*, 1600. (b) Murata, Y.; Murata, M.; Komatsu, K. *J*. *Am*. *Chem*. *Soc*. **2003**, *125*, 7152. (c) Komatsu, K.; Murata, M.; Murata, Y. *Science* **2005**, *307*, 238. (d) Murata, M.; Murata, Y.; Komatsu, K. *J*. *Am*. *Chem*. *Soc*. **2006**, *128*, 8024. (e) Murata, M.; Murata, Y.; Komatsu, K. *Chem*. *Commun*. **2008**, 6083. (f) Wudl, F.; Nagase, S.; Akasaka, T. *Chemistry of Nanocarbons*; Wiley-Blackwell, Oxford, **2010**.

(2) Rubin, Y. *Chem*. *Eur*. *J*. **1997**, *3*, 1009.

(3) (a) Murata, Y.; Maeda, S.; Murata, M.; Komatsu, K. *J*. *Am*. *Chem*. *Soc*. **2008**, *130*, 6702. (b) Murata, M.; Maeda, S.; Morinaka, Y.; Murata, Y.; Komatsu, K. *J*. *Am*. *Chem*. *Soc*. **2008**, *130*, 15800.

(4) Lamparth, I.; Maichle-Mössmer, C.; Hirsch, A. *Angew*. *Chem*. *Int*. *Ed*. **1995**, *34*, 1607.

(5) (a) Saunders, M.; Cross, R. J.; Jiménez-Vázquez, H. A.; Shimshi, R.; Khong, A. *Science* **1996**, *271*, 1693. (b) Saunders, M.; Jiménez-Vázquez, H. A.; Cross, R. J.; Mroczkowski, S.; Freedberg, D. I.; Anet, F. A. L. *Nature* **1994**, *367*, 256. (c) Saunders, M.; Jiménez-Vázquez, H. A.; Cross, R. J.; Mroczkowski, S.; Gross, M. L.; Giblin, D. E.; Poreda, R. J. *J*. *Am*. *Chem*. *Soc*. **1994**, *116*, 2193. (d) Saunders, M.; Jiménez-Vázquez, H. A.; Bangerter, B. W.; Cross. R. J.; Mroczkowski, S.; Freedberg, D. I.; Anet, F. A. L. *J*. *Am*. *Chem*. *Soc*. **1994**, *116*, 3621. (e) Smith III, A. B; Strongin, R. M.; Brard, L.; Romanow, W. J.; Saunders, M.; Jiménez-Vázquez, H. A.; Cross, R. J. *J*. *Am*. *Chem*. *Soc*. **1994**, *116*, 10831. (f) Rüttimann, M.; Haldimann, R. F.; Isaacs, L.; Diederich, F.; Khong, A.; Jiménez-Vázquez, H. A.; Cross, R. J.; Saunders, M. *Chem*. *Eur*. *J*. **1997**, *3*, 1071. (g) Akasaka, T.; Nagase, S. *Endofullerenes*: *A New Family of Carbon Clusters*; Kluwer Academic, Dordrecht, **2002**.

(6) Syamala, M. S.; Cross, R. J.; Saunders, M. *J*. *Am*. *Chem*. *Soc*. **2002**, *124*, 6216.

(7) Wang, G.-W.; Saunders, M.; Cross, R. J. *J*. *Am*. *Chem*. *Soc*. **2001**, *123*, 256.

(8) Frunzi, M.; Cross, R. J.; Saunders, M. *J*. *Am*. *Chem*. *Soc*. **2007**, *129*, 13343.

(9) Frunzi, M.; Xu, H.; Cross, R. J.; Saunders, M. *J*. *Phys*. *Chem*. *A* **2009**, *113*, 4996.

(10) (a) Murata, M.; Ochi, Y.; Tanabe, F.; Komatsu, K.; Murata, Y. *Angew*. *Chem*. *Int*. *Ed*. **2008**, *47*, 2039. (b) Murata, M.; Ochi, Y.; Kitagawa, T.; Komatsu, K.; Murata, Y. *Chem*. *Asian J*. **2008**, *3*, 1336. (c) Matsuo, Y.; Isobe, H.; Tanaka, T.; Murata, Y.; Murata, M.;

Komatsu, K.; Nakamura, E. *J*. *Am*. *Chem*. *Soc*. **2005**, *127*, 17148.

(11) Zhao, Y.; Truhlar, D. G. *Theor*. *Chem*. *Acc*. **2008**, *120*, 215.

(12) Frisch, M. J. ; Trucks, G. W.; Schlegel, H. B.; Scuseria, G. E.; Robb, M. A.; Cheeseman, J. R.; Scalmani, G.; Barone, V.; Mennucci, B.; Petersson, G. A.; Nakatsuji, H.; Caricato, M.; Li, X.; Hratchian, H. P.; Izmaylov, A. F.; Bloino, J.; Zheng, G.; Sonnenberg, J. L.; Hada, M.; Ehara, M.; Toyota, K.; Fukuda, R.; Hasegawa, J.; Ishida, M.; Nakajima, T.; Honda, Y.; Kitao, O.; Nakai, H.; Vreven, T.; Montgomery, Jr. J. A.; Peralta, J. E.; Ogliaro, F.; Bearpark, M.; Heyd, J. J.; Brothers, E.; Kudin, K. N.; Staroverov, V. N.; Kobayashi, R.; Normand, J.; Raghavachari, K.; Rendell, A.; Burant, J. C.; Iyengar, S. S.; Tomasi, J.; Cossi, M.; Rega, N.; Millam, J. M.; Klene, M.; Knox, J. E.; Cross, J. B.; Bakken, V.; Adamo, C.; Jaramillo, J.; Gomperts, R.; Stratmann, R. E.; Yazyev, O.; Austin, A. J.; Cammi, R.; Pomelli, C.; Ochterski, J. W.; Martin, R. L.; Morokuma, K.; Zakrzewski, V. G.; Voth, G. A.; Salvador, P.; Dannenberg, J. J.; Dapprich, S.; Daniels, A. D.; Farkas, O.; Foresman, J. B.; Ortiz, J. V.; Cioslowski, J.; Fox, D. J.; *GAUSSIAN 09*, Revision B. 01; Gaussian Inc.: Wallingford CT, **2010**.

(13) (a) Osuna, S.; Swart, M.; Solá, M. *Phys*. *Chem*. *Chem*. *Phys*. **2011**, *13*, 3585. (b) Osuna, S.; Swart, M.; Solá, M. *Chem*. *Eur*. *J*. **2009**, *15*, 13111.

(14) (a) Bondi, A. *J*. *Phys*. *Chem*. **1964**, *68*, 441. (b) Dekock, R. L.; Gray, H. B. *Chemical Structure and Bonding*; University Science Books, **1989**.

(15) (a) Zhao, Y.; Truhlar, D. G. *J*. *Phys*. *Chem*. *A* **2004**, *108*, 6908. (b) Zhao, Y.; Truhlar, D. G. *J*. *Chem*. *Theory Comput*. **2005**, *1*, 415.

(16) Møller, C.; Plesset, M. S. *Phys*. *Rev*. **1934**, *46*, 618.

(17) Slanina, Z.; Pulay, P.; Nagase, S. *J*. *Chem*. *Theory Comput*. **2006**, *2*, 782.

(18) (a) Kruse, H.; Grimme, S. *J*. *Phys*. *Chem*. *C* **2009**, *113*, 17006. (b) Sebastianelli, F.; Xu, M.; Bačić, Z.; Lawler, R.; Turro, N. J. *J*. *Am*. *Chem*. *Soc*. **2010**, *132*, 9826. (c) Konona, T.; Dodziuk, H. *J*. *Chem*. *Theory Comput*. **2011**, *7*, 1476.

Chapter 2

Rational Synthesis, Enrichment, and ^{13}C NMR Spectra of Endohedral C_{60} and C_{70} Encapsulating a Helium Atom

Abstract: Endohedral C_{60} and C_{70} encapsulating a helium atom, i.e. He@C_{60} and He@C_{70}, at occupation levels of 30% were synthesized by a molecular surgery method. The ^{13}C NMR spectra of He@C_{60} and He@C_{70} showed a slight shift to downfield relative to those of empty C_{60} and C_{70}, indicating a weak interaction between the inner helium atom and the outer fullerene cage. Although the He@C_{60} and He@C_{70} were obtained as mixtures of empty fullerenes, the enrichment of He@C_{60} and He@C_{70} is feasible by the use of recycling HPLC.

Introduction

The endohedral C_{60} encapsulating a ^3He atom, i.e. $^3He@C_{60}$, was first reported by Saunders et al. in 1994.[1] The inner ^3He atom of $^3He@C_{60}$ has opened up an important role as a powerful NMR probe not only to follow chemical reactions taking place at the exterior of the C_{60} framework[2] but also to investigate the internal magnetic field of C_{60} cage.[1,3]

As mentioned in General Introduction, the van der Waals interaction between inner helium atom and outer C_{60} cage of $He@C_{60}$ is expected to be the weakest among the endohedral C_{60} encapsulating a noble-gas atom (He, Ne, Ar, Kr, and Xe). However, the studies on the interaction of $He@C_{60}$ have been limited only in computational chemistry[4] because the production has relied on rather low yielding physical method; high-pressure/high-temperature treatment gave the desired endohedral fullerenes at an occupation level of ca. 0.1%.[5] Although attempts for efficient production of $He@C_{60}$ have been reported by several groups, the occupation levels have remained low (ca. 1%).[6]

On the other hand, "molecular surgery"[7] should have a potential to achieve rational synthesis of $He@C_{60}$. Actually, Rubin et al. reported the insertion of a ^3He atom into an open-cage C_{60} derivative **1**[8] at an occupation level of 1.5% (Scheme 1).[9] Murata et al. also succeeded in the insertion of a ^4He atom into open-cage C_{60} derivative **2**[10] and subsequent size-reduction of the opening to give He@**3** at an occupation level of 35% (Scheme 2).[11] Unfortunately, the complete closure of the complicated openings of He@**1** and He@**3** has not been accomplished.

Scheme 1. Insertion of a ^3He atom into open-cage C_{60} derivative **1**

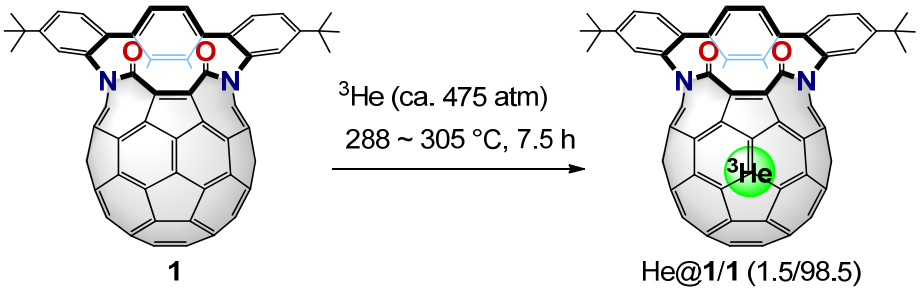

1 He@**1**/**1** (1.5/98.5)

Scheme 2. Encapsulation of a ^{4}He atom inside open-cage C_{60} derivative **3**

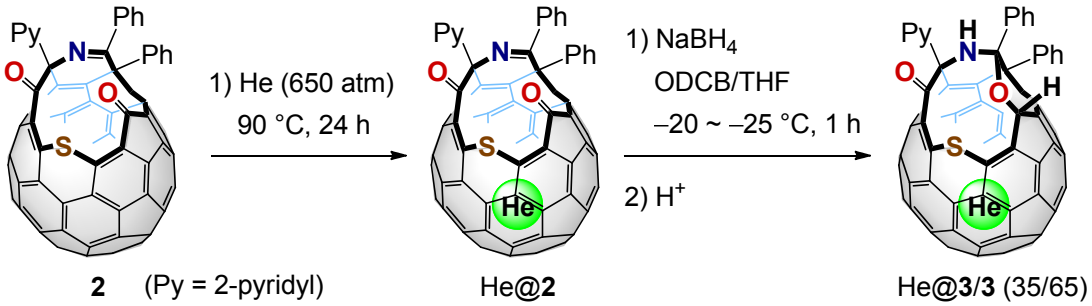

By applying the synthetic methodology of $H_2@C_{60}$[12] and $H_2@C_{70}$,[13] the author succeeded in the synthesis of $He@C_{60}$ and $He@C_{70}$ at occupation levels of 30%. The interaction between the inner helium atom and the outer fullerene cage was studied by the measurement of the ^{13}C NMR signals of $He@C_{60}$ and $He@C_{70}$. Furthermore, the separation of $He@C_{60}$ and $He@C_{70}$ from empty C_{60} and C_{70} was conducted by the use of recycling HPLC on Cosmosil Buckyprep columns. In this chapter, synthesis, ^{13}C NMR spectra, and enrichment of $He@C_{60}$ and $He@C_{70}$ are described.

Results and Discussion

The size of the opening of **2** is so large that a helium atom can freely go in and out through the opening even at room temperature.[14] In the present work, the author selected sulfoxide derivative **4**,[12] instead of **2** so that the author could carry out the size-reduction of the opening by removing the SO unit immediately after the insertion of He (Scheme 3). Thus, powdery **4** was heated at 115 ºC under pressurized ^{4}He gas (1230 atm) for 1 h. The resulting powder was immediately dissolved in benzene and irradiated with high-pressure mercury lamp to afford He@**5** with a 12-membered-ring opening.[12] The occupation level of He was determined to be 30% by atmospheric pressure chemical ionization (APCI) mass analysis (Figure 1). Two peaks were observed at *m*/*z* 1038.6 and 1034.6, corresponding to He@**5** and empty **5**, respectively, with an intensity ratio being 3 : 7.

Scheme 3. Insertion of a ^{4}He atom into **4** and subsequent size-reduction of the opening

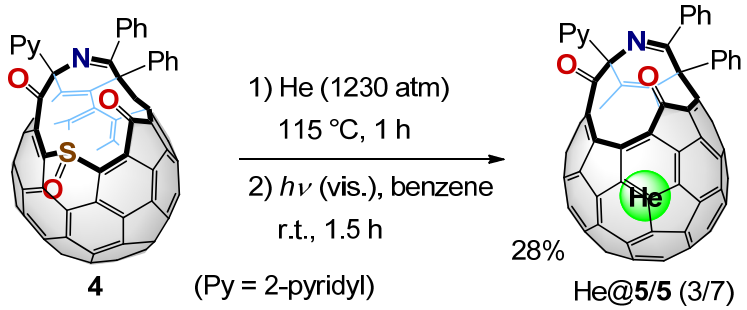

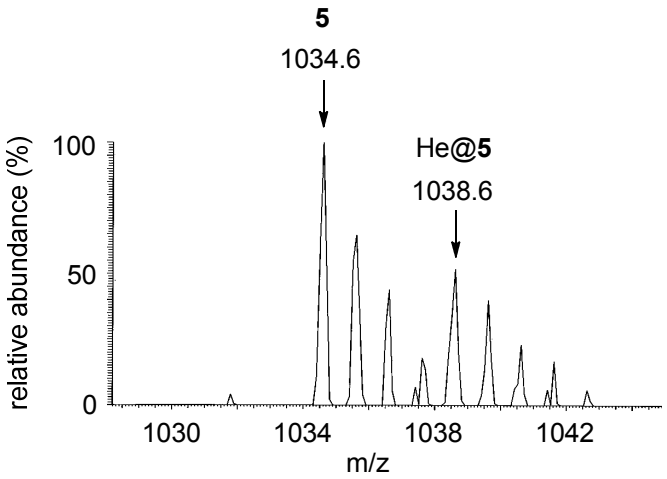

Figure 1. APCI-MS spectrum (negative-ion mode) of He@**5**/**5** (3/7).

As for the incorporation of a helium atom in C_{60}, the binding energy (ΔE = –1.99 kcal mol^{-1}) and the equilibrium constants (K_{eq} = 6.41 × 10^{-4} atm^{-1} at 300 K) were theoretically evaluated based on the results from MP2 calculations with a very large basis set (EXT).[15] On the other hand, the K_{eq} value for ^{3}He@**2** was experimentally determined at 50 ºC, with uncertainty of 40%, to be 3.1 × 10^{-4} atm^{-1}, which is comparable to the K_{eq} value calculated for the equilibrium: (He + C_{60} ⇌ He@C_{60} (*vide supra*)). In this equilibrium, the occupation level of He inside C_{60} under 1230 atm was estimated to be 44% at 300 K and 17% at 500 K.[15] Thus, the incorporation of He inside **4** at the occupation level of 30% (determined after transformation to He@**5**) under the present conditions (1230 atm, 388K) appears to indicate that the equilibrium state has been reached. This lower occupation level for He@**5** than that of 100% for H_2@**2**[12a] can be

ascribed to smaller incorporation energy of He inside **5** than that of H_2 inside **2**. Actually, the calculations at the M06-2X/6-31G(d,p) level[16] showed stabilization caused by the encapsulation of one atom of He inside **4** (ΔE) to be –2.98 kcal mol^{-1} after BSSE (basis set superposition error) correction, which is smaller than the value for one molecule of H_2 inside **2** (ΔE = –7.59 kcal mol^{-1}) (Figure 2).[17]

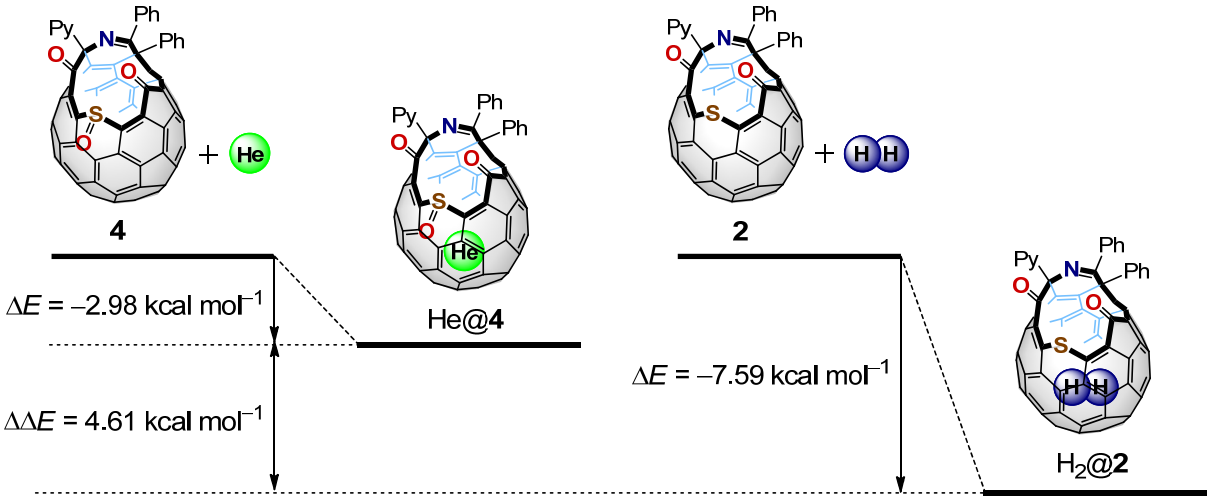

Figure 2. The stabilization energies after BSSE correction. The calculations were conducted at M06-2X/6-31G(d,p) level.

The author then moved on complete closure of the opening of He@**5** to synthesize He@C_{60} (Scheme 4). The opening of He@**5** (He@**5**/**5** = 3/7) was transformed to an 8-membered-ring by the McMurry reaction to give open-cage C_{60} derivative He@**6** (He@**6**/**6** = 3/7).[12b,c] Then, thermal treatment of powdery He@**6** at 400 ºC under vacuum successfully gave endohedral fullerene He@C_{60} in 76% isolated yield.[12b,c] In these reactions, no appreciable escape of inner He took place as judged from the APCI mass analysis, which showed two peaks at *m*/*z* 724.3 and 720.2, corresponding to He@C_{60} and empty C_{60}, respectively, with the same intensity ratio of 3 : 7 as that for He@**5** (Figure 3).

Scheme 4. Synthesis of endohedral C_{60} encapsulating a ^4He atom

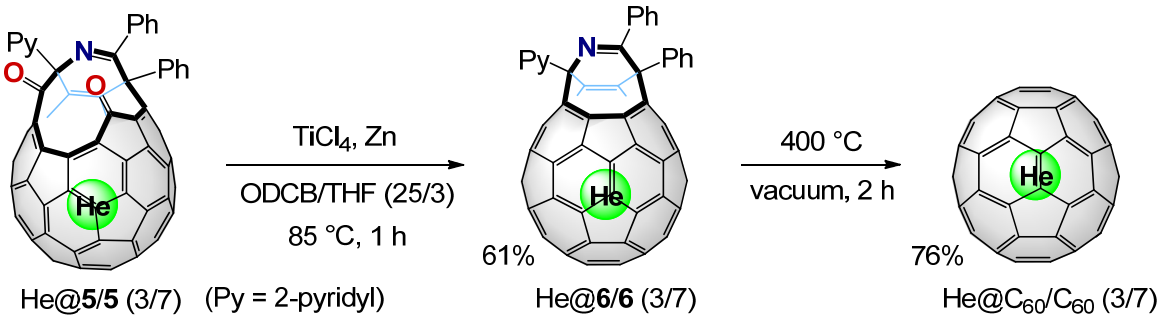

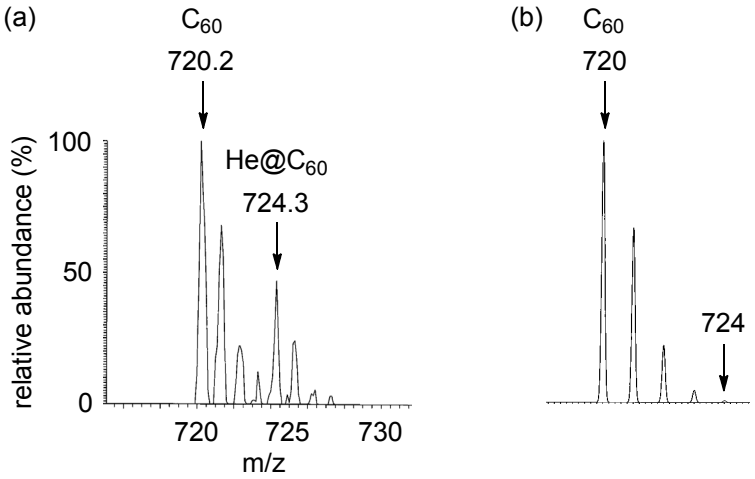

Figure 3. (a) APCI-MS spectrum (negative-ion mode) of $He@C_{60}/C_{60}$ (3/7) and (b) theoretical isotopic pattern for C_{60}.

The ^{13}C NMR spectrum exhibited a signal for $He@C_{60}$ at δ = 142.80, which was slightly shifted to downfield by $\Delta\delta$ = 0.02 relative to that of empty C_{60} (δ = 142.78) (Figure 4). This $\Delta\delta$ value was apparently smaller than that observed for $H_2@C_{60}$ ($\Delta\delta$ = 0.08),[12b,c] $Ar@C_{60}$ ($\Delta\delta$ = 0.17),[18] $Kr@C_{60}$ ($\Delta\delta$ = 0.39),[19] and $Xe@C_{60}$ ($\Delta\delta$ = 0.95),[20] indicating the quite minute electronic interaction exerted on the C_{60} π-system by the encapsulated He.

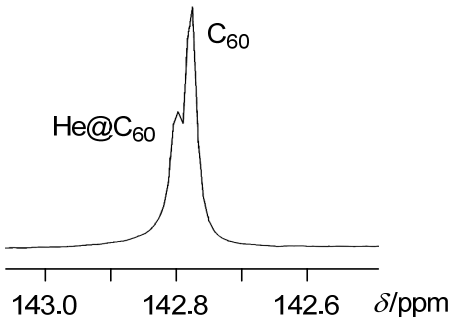

Figure 4. ^{13}C NMR spectra (75 MHz, ODCB-d_4) of $He@C_{60}/C_{60}$ (3/7).

Komatsu et al. reported that complete separation of $H_2@C_{60}$ or $H_2@C_{70}$ from empty counterparts was possible by the use of recycling HPLC on Cosmosil Buckyprep column (two directly connected columns; 250 mm length, 20 mm inner diameter; mobile phase, toluene; 50 °C).[12b,c] Not surprisingly, separation of $He@C_{60}$ from empty C_{60} was rather laborious. Thus, considering the slightly longer retention time of $H_2@C_{60}$ relative to empty C_{60}, the author first collected a latter part of a single fraction eluted after 10th recycle,[12b,c] which was concentrated and further subjected to the same HPLC (Figure 5). After 20th recycle, a detectable shoulder appeared, and after 40th recycle, a split of the peaks was recognized. The latter fraction contained $He@C_{60}$ at an improved occupation level of 60% (Figure 6).

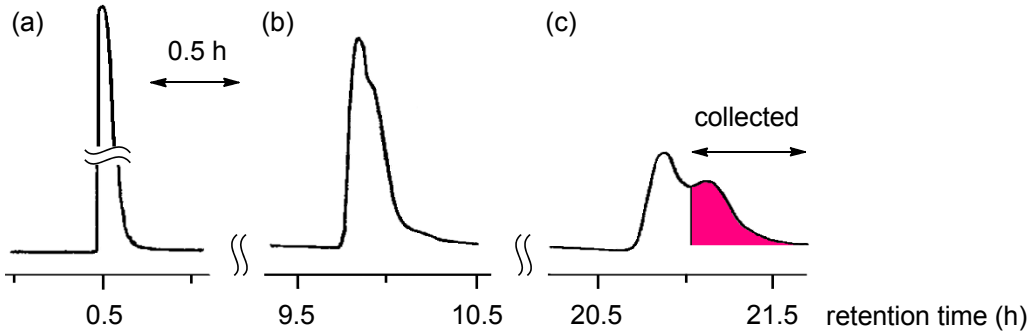

Figure 5. Recycling HPLC chart (flow rate 9.9 mL min^{-1}) for the separation of $He@C_{60}$ from empty C_{60}. (a) The first cycle, (b) 20th recycle, and (c) 40th recycle.

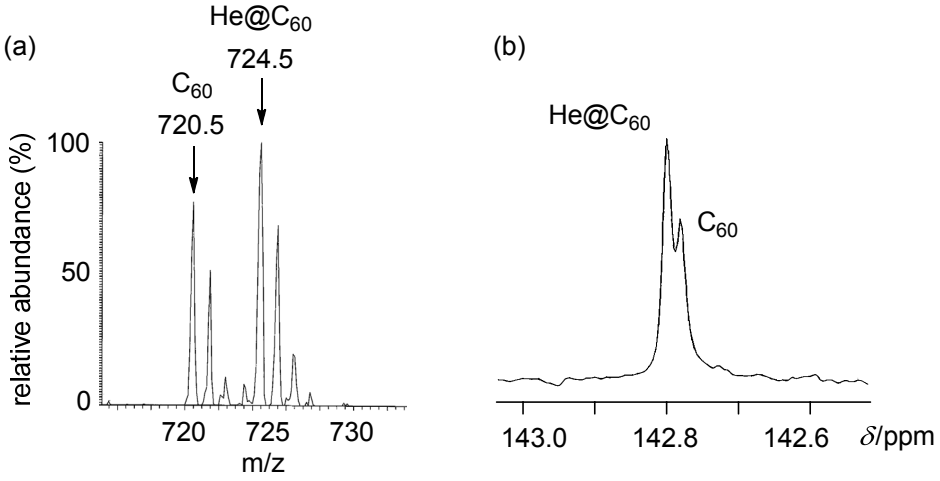

Figure 6. (a) APCI-MS spectrum (negative-ion mode) and (b) ^{13}C NMR spectra (75 MHz, ODCB-d_4) of He@C_{60}/C_{60} (6/4).

Next, the author applied this methodology to C_{70} with an expectation to incorporate two atoms of He.[21] Thus, powder of sulfoxide derivative **7** with a 13-membered-ring opening[13b] was treated with pressurized He gas (1120 atm) at 115 ºC for 1 h (Scheme 5). The resulting powder was immediately subjected to irradiation in the same manner to give He@**8** with a 12-membered-ring opening. Upon APCI mass analysis, two peaks corresponding to He@**8** and empty **8** appeared with an intensity ratio being 3 : 7 (Figure 7). However, regrettably the author could not observe any evidence of the formation of He_2@**8** under these conditions, in contrast to the formation of $(H_2)_2$@**9** (shown in Figure 8) in 3% yield under similar conditions.[13]

Scheme 5. Insertion of a ^{4}He atom into **7** and subsequent size-reduction of the opening

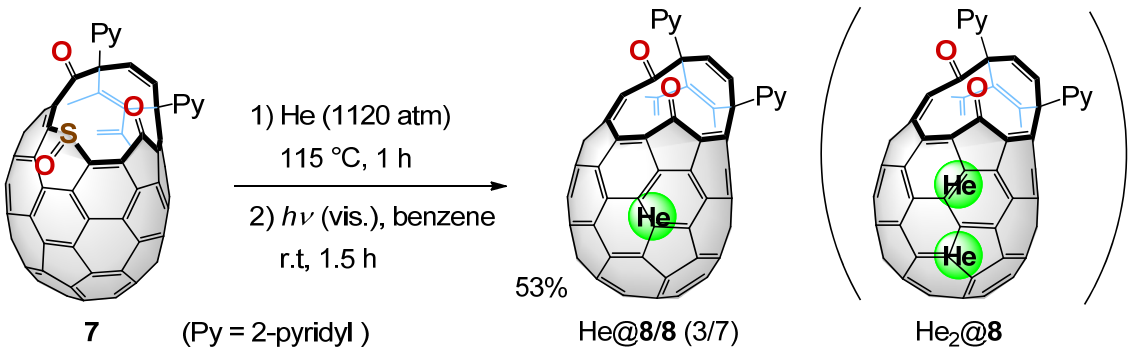

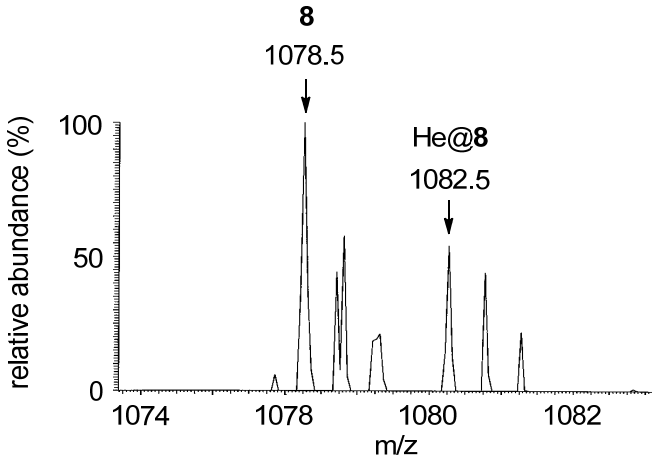

Figure 7. APCI-MS spectrum (negative-ion mode) of He@**8**/**8** (3/7).

The DFT calculations at M06-2X/6-31G(d,p) level showed that incorporation energy of two atoms of He inside **8** is –5.26 kcal mol^{-1} after BSSE correction, while that of two molecules of H_2 inside **9** is –12.63 kcal mol^{-1} (Figure 8). This result suggests that the attractive interaction between two atoms of He and the open-cage C_{70} is weaker than that involving two molecules of H_2. Possibly this is the reason for a too low yield for $He_2@C_{70}$ to be detected by mass spectroscopy.

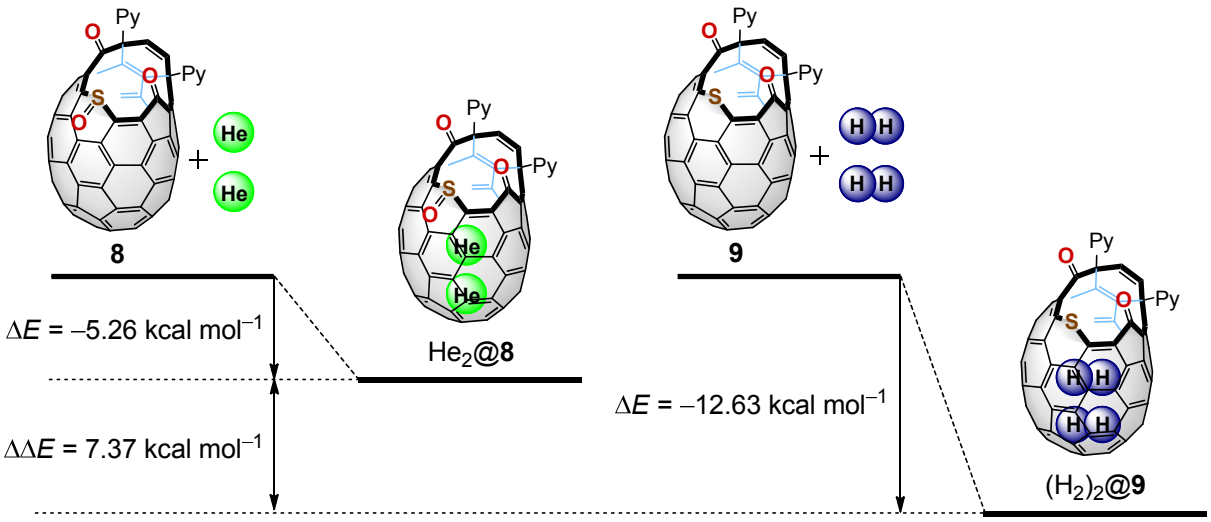

Figure 8. The stabilization energies after BSSE correction. The calculations were conducted at M06-2X/6-31G(d,p) level.

In the same way as the closure of the opening of He@**5**, the opening of He@**8** (He@**8**/**8** = 3/7) was closed by two-step reactions to afford He@C_{70} (Scheme 6) at the occupation level of 30% based on the APCI mass analysis (Figure 9).

Scheme 6. Synthesis of endohedral C_{70} encapsulating a ^{4}He atom

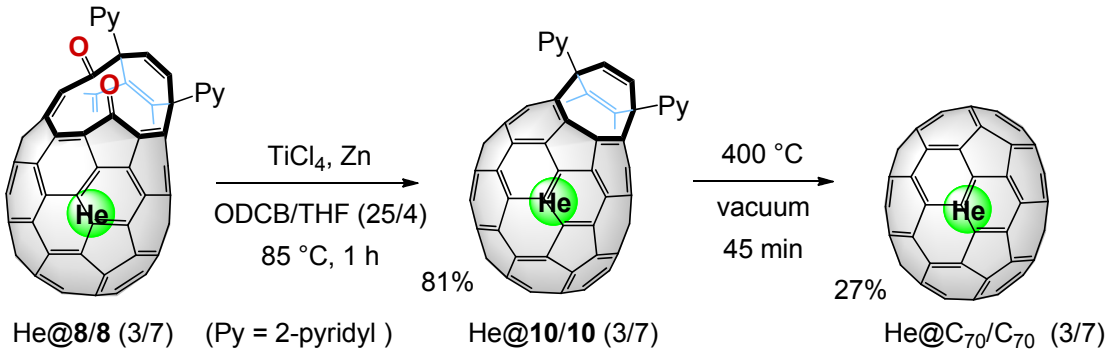

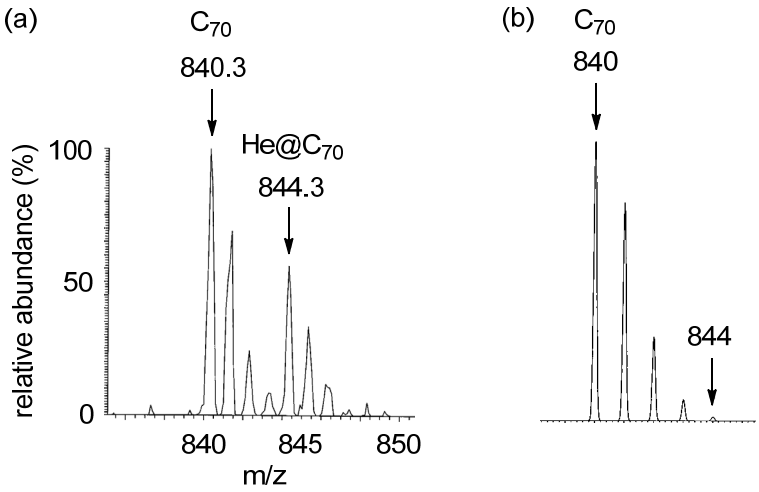

Figure 9. (a) APCI-MS spectrum (negative-ion mode) of He@C_{70}/C_{70} (3/7) and (b) theoretical isotopic pattern for C_{70}.

The ^{13}C NMR spectrum of He@C_{70} (He@C_{70}/C_{70} = 3/7) exhibited five sharp signals for empty C_{70} (δ = 150.91, 148.36, 147.67, 145.64, and 131.15) (Figure 10a) and two weak signals for He@C_{70} (Figure 10b and 10c). Other three out of five signals for He@C_{70} most likely overlapped with those for empty C_{70}. As compared to the signals for empty

C_{70}, those for He@C_{70} (δ = 145.66 and 131.18) slightly shifted to downfield by $\Delta\delta$ = 0.02 and 0.03, respectively, which are very close to that for He@C_{60}. The $\Delta\delta$ values were smaller than those for H_2@C_{70} ($\Delta\delta$ = 0.05 and 0.07, respectively),[13b] showing the extremely weak interaction of the encapsulated He atom with the outer C_{70} cage. Since these resonances are assigned to the carbons at the equatorial belt region of C_{70} cage,[22] the encapsulated He is considered to exist mostly at the center of the cage.

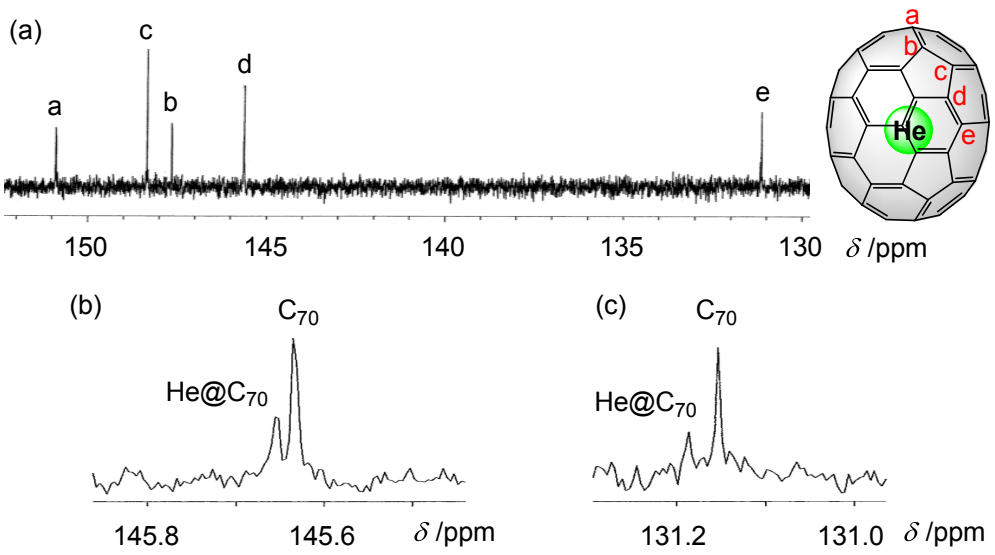

Figure 10. ^{13}C NMR spectra (100 MHz, CS_2/CD_2Cl_2 (1/1, v/v)) of He@C_{70}/C_{70} (3/7). (a) The sp^2 carbon region, and (b, c) the expanded spectra of selected signals.

The enrichment of He@C_{70} was also conducted. After 20th recycle, a detectable shoulder of He@C_{70} appeared and it became prominent after 25th recycle (Figure 11). Thus, the occupation level of He@C_{70} was enhanced from 30% to 60% in the same way as that of He@C_{60}, despite the minute interaction between He and C_{70} (Figure 12).

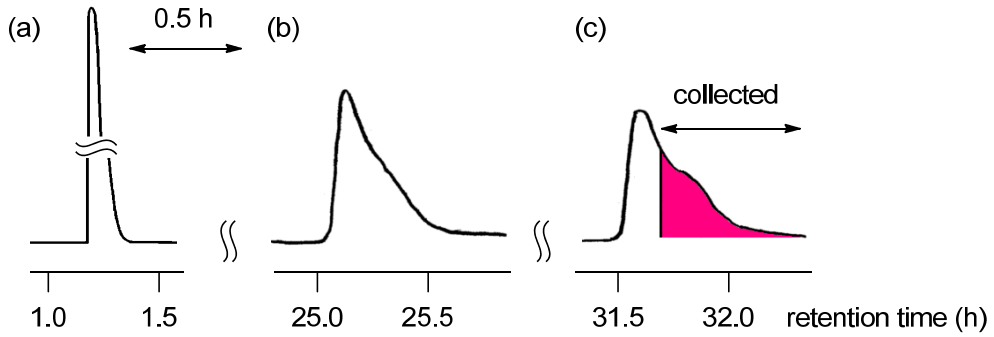

Figure 11. Recycling HPLC chart (flow rate 6.0 mL min^{-1}) for the separation of $He@C_{70}$ and empty C_{70}. (a) The first cycle, (b) 20th recycle, and (c) 25th recycle.

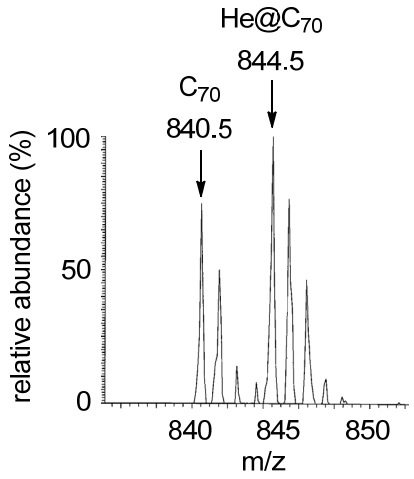

Figure 12. APCI-MS spectrum (negative-ion mode) of $He@C_{70}/C_{70}$ (6/4).

Conclusion

In summary, the encapsulation of a helium atom inside open-cage C_{60} derivative **5** at occupation level of 30% was achieved by a treatment of powdery **4** with He gas (1230 atm) at 115 ºC for 1 h and subsequent irradiation with a high-pressure mercury lamp. Theoretical calculations at the M06-2X/6-31G (d,p) level supported the experimental result of the lower occupation level for He@**5** than that for H_2@**2**; the stabilization energy between **4** and He was smaller (–2.98 kcal mol^{-1}) than that between **2** and H_2 (–7.59 kcal mol^{-1}) after BSSE correction. The McMurry reaction of He@**5**/**5** (3/7) having a 12-membered-ring opening

gave He@**6**/**6** (3/7) with an 8-membered-ring opening. The complete closure of the opening was accomplished by heating powdery He@**6**/**6** (3/7) at 400 ºC under vacuum and the desired He@C_{60} was obtained at occupation level of 30% without a severe loss of the inner He atom. Furthermore, the separation of He@C_{60} from empty C_{60} was conducted by the use of recycling HPLC on Cosmosil Buckyprep columns and the enriched He@C_{60} was demonstrated by the APCI-MS analysis and the ^{13}C NMR measurement. This methodology is applicable to the synthesis of He@C_{70} and the enrichment of He@C_{70} at occupation level from 30% to 60% was also achieved by the use of recycling HPLC. The syntheses of He@C_{60} and He@C_{70} is a good certification that the rational synthesis of endohedral fullerenes encapsulating inert species, which little interact with fullerene cage, would be realistic by developing the ‘‘molecular surgery’’ method.

Experimental Section

General. The ^{1}H and ^{13}C NMR measurements were carried out with a Varian Mercury 300 instrument and a JEOL AL-400 instrument. The NMR chemical shifts are reported in ppm with reference to residual protons and carbons of $CDCl_3$ (δ 7.26 ppm in ^{1}H NMR, δ 77.0 ppm in ^{13}C NMR), CD_2Cl_2 (δ 5.32 ppm in ^{1}H NMR, δ 53.5 ppm in ^{13}C NMR), acetone-d_6 (δ 2.04 ppm in ^{1}H NMR), benzene-d_6 (δ 7.20 ppm in ^{1}H NMR), and 1,2-dichlorobenzene-d_4 (ODCB-d_4) (δ 132.35 ppm in ^{13}C NMR). FAB mass spectra were recorded on a JEOL MStation JMS-700. APCI mass spectra were measured on a Finnigan-MAT TSQ 7000 spectrometer. The high-pressure liquid chromatography (HPLC) was performed with the use of a Cosmosil Buckyprep column (250 mm length, 4.6-mm inner diameter) for analytical purpose, and the same column (two directly connected columns; 250 mm length, 20 mm inner diameter) for preparative purpose. ODCB-d_4 was purchased from Aldrich Co. Zinc (sandy, 99.9%), titanium (IV) chloride, carbon disulfide (CS_2), benzene, and tetrahydrofuran (THF) were purchased from Wako Pure Chemical Industries, Ltd, and THF was distilled from sodium benzophenone ketyl under argon before use.

Computational Method. All calculations were conducted with Gaussian 09 packages. The structures were fully optimized with the M06-2X functional and 6-31G(d,p) basis set

without any symmetry assumptions. The stabilization energies were estimated after BSSE correction. Frequency calculations at the optimized structures produced no imaginary frequencies in all cases.

Synthesis of He@5 with a 12-membered-ring opening. A powder of open-cage C_{60} derivative **4** (600 mg, 0.553 mmol) wrapped in aluminum foil was heated at 115 ºC in an autoclave under pressurized He gas (1230 atm) for 1 h. This high pressure (1230 atm) was generated by (i) introducing He gas (100 atm) into the autoclave, (ii) elevating the pressure up to 1050 atm by the use of a hydraulic compressor at room temperature, and (iii) heating the autoclave at 115 ºC. After cooling to ambient temperature, the resulting powder was recovered from the autoclave and dissolved in benzene (1 L). The solution was irradiated with a high-pressure mercury lamp for 1.5 h at room temperature through Pyrex glass. The solvent was removed *in vacuo* and the residual brown solid was subjected to flash column chromatography over silica gel. Elution with toluene-EtOAc (20:1) gave He@**5**/**5** (3/7) (158.8 mg, 0.153 mmol, 28%) as a brown solid, and following elution with toluene-EtOAc (5:1) gave unreacted **4** (307.4 mg, 0.284 mmol, 51%).

He@**5**/**5** (3/7): ^{1}H NMR (300 MHz, CS_2-acetone-d_6 (7:1)) δ 8.52 (m, 1H), 8.32 (m, 1H), 7.98-8.08 (m, 3H), 7.85 (m, 1H), 7.03-7.39 (m, 8H); ^{13}C NMR (75 MHz, CS_2-$CDCl_3$ (1:1)) δ 196.35, 189.11, 167.75, 161.87, 149.74, 148.48, 148.48, 148.43, 148.24, 147.63, 147.54, 147.52, 147.18, 147.14, 146.57, 146.24, 146.24, 146.06, 145.91, 145.75, 145.68, 145.57, 145.47, 145.42, 145.41, 145.18, 145.08, 145.03, 144.89, 144.56, 144.41, 144.03, 143.92, 143.72, 143.08, 142.59, 142.38, 142.15, 141.78, 141.64, 141.31, 140.98, 140.76, 140.45, 140.20, 140.11, 139.92, 139.79, 139.55, 139.45, 139.35, 139.35, 139.32, 138.47, 137.50, 137.11, 137.02, 137.02, 136.13, 135.57, 133.07, 132.60, 131.24, 130.85, 130.34, 129.93, 129.88, 129.65, 129.11, 128.89, 128.89, 128.57, 127.48, 127.48, 127.42, 126.94, 123.15, 122.65, 75.06, 52.44.

Synthesis of He@6 with an 8-membered-ring opening. To a stirred suspension of zinc powder (600 mg, 9.176 mmol) in dry THF (20 mL) was added titanium (IV) tetrachloride (500 μL, 4.560 mmol) drop by drop at 0 ºC under argon atmosphere, and the mixture was refluxed for 2 h. A 3.0 mL portion of the resulting black slurry was added to a stirred

solution of He@**5**/**5** (3/7) (143.0 mg, 0.138 mmol) in dry ODCB (25 mL) at room temperature under argon atmosphere. After heating at 85 ºC for 1 h, the resulting brownish purple solution was cooled to room temperature. Then the solution was diluted with CS_2 (30 mL) and washed with aqueous solution of $NaHCO_3$ (saturated, 50 mL). The organic layer was dried over $MgSO_4$ and evaporated under reduced pressure to give a residual brown solid, which was then subjected to flash column chromatography over silica gel. Elution with toluene-EtOAc (20:1) gave He@**6**/**6** (3/7) (84.5 mg, 0.084 mmol, 61%) as a brown solid.

He@**6**/**6** (3/7): ^{1}H NMR (300 MHz, CS_2-acetone-d_6 (7:1)) δ 8.67 (m, 1H), 7.90-8.00 (m, 2H), 7.69-7.76 (m, 2H), 7.37-7.44 (m, 2H), 7.10-7.22 (m, 7H); ^{13}C NMR (75 MHz, CS_2-$CDCl_3$ (1:2)) δ 168.70, 165.32, 149.51, 148.62, 148.62, 148.30, 145.77, 145.60, 145.52, 145.45, 145.29, 144.74, 144.74, 144.59, 144.57, 144.33, 144.33, 144.19, 144.19, 144.04, 144.04, 143.92, 143.87, 143.78, 143.73, 143.59, 143.58, 143.40, 143.21, 141.69, 140.91, 140.91, 140.69, 140.68, 140.60, 140.34, 139.53, 139.14, 138.47, 138.32, 137.08, 137.03, 137.03, 136.71, 135.51, 135.38, 135.22, 134.89, 131.21, 131.01, 128.66, 128.58, 128.31, 128.31, 127.56, 127.42, 127.42, 127.36, 125.55, 122.90, 73.19, 56.56.

Synthesis of He@C_{60}. A powder of He@**6**/**6** (3/7) (70.0 mg, 0.070 mmol) lightly wrapped with a piece of aluminum foil was placed in a glass tube (inner diameter 20 mm), which was heated with an electric furnace at 400 ºC for 2 h under vacuum (1 mmHg). The resulting black solid was dissolved in CS_2 (50 mL) and subjected to flash column chromatography over silica gel. Elution with CS_2 gave He@C_{60}/C_{60} (3/7) (38.3 mg, 0.053 mmol, 76%) as a brown solid.

He@C_{60}/C_{60} (3/7): ^{13}C NMR (75 MHz, ODCB-d_4) δ 142.80 (He@C_{60}), 142.78 (C_{60}); HRMS (+FAB), calcd for C_{60}He (M^+) 724.0026, found 724.0026.

Enrichment of He@C_{60}. The sample of He@C_{60}/C_{60} (3/7) was subjected to the recycle HPLC on Cosmosil Buckyprep column (two directly connected columns; 250 mm length, 20 mm inner diameter; mobile phase, toluene; 50 ºC; flow rate was 9.9 mL/min). After 10 recycling, the separated latter portion was evaporated and further subjected to the same HPLC. After 40 recycling, the latter potion was collected and evaporated to give He@C_{60}/C_{60} (6/4). By repeating this procedure He@C_{60} at occupation level of 95% was

obtained.

Synthesis of He@7 with a 12-membered-ring opening. A powder of open-cage C_{70} derivative **7** (441.0 mg, 0.391 mmol) wrapped in aluminum foil was heated at 115 ºC in an autoclave under pressurized He gas (1120 atm) for 1 h. This high pressure (1120 atm) was generated by (i) introducing He gas (110 atm) into the autoclave, (ii) elevating the pressure up to 1030 atm by the use of a hydraulic compressor at room temperature, and (iii) heating the autoclave at 115 ºC. After cooling to ambient temperature, the resulting powder was recovered from the autoclave and dissolved in benzene (1 L). The solution was irradiated with a high-pressure mercury lamp for 1.5 h at room temperature through Pyrex glass. The solvent was removed *in vacuo* and the residual brown solid was subjected to flash column chromatography over silica gel. Elution with toluene-EtOAc (10:1) gave He@**8**/**8** (3/7) (225.9 mg, 0.208 mmol, 53%) as a brown solid.

He@**8/8** (3/7): ^{1}H NMR (300 MHz, CS_2-CD_2Cl_2 (1:1)) δ 8.80 (m, 1H), 8.51 (m, 1H), 7.94 (m, 1H), 7.76 (m, 2H), 7.70 (m, 1H), 7.40 (m, 1H), 7.22 (m, 1H), 6.72 (d, J = 9.9 Hz, 1H), 6.59 (d, J = 9.9 Hz, 1H); ^{13}C NMR (75 MHz, ODCB-d_4) δ 198.37, 187.50, 165.81, 164.11, 151.17, 150.84, 150.71, 150.61, 150.45, 150.31, 149.91, 149.32, 149.19, 149.19, 148.87, 148.68, 148.37, 148.34, 148.13, 148.09, 148.05, 147.89, 147.89, 147.75, 147.69, 147.48, 146.93, 146.69, 146.58, 145.86, 145.60, 145.37, 145.29, 144.45, 144.21, 144.01, 143.70, 143.70, 143.32, 143.17, 142.92, 142.78, 142.17, 142.07, 141.60, 140.66, 139.79, 138.43, 138.15, 137.99, 137.91, 137.81, 137.09, 137.09, 136.73, 136.73, 135.12, 134.52, 133.63, 133.32, 132.85, 123.19, 122.79, 122.42, 122.03, 59.98, 52.92 (the signals at the range of δ 126.0 ~ 132.5 were overlapped with the signals of ODCB-d_4).

Synthesis of He@10 with an 8-membered-ring opening. To a stirred suspension of zinc powder (600 mg, 9.176 mmol) in dry THF (20 mL) was added titanium (IV) tetrachloride (500 μL, 4.560 mmol) drop by drop at 0 ºC under argon atmosphere, and the mixture was refluxed for 2 h. A 4.1 mL portion of the resulting black slurry was added to a stirred solution of He@**8**/**8** (3/7) (200.0 mg, 0.185 mmol) in dry ODCB (25 mL) at room temperature under argon atmosphere. After heating at 85 ºC for 1 h, the resulting brown solution was cooled to room temperature. Then the solution was diluted with CS_2 (30 mL) and washed

with aqueous solution of $NaHCO_3$ (saturated, 50 mL). The organic layer was dried over $MgSO_4$ and evaporated under reduced pressure to give a residual brown solid, which was then subjected to flash column chromatography over silica gel. Elution with toluene-EtOAc (10:1) gave He@**10**/**10** (3/7) (157.6 mg, 0.150 mmol, 81%) as a brown solid.

He@**10/10** (3/7): ^{1}H NMR (300 MHz, CS_2-$CDCl_3$ (1:1)) δ 9.00 (m, 1H), 8.59 (m, 1H), 8.40 (m, 1H), 8.09 (m, 1H), 7.88 (m, 1H), 7.73 (m, 1H), 7.49 (m, 1H), 6.50 (d, J = 9.6 Hz, 1H), 6.30 (d, J = 9.3 Hz, 1H); ^{13}C NMR (75 MHz, CS_2-$CDCl_3$ (1:1)) δ 168.20, 165.41, 153.42, 150.79, 150.61, 150.40, 150.13, 150.00, 150.00, 149.82, 149.34, 149.34, 149.03, 148.46, 148.42, 148.27, 148.33, 148.02, 147.94, 147.89, 147.87, 147.82, 147.75, 147.44, 147.23, 147.20, 147.17, 147.11, 146.84, 146.18, 145.78, 145.72, 145.29, 145.22, 144.99, 144.86, 144.67, 144.27, 144.14, 143.91, 143.91, 143.82, 143.80, 143.12, 142.42, 142.03, 141.67, 141.43, 140.92, 140.43, 139.90, 139.55, 139.15, 138.16, 137.15, 137.08, 136.91, 136.30, 136.02, 135.36, 134.99, 133.29, 132.20, 132.02, 131.66, 131.03, 130.88, 130.49, 128.86, 127.58, 126.46, 124.93, 124.62, 124.41, 124.06, 123.37, 122.27, 122.05, 121.90, 117.49, 54.29, 52.87.

Synthesis of He@C_{70}. A powder of He@**10/10** (3/7) (137.1 mg, 0.130 mmol) lightly wrapped with a piece of aluminum foil was placed in a glass tube (inner diameter 20 mm), which was heated with an electric furnace at 400 ºC for 45 min under vacuum (1 mmHg). The resulting black solid was dissolved in CS_2 (50 mL) and subjected to flash column chromatography over silica gel. Elution with CS_2 gave He@C_{70}/C_{70} (3/7) (29.9 mg, 0.041 mmol, 27%) as a brown solid.

He@C_{70}/C_{70} (3/7): ^{13}C NMR (100 MHz, CS_2-CD_2Cl_2 (1:1)) δ 150.91 (He@C_{70} & C_{70}), 148.36 (He@C_{70} & C_{70}), 147.67(He@C_{70} & C_{70}), 145.66 (He@C_{70}), 145.64 (C_{70}), 131.18 (He@C_{70}), 131.15 (C_{70}); HRMS (+FAB), calcd for C_{70}He (M^+) 844.0026, found 844.0031.

Enrichment of He@C_{70}. The sample of He@C_{70}/C_{70} (3/7) was subjected to the recycle HPLC on Cosmosil Buckyprep column (two directly connected columns; 250 mm length, 20 mm inner diameter; mobile phase, toluene; 50 ºC; flow rate was 6.0 mL/min). After 25 recycling, the latter portion was collected and evaporated to give He@C_{70}/C_{70} (6/4).

References

(1) Saunders, M.; Jiménez-Vázquez, H. A.; Cross, R. J.; Mroczkowski, S.; Freedberg, D. I.; Anet, F. A. L. *Nature* **1994**, *367*, 256.

(2) (a) Saunders, M.; Jiménez-Vázquez, H. A.; Bangerter, B. W.; Cross. R. J.; Mroczkowski, S.; Freedberg, D. I.; Anet, F. A. L. *J*. *Am*. *Chem*. *Soc*. **1994**, *116*, 3621. (b) Smith III, A. B; Strongin, R. M.; Brard, L.; Romanow, W. J.; Saunders, M.; Jiménez-Vázquez, H. A.; Cross, R. J. *J*. *Am*. *Chem*. *Soc*. **1994**, *116*, 10831. (c) Cross, R. J.; Jiménez-Vázquez, H. A.; Lu, Q.; Saunders, M.; Schuster, D. I.; Wilson, S. R.; Zhao, H. *J*. *Am*. *Chem*. *Soc*. **1996**, *118*, 11454. (d) Wang, G.-W.; Saunders, M.; Cross, R. J. *J*. *Am*. *Chem*. *Soc*. **2001**, *123*, 256. (e) Zhou, Z.; Schuster, D. I.; Wilson, S. R. *J*. *Org*. *Chem*. **2003**, *68*, 7612.

(3) (a) Rüttimann, M.; Haldimann, R. F.; Isaacs, L.; Diederich, F.; Khong, A.; Jiménez-Vázquez, H. A.; Cross, R. J.; Saunders, M. *Chem*. *Eur*. *J*. **1997**, *3*, 1071. (b) Sternfeld, T.; Hoffman, R. E.; Saunders, M.; Cross, R. J.; Syamala, M. S.; Rabinovitz, M. *J*. *Am*. *Chem*. *Soc*. **2002**, *124*, 8786.

(4) (a) Son, M.-S.; Sung, Y. K. *Chem*. *Phys*. *Lett*. **1995**, *245*, 113. (b) Bühl, M.; Patchkovskii, S.; Thiel, W. *Chem*. *Phys*. *Lett*. **1997**, *275*, 14. (c) Albert, V. V.; Sabin, J. R.; Harris, F. E. *Int*. *J*. *Quant*. *Chem*. **2007**, *107*, 3061. (d) Hesselmann, A.; Korona, T. *Phys*. *Chem*. *Chem*. *Phys*. **2011**, *13*, 732. (e) Varandas, A. J. C. *Int*. *J*. *Quant*. *Chem*. **2011**, *111*, 416.

(5) (a) Saunders, M.; Cross, R. J.; Jiménez-Vázquez, H. A.; Shimshi, R.; Khong, A. *Science* **1996**, *271*, 1693. (b) Saunders, M.; Jiménez-Vázquez, H. A.; Cross, R. J.; Mroczkowski, S.; Gross, M. L.; Giblin, D. E.; Poreda, R. J. *J*. *Am*. *Chem*. *Soc*. **1994**, *116*, 2193.

(6) (a) Shimshi, R.; Cross, R. J.; Saunders, M. *J*. *Am*. *Chem*. *Soc*. **1997**, *119*, 1163. (b) Cross, R. J.; Khong, A.; Saunders, M. *J*. *Org*. *Chem*. **2003**, *68*, 8281. (c) Peng, R.-F.; Chu, S.-J.; Huang, Y.-M.; Yu, H.-J.; Wang, T.-S.; Jin, B.; Fu, Y.-B.; Wang, C.-R. *J*. *Mater*. *Chem*. **2009**, *19*, 3602.

(7) Rubin, Y. *Chem*. *Eur*. *J*. **1997**, *3*, 1009.

(8) Schick, G.; Jarrosson, T.; Rubin, Y. *Angew*. *Chem*. *Int*. *Ed*. **1999**, *38*, 2360.

(9) Rubin, Y.; Jarrosson, T.; Wang, G.-W.; Bartberger, M. D.; Houk, K. N.; Schick, G.; Sanuders, M.; Cross, R. J. *Angew*. *Chem*. *Int*. *Ed*. **2001**, *40*, 1543.

(10) Murata, Y.; Murata, M.; Komatsu, K. *Chem*. *Eur*. *J*. **2003**, *9*, 1600.

(11) Chuang, S.-C.; Murata, Y.; Murata, M.; Komatsu, K. *Chem*. *Commun*. **2007**, 1751.

(12) (a) Murata, Y.; Murata, M.; Komatsu, K. *J*. *Am*. *Chem*. *Soc*. **2003**, *125*, 7152. (b) Komatsu, K.; Murata, M.; Murata, Y. *Science* **2005**, *307*, 238. (c) Murata, M.; Murata, Y.; Komatsu, K. *J*. *Am*. *Chem*. *Soc*. **2006**, *128*, 8024.

(13) (a) Murata, Y.; Maeda, S.; Murata, M.; Komatsu, K. *J*. *Am*. *Chem*. *Soc*. **2008**, *130*, 6702. (b) Murata, M.; Maeda, S.; Morinaka, Y.; Murata, Y.; Komatsu, K. *J*. *Am*. *Chem*. *Soc*. **2008**, *130*, 15800.

(14) Stanisky, C. M.; Cross, R. J.; Saunders, M.; Murata, M.; Murata, Y.; Komatsu, K. *J*. *Am*. *Chem*. *Soc*. **2005**, *127*, 299.

(15) Patchkovskii, S.; Thiel, W. *J*. *Chem*. *Phys*. **1997**, *106*, 1796.

(16) Zhao, Y.; Truhlar, D. G. *Theor. Chem. Acc*. **2008**, *120***,** 215.

(17) Frisch, M. J. ; Trucks, G. W.; Schlegel, H. B.; Scuseria, G. E.; Robb, M. A.; Cheeseman, J. R.; Scalmani, G.; Barone, V.; Mennucci, B.; Petersson, G. A.; Nakatsuji, H.; Caricato, M.; Li, X.; Hratchian, H. P.; Izmaylov, A. F.; Bloino, J.; Zheng, G.; Sonnenberg, J. L.; Hada, M.; Ehara, M.; Toyota, K.; Fukuda, R.; Hasegawa, J.; Ishida, M.; Nakajima, T.; Honda, Y.; Kitao, O.; Nakai, H.; Vreven, T.; Montgomery, Jr. J. A.; Peralta, J. E.; Ogliaro, F.; Bearpark, M.; Heyd, J. J.; Brothers, E.; Kudin, K. N.; Staroverov, V. N.; Kobayashi, R.; Normand, J.; Raghavachari, K.; Rendell, A.; Burant, J. C.; Iyengar, S. S.; Tomasi, J.; Cossi, M.; Rega, N.; Millam, J. M.; Klene, M.; Knox, J. E.; Cross, J. B.; Bakken, V.; Adamo, C.; Jaramillo, J.; Gomperts, R.; Stratmann, R. E.; Yazyev, O.; Austin, A. J.; Cammi, R.; Pomelli, C.; Ochterski, J. W.; Martin, R. L.; Morokuma, K.; Zakrzewski, V. G.; Voth, G. A.; Salvador, P.; Dannenberg, J. J.; Dapprich, S.; Daniels, A. D.; Farkas, O.; Foresman, J. B.; Ortiz, J. V.; Cioslowski, J.; Fox, D. J.; *GAUSSIAN 09*, Revision B. 01; Gaussian Inc.: Wallingford CT, **2010**.

(18) Takeda, A.; Yokoyama, Y.; Ito, S.; Miyazaki, T.; Shimotani, H.; Yakigaya, K.; Kakiuchi, T.; Sawa, H.; Takagi, H.; Kitazawa, K.; Dragoe, N. *Chem*. *Commun*. **2006**, 912.

(19) Yamamoto, K.; Saunders, M.; Khong, A.; Cross, R. J.; Grayson, M.; Gross, M. L.; Benedetto, A. F.; Weisman, R. B. *J*. *Am*. *Chem*. *Soc*. **1999**, *121*, 1591.

(20) Syamala, M. S.; Cross, R. J.; Saunders, M. *J*. *Am*. *Chem*. *Soc*. **2002**, *124*, 6216.

(21) Khong, A.; Jiménez-Vázquez, H. A.; Saunders, M.; Cross, R. J.; Laskin, J.; Peres, T.;

Lifshitz, C.; Strongin, R.; Smith III, A. B. *J. Am. Chem. Soc.* **1998**, *120*, 6380.

(22) Taylor, R.; Hare, J. P.; Abdul-Sada, A. K.; Kroto, H. W. *J. Chem. Soc., Chem. Commun.* **1990**, 1423.

Chapter 3

Single Crystal X-ray Observation of a Helium Atom and Placing a Nitrogen Atom inside $He@C_{60}$ and $He@C_{70}$

Abstract: X-ray diffraction study of $He@C_{60}$ is demonstrated as the clear observation of a single helium atom inside C_{60}. In addition, the close packing of a helium atom and a nitrogen atom inside fullerenes was realized by the use of two stepwise insertion techniques, i.e. ‘‘molecular surgery’’ to synthesize the fullerenes encapsulating a He atom followed by ‘‘nitrogen radio-frequency plasma’’ methods to generate the fullerenes encapsulating both He and N atoms. The ESR analysis revealed that the encapsulated He atom gives a small but detectable influence on the electronic properties of the highly reactive N atom coexisting inside the fullerenes, indicating the new usage of helium for controlling electronic properties of reactive species.

Introduction

The importance of helium is widely seen in the common use as helium balloons or respirator gas as well as in the scientific use as refrigerant for superconductive magnets and physical research works at low temperature. Helium is well known as the smallest noble gas atom and it has been refusing to be directly observed by single crystal X-ray analysis, a powerful method to determine the molecular structure. This is because helium or a helium-incorporating material neither becomes crystalline solid under atmospheric pressure even at the vicinity of 0 K.[1] Thus, it is crucial to embed a helium atom selectively into some crystalline material with a discrete structure if one wishes to observe it by X-ray analysis.

Since the strength of the X-ray diffraction on single crystal X-ray analyses depends on the total number of electrons of all atoms existing in the unit cell, it is usually difficult to observe atoms with poor electron density such as hydrogen after structural refinements. In contrast, if a proper single crystal is available, a helium atom should be observable by the single X-ray analysis because a helium atom possesses two electrons in its 1s electronic shell having the isoelectronic structure with lithium cation widely observed in the literature.[2] Fullerene C_{60} is a good candidate to entrap a helium atom. Endohedral C_{60} and C_{70} encapsulating a ^{3}He atom, i.e. ^{3}He@C_{60} and ^{3}He@C_{70}, were first reported by Saunders et al. in 1994[3] in which ^{3}He atom was forced to be inserted into pristine C_{60} and C_{70} under drastic conditions such as 650 ºC under 3000 atm of helium gas (Figure 1).[3,4] However, the encapsulation level of the helium atom was quite low such as 0.15[5]-0.4%[6] due to the inefficiency of this physical method although the inner ^{3}He atom is useful for the clarification of the internal magnetic field of fullerenes.[5,7]

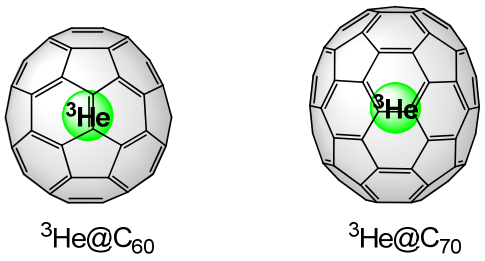

Figure 1. Structure of ^{3}He@C_{60} and ^{3}He@C_{70}.[3]

On the other hand, as mentioned in General Introduction, Komatsu and Murata et al. developed rational synthetic methodology, so-called "molecular surgery",[8] and the syntheses of H_2@C_{60},[9] H_2@C_{70},[10] and H_2O@C_{60}[11] were achieved (Figure 2). As described in Chapter 2, the author also succeeded in the chemical syntheses of He@C_{60} and He@C_{70} with ca. 30% encapsulation levels in macroscopic scales.[12] In the present work, the author succeeded in the enrichment of He@C_{60} at the encapsulation level of 95% by purification with recycling HPLC[12] and the single crystal X-ray observation of the He atom inside C_{60} cage. In addition, there are reports on the endohedral C_{60} and C_{70} encapsulating two species such as He_2@C_{60},[6,7b] He_2@C_{70},[7b,13] $^3He^{22}Ne$@C_{70},[14] $^{22}Ne_2$@C_{70},[15] and $(H_2)_2$@C_{70} (Figure 3).[10] Therefore, the author considered that there is still room for He@C_{60} and He@C_{70} to encapsulate an additional atom or molecule inside the cavities. If such insertion into endohedral fullerenes becomes possible, the studies on the interaction between different inner guests inside fullerenes would open up.

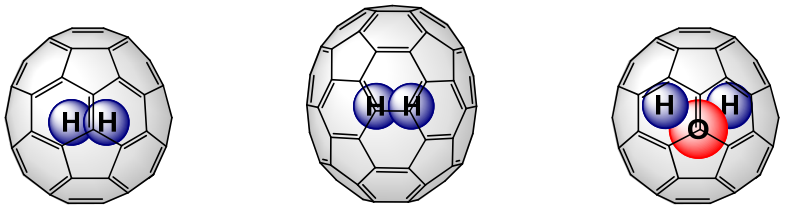

H_2@C_{60}[9] H_2@C_{70}[10] H_2@C_{60}[11]

Figure 2. Structure of H_2@C_{60}, H_2@C_{70}, and H_2O@C_{60}.

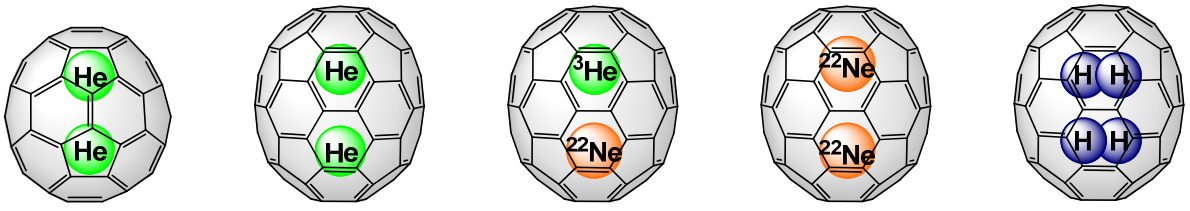

He_2@C_{60}[6] He_2@C_{70}[13] $^3He^{22}Ne$@C_{70}[14] $^{22}Ne_2$@C_{70}[15] $(H_2)_2$@C_{70}[10]

Figure 3. Endohedral C_{60} and C_{70} encapsulating two guest species.

In this chapter, the X-ray diffraction study of $He@C_{60}$ is demonstrated as the clear observation of a single atom of He inside C_{60} cage. Moreover, the chapter describes the generation, ESR spectra, and theoretical studies of endohedral C_{60} and C_{70} encapsulating both He and N atoms, i.e. $HeN@C_{60}$ and $HeN@C_{70}$.

Results and Discussion

Although C_{60} is a crystalline material, a C_{60} cage is known to rotate even in the solid-state.[16] To prevent such a rotational or orientational disorder in the single crystal, co-crystals of the $He@C_{60}$ and nickel(II) octaethylporphyrin (NiOEP) were prepared from the solution in *o*-xylene.[11,17] The X-ray diffraction data were collected using synchrotron radiation at 173 K at SPring-8. The least-square refinements gave the structure of $He@C_{60}\cdot(NiOEP)_2$ without any disorders of the C_{60} cage. As shown in Figure 4, the encapsulated helium atom was unambiguously observed at the center of the C_{60} cage with 100% occupation level, probably owing to the enrichment during crystallization. The relatively larger ellipsoid of the helium implies its translational motion at this temperature since there remains small space for the encapsulated helium atom inside C_{60} (estimated diameter of the hollow space is ca. 3.7 Å and the van der Waals diameter of helium is 2.80 Å).[18]

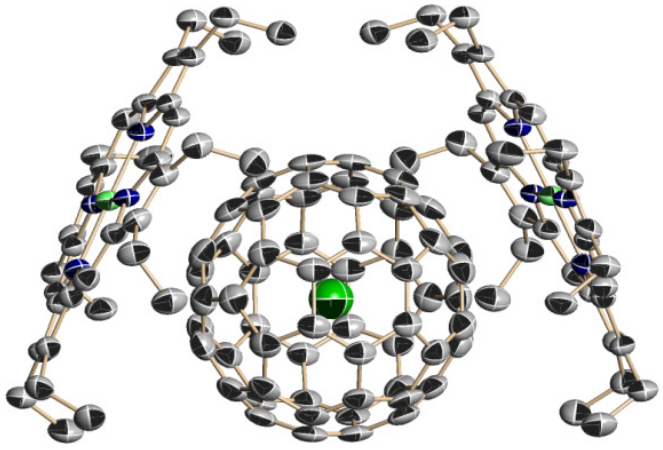

Figure 4. X-Ray crystal structure of $He@C_{60}\cdot(NiOEP)_2$ with thermal ellipsoids at the 50% probability level. Hydrogen atoms are omitted for clarity.

After confirming the existence of one helium atom inside C_{60}, the author wondered about the capability of this complex to further accommodate an additional guest species. It seemed intriguing to see if so-believed ‘‘inert’’ helium could affect the properties of a neighbor atom in tightly confined space inside He@C_{60} and He@C_{70}. For this purpose, a nitrogen atom was selected as the guest. It is reported that a sharp triplet ESR signal is observed for the reaction products of C_{60} and C_{70} with a nitrogen atom source (see below), indicating the generation of N@C_{60} and N@C_{70}.[19] The inner nitrogen atom of these endohedral fullerenes retains its electron spin of 3/2 without any covalent bond formation with carbons of the C_{60} or C_{70} cage. These products are believed to be endohedral fullerenes which are promising materials for quantum computers.[20]

Insertion of a nitrogen atom into He@C_{70} (ca. 30% encapsulation level), whose inner space (estimated long axis diameter is ca. 4.7 Å) is larger than that of He@C_{60}, was conducted under the nitrogen radio-frequency (RF) plasma conditions.[21] As shown in Figure 5, the ESR spectrum of the resulting material showed a new triplet signal in addition to a larger triplet corresponding to N@C_{70} with the hyperfine coupling constant (hfcc) of 5.39 Gauss as reported.[21a] In spite of a partial overlap with the known triplet corresponding to N@C_{70}, a simulated spectrum revealed the presence of a new species with the hfcc of 5.65 Gauss (Figure 6). This result is most reasonably interpreted by the generation of C_{70} encapsulating both helium and nitrogen atoms (HeN@C_{70}; Scheme 1).

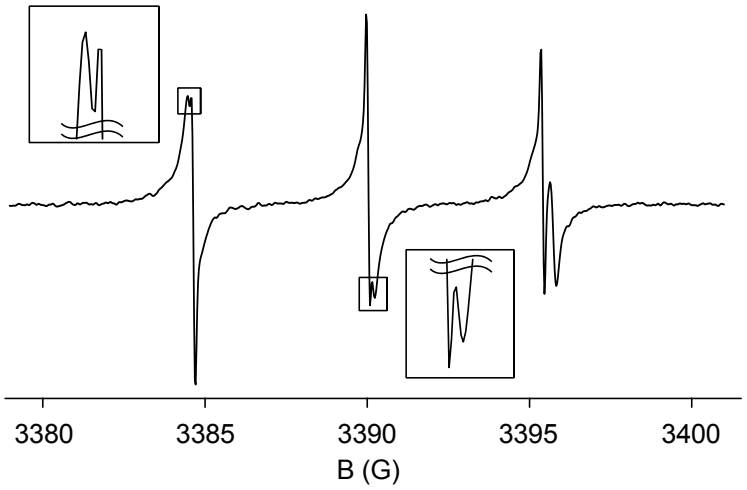

Figure 5. ESR spectrum of a mixture of HeN@C_{70} and N@C_{70} in CS_2 at 220 K.

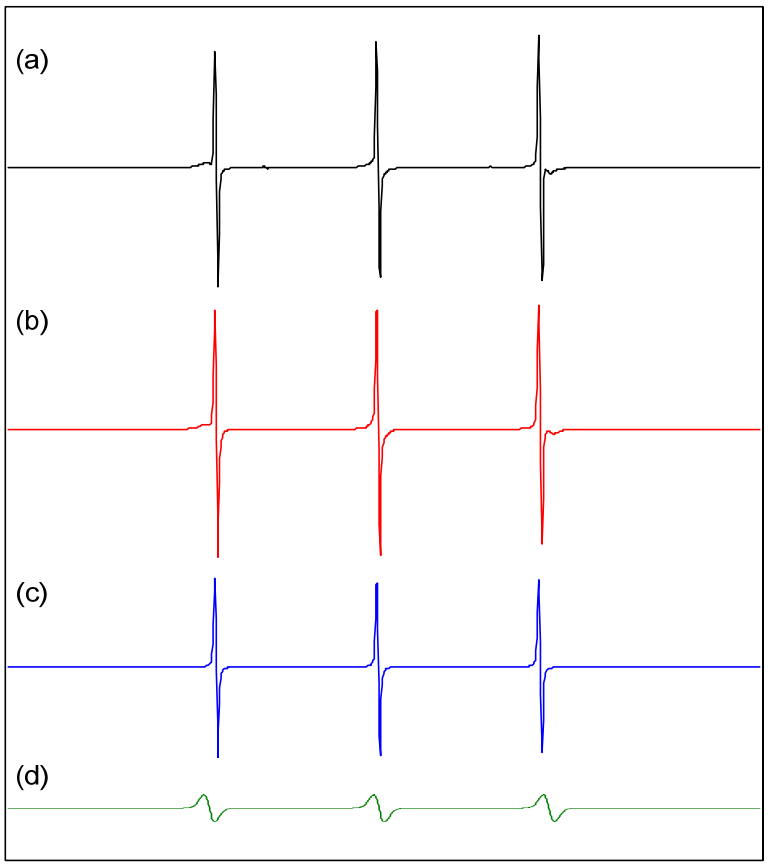

Figure 6. (a) Experimental spectrum of the mixture of HeN@C_{70} and N@C_{70} in CS_2 at room temperature. The spectrometer was operated at 9.8 GHz with a microwave power of 0.6 mW, a modulation frequency of 100 kHz, and modulation amplitude of 100 mG. (b) Simulated spectrum of the mixture. (c) Simulated spectrum of N@C_{70} (hfcc = 5.39 Gauss), and (d) Simulated spectrum of HeN@C_{70} (hfcc = 5.65 Gauss).

Scheme 1. Insertion of a nitrogen atom into He@C_{70} with ca. 30% encapsulation level of He

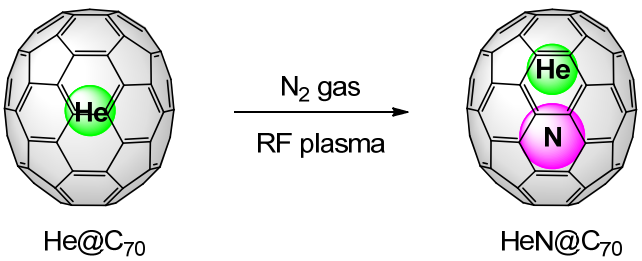

The existence of HeN@C_{70} was also confirmed by mass spectrometry of the enriched sample prepared by repeated recycling HPLC (Figure 7).

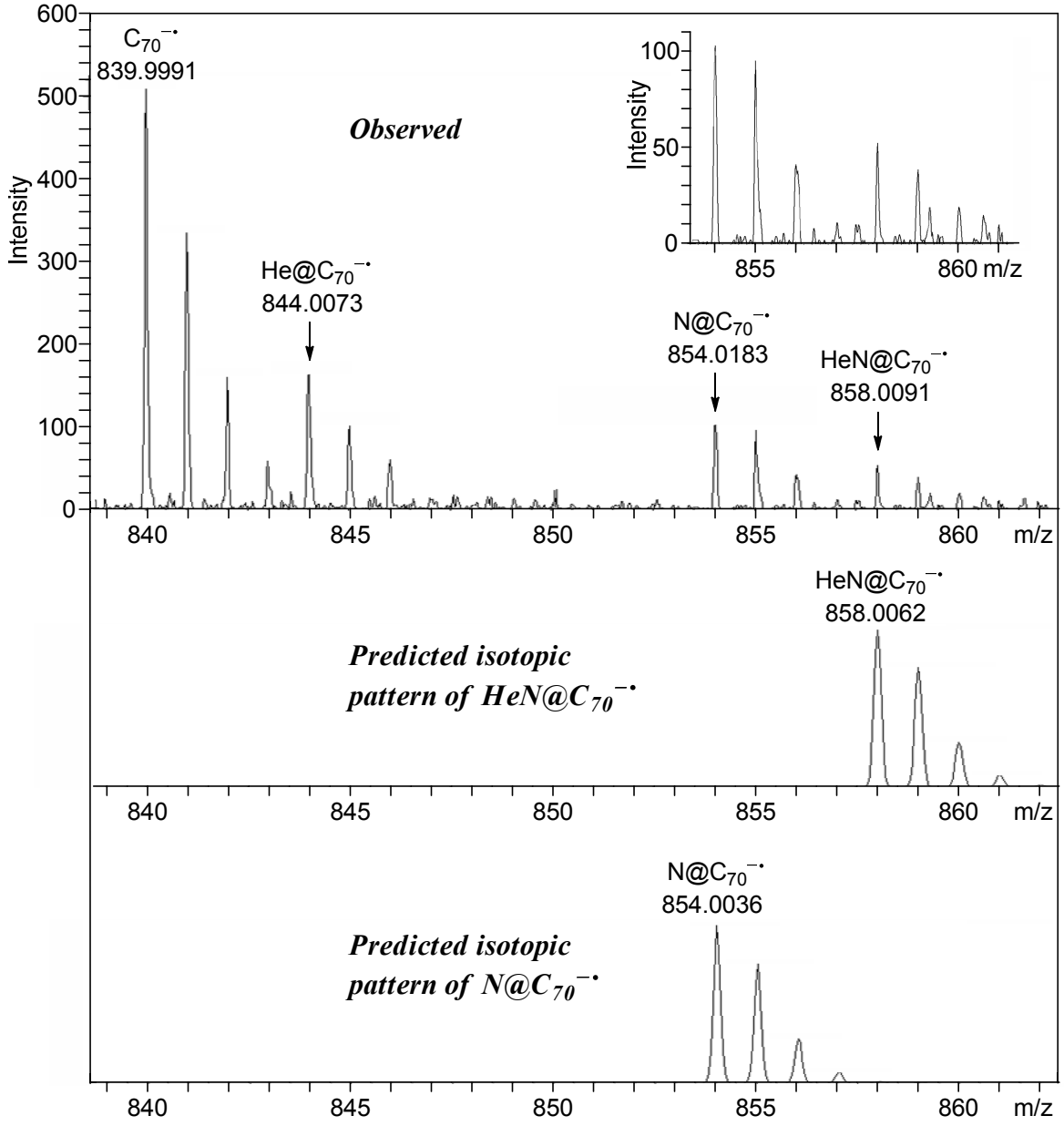

Figure 7. APCI-MS spectrum (negative ionization mode) of the mixture of HeN@C_{70}, N@C_{70}, He@C_{70}, and empty C_{70}. The middle and bottom panels show the predicted isotopic patterns of HeN@C_{70} and N@C_{70}, respectively.

Moreover, though the inner space of He@C_{60} seemed too small to accommodate a nitrogen atom as an additional guest, similarly overlapped ESR signals were obtained when He@C_{60} (ca. 30% encapsulation level) was used for the nitrogen insertion (Figure 8 and 9), indicating the generation of HeN@C_{60} (Scheme 2). The hfcc of HeN@C_{60} (5.99 Gauss) is slightly larger than that of N@C_{60} (5.67 Gauss).

The ratio of the integrated peak areas of HeN@C_{70}/N@C_{70} (3/7) was in good accordance with that of the starting He@C_{70}/C_{70} (3/7), indicating that the nitrogen atoms were inserted into He@C_{70} and C_{70} in the order of 10^{-4} to 10^{-5}.[19] On the other hand, the ratio of the integrated peak areas of HeN@C_{60}/N@C_{60} (1/9) was lower than that of HeN@C_{70}/N@C_{70}. This difference implies that it is easier for a nitrogen atom to access to the larger inner space of He@C_{70} than that of He@C_{60}.

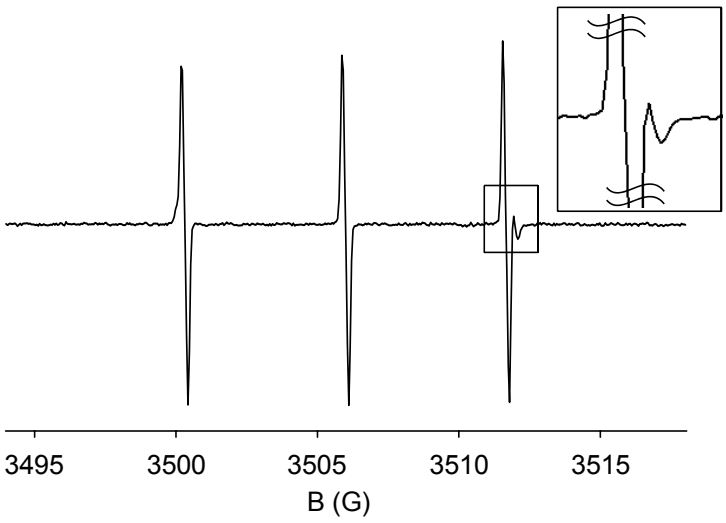

Figure 8. ESR spectrum of a mixture of HeN@C_{60} and N@C_{60} in CS_2 at room temperature.

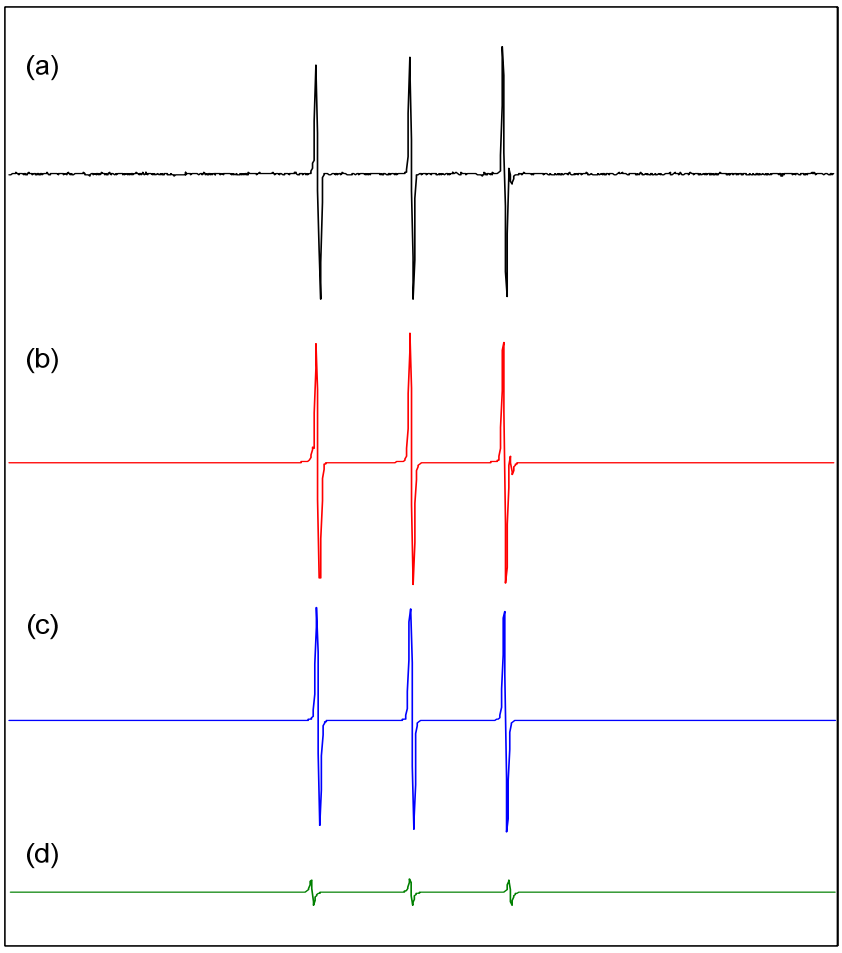

Figure 9. (a) Experimental spectrum of the mixture of HeN@C_{60} and N@C_{60} in CS_2 at room temperature. The spectrometer was operated at 9.8 GHz with a microwave power of 0.2 mW, a modulation frequency of 100 kHz, and modulation amplitude of 250 mG. (b) Simulated spectrum of the mixture. (c) Simulated spectrum of N@C_{60} (hfcc = 5.67 Gauss), and (d) Simulated spectrum of HeN@C_{60} (hfcc = 5.99 Gauss).

Scheme 2. Insertion of a nitrogen atom into He@C_{60} with ca. 30% encapsulation level of He

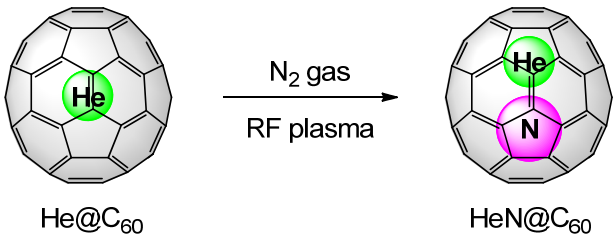

The inner nitrogen atoms of HeN@C_{60} and HeN@C_{70} still retain the electron spin state of 3/2 in spite of the existence of the tightly packed helium atom, showing the entire inertness of helium. However, the line widths of three signals for HeN@C_{60} and HeN@C_{70} are clearly broadened compared to those for N@C_{60} and N@C_{70}. This is because placing a helium atom inside N@C_{60} and N@C_{70} causes lower symmetry of the resulting HeN@C_{60} and HeN@C_{70} compared with high symmetry of the starting materials. Such lower symmetry of the molecules breaks the degeneracy of the three 2p-orbitals of the inner nitrogen atom, giving rise to appearance of the broad signals in which possible fine structures are about to appear. This is consistent with the reported observations on N@C_{60} derivatives with ‘‘external modification’’.[22]

In order to gain insight into the structures and properties of HeN@C_{60}, theoretical consideration was essential. The structures of the related molecules were fully optimized at the M06-2X method[23] using basis sets of 6-31G(d)[24] for C and 6-311G(2df)[25] for He and N atoms.[26] It was shown that the encapsulation of both helium and nitrogen atoms into C_{60} is exothermic by –7.1 kcal mol^{-1} after correction of basis set superposition error (BSSE) (Figure 10). This stabilization energy of HeN@C_{60} is lower than that of N@C_{60} (–23.4 kcal mol^{-1}), but higher than that of He@C_{60} (–3.2 kcal mol^{-1}), indicating that the coexistence of the two atoms in a small space inside C_{60} is possible. It is considered that these atoms are packed tightly inside the C_{60} cage because the distance between the helium and the nitrogen atoms (2.07 Å) were obviously shorter than that at the most stable position (3.75 Å) calculated at the CCSD(T)/6-311+G(2df) level of theory.

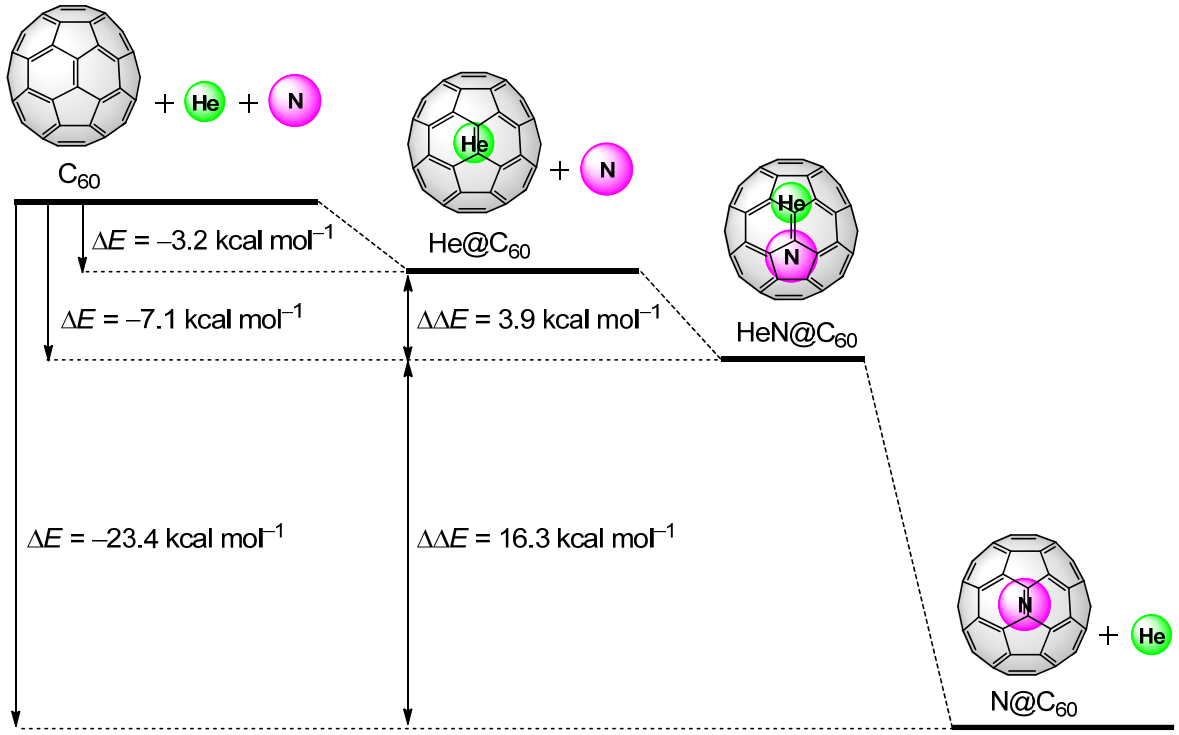

Figure 10. The stabilization energies after BSSE correction. Geometries were fully optimized with hybrid density functional theory at the M06-2X level. The 6-311+G(2df) basis set was used for He and N, while the 6-31G(d) basis set was used for C.

Using the optimized structures at the M06-2X method, the hfcc values were studied by the single-point calculations at MP2 method[27] using basis sets of 6-31G(d) for C and 6-311++G(3df,3pd) for He and N atoms. The calculated hfcc values were found to highly depend on the basis sets. Among the tested basis sets, the use of 6-311++G(3df,3pd) gave the acceptable results for N@C_{60} as a benchmark compound; the calculated and experimental hfcc values are 5.44 and 5.67 Gauss, respectively. As shown in Figure 11a, the calculated hfcc values reproduced the experimental tendency that the smaller space for a nitrogen atom results in the larger hfcc (5.57 Gauss for HeN@C_{60}), most probably owing to the increased s electron density on the nucleus of the nitrogen. To clarify the contributing factors of this phenomenon, the He atom in the optimized structure of HeN@C_{60} was removed and the hfcc

of the remaining N atom located at off-center inside C_{60} was calculated as the hypothetical molecule to afford the larger hfcc value of 5.80 Gauss (Figure 11a: $HeN@C_{60}$–He). These results indicated that the hfcc of the nitrogen is larger as the distance between the N atom and the fullerene cage becomes shorter. On the contrary, the hfcc value of a nitrogen atom with a neighboring helium atom in a distance of 2.07 Å (3.52 Gauss) was smaller than that with a helium atom at the optimized distance of 3.75 Å (3.66 Gauss) or without a helium atom (3.69 Gauss). These results showed that the hfcc values decrease as the helium atom gets closer to the nitrogen atom. Thus, the experimentally observed increase in hfcc value for $HeN@C_{60}$ compared with that of $N@C_{60}$ is rationalized in terms of the compensation of the increase by the C_{60} cage and the decrease by the neighboring helium atom.

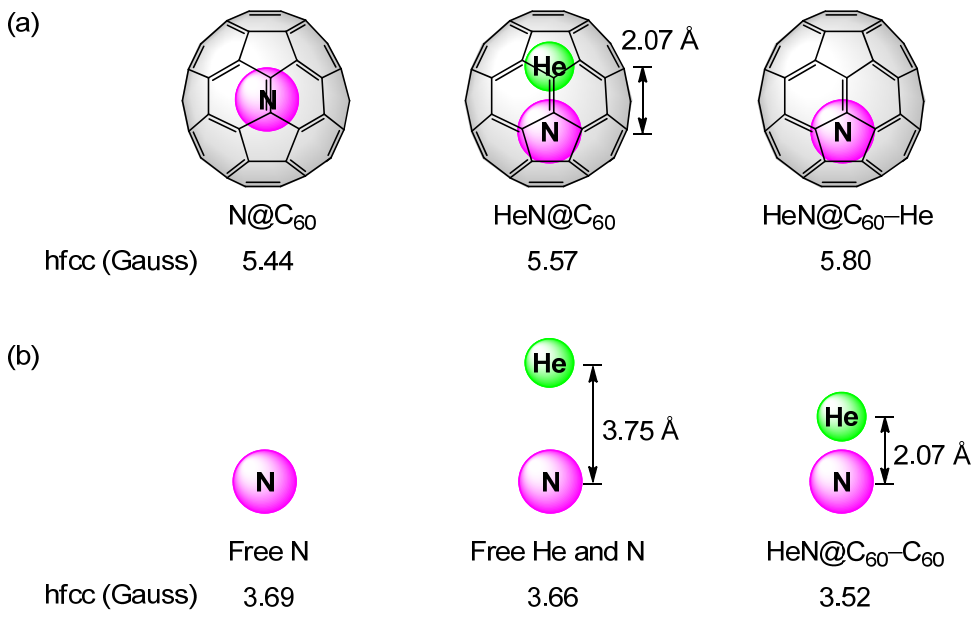

Figure 11. (a) The hfccs of $N@C_{60}$, $HeN@C_{60}$ and $HeN@C_{60}$–He (the helium atom being removed from the optimized structure of $HeN@C_{60}$). (b) The hfccs of a free nitrogen atom and the nitrogen atoms with a neighboring helium atom at the distance of 3.75 Å (optimized distance) and 2.07 Å (extracted distance from $HeN@C_{60}$).

To obtain more information on the inner encapsulated atoms of helium and nitrogen, the Atoms-in-Molecules (AIM) analysis[28,29] was carried out at the MP2 level using the optimized structure at the M06-2X method described above. In the AIM analysis, if the bond path through the bond critical point (BCP) connects two atoms, it is defined to be an interaction existing between these atoms. As shown in Figure 12, there is a bond path between the He atom and the N atom. There are also three He-C and four N-C bond paths in the C_{60} cage (Figure 12a). These results imply that not only the C_{60} cage but also the He atom interact with the N atom. By the analysis at the BCP,[30] the inner N atom is not covalently bound with the He atom nor C_{60} cage. Comprehensively, the He atom and the N atom interacts each other only through a van der Waals interaction inside the C_{60} cage, whose situation is similar to that of $He_2@C_{60}$.[31]

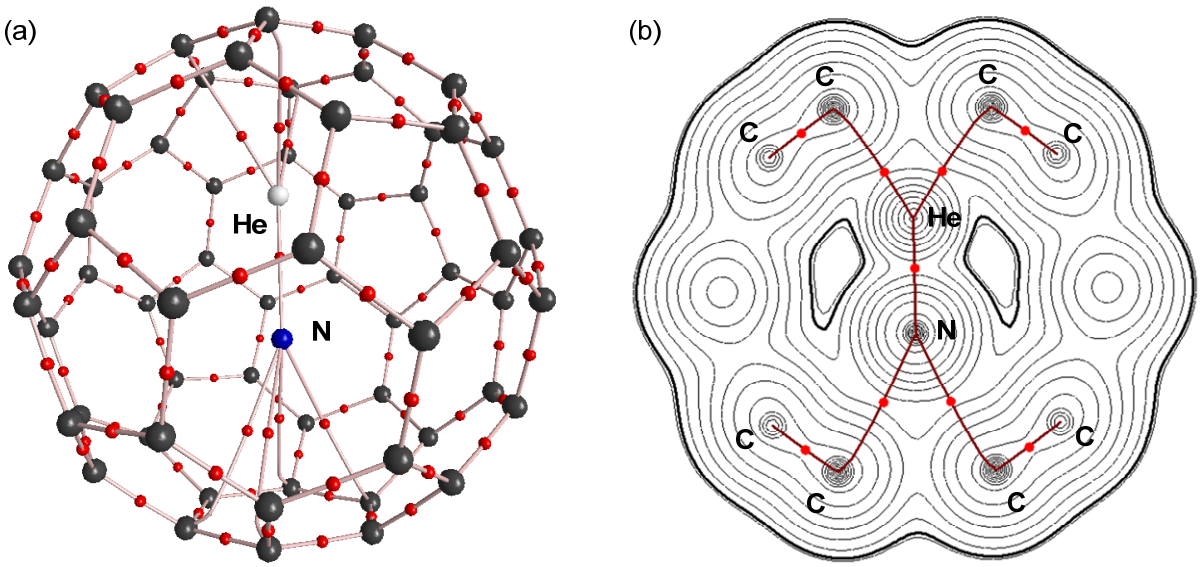

Figure 12. AIM analysis of HeN@C_{60} at the MP2 method. (a) Molecular depiction with displaying BCPs in red. (b) Cross-section contour map of electron density with displaying bond paths in brown and BCPs in red. The ring and cage critical points are omitted for clarity.

Conclusion

In summary, it was demonstrated that a single atom of helium in C_{60} is observable by means of single crystal X-ray analyses. Thus, the element of helium newly joined the libraries of X-ray crystallographic study.[32] The encapsulated helium was confirmed to be located at the center inside the C_{60}. In addition, the stepwise insertion of different atoms into fullerenes was achieved by the combined ‘‘molecular surgery’’ and ‘‘nitrogen RF plasma’’ methods. Even highly reactive nitrogen atom was found to coexist with a helium atom in a small space inside fullerenes. The ESR signals of the nitrogen atom were influenced by the helium coexisting in the same fullerene cages. Thus, these results are considered to be pieces of evidence for encapsulation of a nitrogen atom *INSIDE* fullerenes. This technique is expected to create a variety of endohedral fullerenes encapsulating heterogeneous atoms in the near future.

Experimental Section

General. ESR spectra were measured with Bruker EMX and EMX plus spectrometers. The temperature was controlled with an OXFORD ESR900 helium-flow type cryostat and an OXFORD ITC503 temperature controller for the EMX plus. Simulation of the spectra was carried out on a WinSim program.[33] The atmospheric pressure chemical ionization mass spectrum was recorded on a Bruker micrOTOF-QII.

Single crystal X-ray analysis of $He@C_{60}\cdot(NiOEP)_2$. Single crystal X-ray data were collected on a BL38B1 beamline in SPring-8 with the approval of the Japan Synchrotron Radiation Research Institute (JASRI) with a diffractometer equipped with an ADSC Quantum315 CCD detector. The collected diffraction data were processed with the HKL2000 software program. The structure solutions were obtained by direct method using the SHELXS-97[34] and refined using the SHELXL-97 program.[34]

Experimental details for generation of $HeN@C_{60}$ or $HeN@C_{70}$. $HeN@C_{60}$ or $HeN@C_{70}$ was generated by a nitrogen radio-frequency plasma method.[21] Helium incorporated fullerene, $He@C_{60}$ or $He@C_{70}$, (~ 9 mg, ca. 30% encapsulation level) was put in

a molybdenum boat and placed into the instrument. Under the reduced pressure of nitrogen gas (30 Pa), the material containing N-encapsulating fullerene was generated by sublimation through resistive heating in nitrogen plasma. After cooling to room temperature, the deposit (~ 3 mg) was dissolved in CS_2, followed by filtration and evaporation of the solvent. The resulting material was dissolved in toluene and subjected to recycling HPLC equipped with the Cosmosil Byckyprep column (250 mm length, 20 mm inner diameter, toluene) for further purification. The major fraction was collected and evaporated. The residue was dissolved in CS_2 and placed in an ESR tube, which was connected to a vacuum line. The solution was degassed by three freeze-pump-thaw cycles under reduced pressure, and then sealed.

Enrichment of HeN@C_{70}. After sublimation of HeN@C_{70}/C_{70} (3/7) through resistive heating in nitrogen plasma, the resulting deposit (~ 3 mg) was subjected to the recycle HPLC on Cosmosil Buckyprep columns (two directly connected columns; 250 mm length, 20 mm diameter; mobile phase, toluene, 25 °C; flow rate was 8.0 mL min^{-1}). The retention time of HeN@C_{70} was close to that of N@C_{70}. After 2 recycling, the latter portion of main peak was evaporated and further subjected to the same HPLC to enrich HeN@C_{70}. The existence of HeN@C_{70} and N@C_{70} was monitored by the ESR spectra. After repeating this procedure 5 times, the resulting mixture in toluene solution (100 μL) was subjected to a Bruker micrOTOF-QII to give the mass spectrum shown in Figure 7.

Computational Method. Geometries were fully optimized with hybrid density functional theory at the M06-2X level. The 6-31G(d) basis set was used for C, while the 6-311+G(2df) basis set was used for He and N. The stabilization energies were estimated after BSSE correction. Frequency calculations at the optimized structures produced no imaginary frequencies in all cases. To calculate the hyperfine coupling constants, the M06-2X optimization was followed by single-point MP2 (second-order Møller-Plesset perturbation theory) calculations using 6-31G(d) basis set for C, and 6-311++G(3df,3pd) basis set for He and N. Calculations were carried out using the Gaussian 09 program.

Table 1. Crystal data and structure refinement for $He@C_{60}\cdot(NiOEP)_2$

Identification code	He@C60·(NiOEP)2	
Empirical formula	C132 H88 He N8 Ni2	
Formula weight	1907.52	
Temperature	173(2) K	
Wavelength	0.80000 Å	
Crystal system	Monoclinic	
Space group	C2/c	
Unit cell dimensions	a = 18.7106(3) Å	α = 90º
	b = 20.5179(3) Å	β = 104.2692(6) º
	c = 23.6396(5) Å	γ = 90 º
Volume	8795.3(3) $Å^3$	
Z	4	
Density (calculated)	1.441 Mg/m^3	
Absorption coefficient	0.494 mm^{-1}	
F(000)	3976	
Crystal size	0.05 x 0.02 x 0.01 mm^3	
Theta range for data collection	1.69 to 22.65°.	
Index ranges	-17<=h<=17, -19<=k<=19, -22<=l<=22	
Reflections collected	16998	
Independent reflections	3964 [R(int) = 0.0588]	
Completeness to theta = 20.01º	96.3 %	
Max. and min. transmission	0.9951 and 0.9757	
Refinement method	Full-matrix least-squares on F^2	
Data / restraints / parameters	3964 / 0/ 653	
Goodness-of-fit on F2	1.036	
Final R indices [I>2sigma(I)]	R1 = 0.0401, wR2 = 0.0981	
R indices (all data)	R1 = 0.0551, wR2 = 0.1078	
Largest diff. peak and hole	0.277 and -0.336 e. $Å^{-3}$	

Table 2. Bond lengths [Å] for He@C_{60}·$(NiOEP)_2$. Symmetry transformations used to generate equivalent atoms: #1 -x,y,-z+1/2

C(1)-C(6)	1.384(6)	C(18)-C(30)#1	1.387(6)	C(33)-C(34)	1.430(5)
C(1)-C(2)	1.441(6)	C(18)-C(19)	1.455(6)	C(33)-C(53)	1.495(6)
C(1)-C(7)	1.453(6)	C(19)-C(25)#1	1.366(6)	C(34)-C(35)	1.381(5)
C(2)-C(3)	1.399(6)	C(19)-C(20)	1.453(6)	C(35)-C(36)	1.365(5)
C(2)-C(13)	1.441(6)	C(20)-C(21)	1.375(6)	C(36)-N(2)	1.382(5)
C(3)-C(18)	1.435(6)	C(21)-C(24)	1.434(7)	C(36)-C(37)	1.451(5)
C(3)-C(4)	1.444(6)	C(21)-C(22)	1.445(7)	C(37)-C(38)	1.340(5)
C(4)-C(5)	1.369(6)	C(22)-C(23)	1.372(7)	C(37)-C(55)	1.498(6)
C(4)-C(20)	1.467(7)	C(22)-C(26)	1.454(6)	C(38)-C(39)	1.449(5)
C(5)-C(6)	1.452(7)	C(23)-C(27)	1.452(6)	C(38)-C(57)	1.505(5)
C(5)-C(23)	1.462(7)	C(24)-C(24)#1	1.384(9)	C(39)-C(40)	1.362(5)
C(6)-C(10)	1.456(6)	C(24)-C(25)	1.461(6)	C(39)-N(2)	1.375(5)
C(7)-C(8)	1.378(6)	C(25)-C(19)#1	1.366(6)	C(40)-C(41)	1.369(5)
C(7)-C(12)	1.458(6)	C(25)-C(26)	1.442(6)	C(41)-N(3)	1.398(5)
C(8)-C(11)	1.439(6)	C(26)-C(29)	1.384(6)	C(41)-C(42)	1.424(6)
C(8)-C(9)	1.448(7)	C(27)-C(28)	1.369(6)	C(42)-C(43)	1.363(6)
C(9)-C(10)	1.385(6)	C(28)-C(29)	1.452(6)	C(42)-C(59)	1.510(6)
C(9)-C(16)#1	1.481(6)	C(28)-C(15)#1	1.460(6)	C(43)-C(44)	1.439(6)
C(10)-C(27)	1.437(7)	C(29)-C(30)	1.460(6)	C(43)-C(61)	1.484(6)
C(11)-C(11)#1	1.392(9)	C(30)-C(18)#1	1.387(6)	C(44)-N(3)	1.377(5)
C(11)-C(17)#1	1.468(6)	C(30)-C(14)#1	1.442(6)	C(44)-C(45)	1.384(6)
C(12)-C(17)	1.373(6)	Ni(1)-N(1)	1.931(3)	C(45)-C(46)	1.363(6)
C(12)-C(13)	1.445(6)	Ni(1)-N(3)	1.942(3)	C(46)-N(4)	1.377(5)
C(13)-C(14)	1.389(6)	Ni(1)-N(4)	1.957(3)	C(46)-C(47)	1.454(6)
C(14)-C(30)#1	1.442(6)	Ni(1)-N(2)	1.960(3)	C(47)-C(48)	1.342(6)
C(14)-C(15)	1.447(6)	N(1)-C(34)	1.390(5)	C(47)-C(63)	1.502(6)
C(15)-C(16)	1.385(6)	N(1)-C(31)	1.403(5)	C(48)-C(49)	1.454(6)
C(15)-C(28)#1	1.460(6)	C(31)-C(50)	1.372(5)	C(48)-C(65)	1.492(6)
C(16)-C(17)	1.435(6)	C(31)-C(32)	1.427(6)	C(49)-C(50)	1.356(6)
C(16)-C(9)#1	1.481(6)	C(32)-C(33)	1.357(5)	C(49)-N(4)	1.383(5)
C(17)-C(11)#1	1.468(6)	C(32)-C(51)	1.504(5)	C(51)-C(52)	1.522(6)

C(53)-C(54)	1.517(6)	C(59)-C(60)	1.517(6)	C(65)-C(66)	1.531(6)
C(55)-C(56)	1.513(5)	C(61)-C(62)	1.530(6)		
C(57)-C(58)	1.511(5)	C(63)-C(64)	1.527(6)		

Table 3. Bond angles [º] for He@C_{60}·$(NiOEP)_2$. Symmetry transformations used to generate equivalent atoms: #1 -x,y,-z+1/2

C(6)-C(1)-C(2)	120.1(4)	C(10)-C(9)-C(8)	120.9(5)	C(12)-C(17)-C(16)	120.2(5)
C(6)-C(1)-C(7)	120.4(4)	C(10)-C(9)-C(16)#1	118.8(4)	C(12)-C(17)-C(11)#1	120.1(5)
C(2)-C(1)-C(7)	107.9(4)	C(8)-C(9)-C(16)#1	107.4(4)	C(16)-C(17)-C(11)#1	108.1(4)
C(3)-C(2)-C(13)	120.0(4)	C(9)-C(10)-C(27)	121.0(5)	C(30)#1-C(18)-C(3)	120.3(4)
C(3)-C(2)-C(1)	119.9(4)	C(9)-C(10)-C(6)	118.8(5)	C(30)#1-C(18)-C(19)	119.1(4)
C(13)-C(2)-C(1)	108.2(4)	C(27)-C(10)-C(6)	108.6(4)	C(3)-C(18)-C(19)	108.6(4)
C(2)-C(3)-C(18)	119.6(4)	C(11)#1-C(11)-C(8)	120.7(5)	C(25)#1-C(19)-C(20)	120.0(5)
C(2)-C(3)-C(4)	119.7(4)	C(11)#1-C(11)-C(17)#1	118.9(5)	C(25)#1-C(19)-C(18)	120.9(5)
C(18)-C(3)-C(4)	108.9(4)	C(8)-C(11)-C(17)#1	108.1(4)	C(20)-C(19)-C(18)	107.1(4)
C(5)-C(4)-C(3)	120.0(4)	C(17)-C(12)-C(13)	120.6(5)	C(21)-C(20)-C(19)	119.9(5)
C(5)-C(4)-C(20)	120.6(5)	C(17)-C(12)-C(7)	120.0(5)	C(21)-C(20)-C(4)	119.2(5)
C(3)-C(4)-C(20)	107.0(4)	C(13)-C(12)-C(7)	107.2(4)	C(19)-C(20)-C(4)	108.3(4)
C(4)-C(5)-C(6)	120.7(5)	C(14)-C(13)-C(2)	120.1(4)	C(20)-C(21)-C(24)	120.3(5)
C(4)-C(5)-C(23)	119.8(5)	C(14)-C(13)-C(12)	119.1(4)	C(20)-C(21)-C(22)	120.1(5)
C(6)-C(5)-C(23)	108.0(4)	C(2)-C(13)-C(12)	108.7(4)	C(24)-C(21)-C(22)	108.3(5)
C(1)-C(6)-C(5)	119.4(4)	C(13)-C(14)-C(30)#1	119.6(4)	C(23)-C(22)-C(21)	121.1(5)
C(1)-C(6)-C(10)	120.3(4)	C(13)-C(14)-C(15)	120.3(4)	C(23)-C(22)-C(26)	119.2(4)
C(5)-C(6)-C(10)	107.5(5)	C(30)#1-C(14)-C(15)	108.6(4)	C(21)-C(22)-C(26)	108.0(5)
C(8)-C(7)-C(1)	119.4(5)	C(16)-C(15)-C(14)	119.6(4)	C(22)-C(23)-C(27)	121.3(5)
C(8)-C(7)-C(12)	120.1(5)	C(16)-C(15)-C(28)#1	120.0(4)	C(22)-C(23)-C(5)	119.3(5)
C(1)-C(7)-C(12)	108.0(4)	C(14)-C(15)-C(28)#1	108.4(4)	C(27)-C(23)-C(5)	107.6(5)
C(7)-C(8)-C(11)	120.1(5)	C(15)-C(16)-C(17)	120.1(4)	C(24)#1-C(24)-C(21)	120.4(6)
C(7)-C(8)-C(9)	120.3(5)	C(15)-C(16)-C(9)#1	119.6(4)	C(24)#1-C(24)-C(25)	119.1(6)
C(11)-C(8)-C(9)	108.6(4)	C(17)-C(16)-C(9)#1	107.8(4)	C(21)-C(24)-C(25)	108.1(4)

C(19)#1-C(25)-C(26)	120.0(5)	C(31)-C(32)-C(51)	124.9(4)	C(44)-C(43)-C(61)	124.9(4)
C(19)#1-C(25)-C(24)	120.2(5)	C(32)-C(33)-C(34)	106.3(4)	N(3)-C(44)-C(45)	123.8(4)
C(26)-C(25)-C(24)	107.7(4)	C(32)-C(33)-C(53)	128.3(4)	N(3)-C(44)-C(43)	112.8(4)
C(29)-C(26)-C(25)	120.7(5)	C(34)-C(33)-C(53)	125.3(4)	C(45)-C(44)-C(43)	123.3(4)
C(29)-C(26)-C(22)	120.1(5)	C(35)-C(34)-N(1)	123.5(4)	C(44)-N(3)-C(41)	102.6(3)
C(25)-C(26)-C(22)	107.9(4)	C(35)-C(34)-C(33)	123.7(4)	C(44)-N(3)-Ni(1)	128.2(3)
C(28)-C(27)-C(10)	120.6(5)	N(1)-C(34)-C(33)	112.7(3)	C(41)-N(3)-Ni(1)	129.2(3)
C(28)-C(27)-C(23)	119.2(5)	C(36)-C(35)-C(34)	124.7(4)	C(46)-C(45)-C(44)	124.9(4)
C(10)-C(27)-C(23)	108.3(5)	C(35)-C(36)-N(2)	125.4(4)	C(45)-C(46)-N(4)	125.1(4)
C(27)-C(28)-C(29)	120.5(4)	C(35)-C(36)-C(37)	124.4(4)	C(45)-C(46)-C(47)	124.2(4)
C(27)-C(28)-C(15)#1	120.1(4)	N(2)-C(36)-C(37)	110.1(4)	N(4)-C(46)-C(47)	110.6(4)
C(29)-C(28)-C(15)#1	107.0(4)	C(38)-C(37)-C(36)	107.7(4)	C(48)-C(47)-C(46)	107.0(4)
C(26)-C(29)-C(28)	119.7(4)	C(38)-C(37)-C(55)	129.1(4)	C(48)-C(47)-C(63)	129.3(4)
C(26)-C(29)-C(30)	119.0(4)	C(36)-C(37)-C(55)	123.0(4)	C(46)-C(47)-C(63)	123.5(4)
C(28)-C(29)-C(30)	108.7(4)	C(37)-C(38)-C(39)	106.1(3)	C(47)-C(48)-C(49)	106.9(4)
C(18)#1-C(30)-C(14)#1	120.3(4)	C(37)-C(38)-C(57)	129.3(4)	C(47)-C(48)-C(65)	129.2(4)
C(18)#1-C(30)-C(29)	120.3(4)	C(39)-C(38)-C(57)	124.6(4)	C(49)-C(48)-C(65)	123.8(4)
C(14)#1-C(30)-C(29)	107.4(4)	C(40)-C(39)-N(2)	125.0(4)	C(50)-C(49)-N(4)	124.6(4)
N(1)-Ni(1)-N(3)	177.37(13)	C(40)-C(39)-C(38)	123.6(4)	C(50)-C(49)-C(48)	125.0(4)
N(1)-Ni(1)-N(4)	89.68(14)	N(2)-C(39)-C(38)	111.4(4)	N(4)-C(49)-C(48)	110.4(4)
N(3)-Ni(1)-N(4)	90.62(14)	C(39)-N(2)-C(36)	104.8(3)	C(46)-N(4)-C(49)	105.0(3)
N(1)-Ni(1)-N(2)	90.46(14)	C(39)-N(2)-Ni(1)	128.0(3)	C(46)-N(4)-Ni(1)	127.0(3)
N(3)-Ni(1)-N(2)	89.21(14)	C(36)-N(2)-Ni(1)	127.0(3)	C(49)-N(4)-Ni(1)	127.9(3)
N(4)-Ni(1)-N(2)	179.34(13)	C(39)-C(40)-C(41)	125.1(4)	C(49)-C(50)-C(31)	125.6(4)
C(34)-N(1)-C(31)	102.0(3)	C(40)-C(41)-N(3)	123.0(4)	C(32)-C(51)-C(52)	112.1(3)
C(34)-N(1)-Ni(1)	128.8(3)	C(40)-C(41)-C(42)	124.9(4)	C(33)-C(53)-C(54)	113.9(4)
C(31)-N(1)-Ni(1)	129.1(3)	N(3)-C(41)-C(42)	112.1(4)	C(37)-C(55)-C(56)	112.6(3)
C(50)-C(31)-N(1)	122.8(4)	C(43)-C(42)-C(41)	106.9(4)	C(38)-C(57)-C(58)	113.2(3)
C(50)-C(31)-C(32)	125.0(4)	C(43)-C(42)-C(59)	127.9(4)	C(42)-C(59)-C(60)	112.3(3)
N(1)-C(31)-C(32)	112.2(3)	C(41)-C(42)-C(59)	125.1(4)	C(43)-C(61)-C(62)	112.9(4)
C(33)-C(32)-C(31)	106.8(3)	C(42)-C(43)-C(44)	105.7(4)	C(47)-C(63)-C(64)	111.9(4)
C(33)-C(32)-C(51)	128.3(4)	C(42)-C(43)-C(61)	129.2(4)	C(48)-C(65)-C(66)	112.7(4)

References and Notes

(1) Srivastava, G. P. *The Physics of Phonons*; Adam Hilger, Bristol, **1990**.

(2) Aoyagi, S.; Nishibori, E.; Sawa, H.; Sugimoto, K.; Takata, M.; Miyata, Y.; Kitaura, R.; Shinohara, H.; Okada, H.; Sakai, T.; Ono, Y.; Kawachi, K.; Yokoo, K.; Ono, S.; Omote, K.; Kasama, Y.; Ishikawa, S.; Komuro, T.; Tobita, H. *Nat. Chem*. **2010**, *2*, 678.

(3) Saunders, M.; Jiménez-Vázquez, H. A.; Cross, R. J.; Mroczkowski, S.; Freedberg, D. I.; Anet, F. A. L. *Nature* **1994**, *367*, 256.

(4) (a) Saunders, M.; Cross, R. J.; Jiménez-Vázquez, H. A.; Shimshi, R.; Khong, A. *Science* **1996**, *271*, 1693. (b) Saunders, M.; Jiménez-Vázquez, H. A.; Cross, R. J.; Mroczkowski, S.; Gross, M. L.; Giblin, D. E.; Poreda, R. J. *J. Am. Chem. Soc*. **1994**, *116*, 2193.

(5) Saunders, M.; Jiménez-Vázquez, H. A.; Bangerter, B. W.; Cross. R. J.; Mroczkowski, S.; Freedberg, D. I.; Anet, F. A. L. *J. Am. Chem. Soc*. **1994**, *116*, 3621.

(6) Peng, R.-F.; Chu, S.-J.; Huang, Y.-M.; Yu, H.-J.; Wang, T.-S.; Jin, B.; Fu, Y.-B.; Wang, C.-R. *J. Mater. Chem*. **2009**, *19*, 3602.

(7) (a) Rüttimann, M.; Haldimann, R. F.; Isaacs, L.; Diederich, F.; Khong, A.; Jiménez-Vázquez, H. A.; Cross, R. J.; Saunders, M. *Chem. Eur. J*. **1997**, *3*, 1071. (b) Sternfeld, T.; Hoffman, R. E.; Saunders, M.; Cross, R. J.; Syamala, M. S.; Rabinovitz, M. *J. Am. Chem. Soc*. **2002**, *124*, 8786.

(8) Rubin, Y. *Chem. Eur. J*. **1997**, *3*, 1009.

(9) (a) Murata, Y.; Murata, M.; Komatsu, K. *Chem. Eur. J*. **2003**, *9*, 1600. (b) Murata, Y.; Murata, M.; Komatsu, K. *J. Am. Chem. Soc*. **2003**, *125*, 7152. (c) Komatsu, K.; Murata, M.; Murata, Y. *Science* **2005**, *307*, 238. (d) Murata, M.; Murata, Y.; Komatsu, K. *J. Am. Chem. Soc*. **2006**, *128*, 8024.

(10) (a) Murata, Y.; Maeda, S.; Murata, M.; Komatsu, K. *J. Am. Chem. Soc*. **2008**, *130*, 6702. (b) Murata, M.; Maeda, S.; Morinaka, Y.; Murata, Y.; Komatsu, K. *J. Am. Chem. Soc*. **2008**, *130*, 15800.

(11) Kurotobi, K.; Murata, Y. *Science* **2011**, *333*, 613.

(12) Morinaka, Y.; Tanabe, F.; Murata, M.; Murata, Y.; Komatsu, K. *Chem. Commun*. **2010**, *46*, 4532.

(13) Khong, A.; Jiménez-Vázquez, H. A.; Saunders, M.; Cross, R. J.; Laskin, J.; Peres, T.;

Lifshitz, C.; Strongin, R.; Smith III, A. B. *J*. *Am*. *Chem*. *Soc*. **1998**, *120*, 6380.

(14) Peres, T.; Cao, B.; Cui, W.; Khong, A.; Cross, R. J.; Saunders, M.; Lifshitz, C. *Int*. *J*. *Mass*. *Spectrom*. **2001**, *210*/*211*, 241.

(15) Laskin, J.; Peres, T.; Lifshitz, C.; Saunders, M.; Cross, R. J.; Khong, A. *Chem*. *Phys*. *Lett*. **1998**, *285*, 7.

(16) Yannoni, C. S.; Johnson, R. D.; Meijer, G.; Bethune, D. S.; Salem, J. R. *J*. *Phys*. *Chem*. **1991**, *95*, 9.

(17) Lee, H. M.; Olmstead, M. M.; Suetsuna, T.; Shimotani, H.; Dragoe, N.; Cross, R. J.; Kitazawa, K.; Balch, A. L. *Chem*. *Commun*. **2002**, 1352.

(18) Bondi, A. *J*. *Phys*. *Chem*. **1964**, *68*, 441.

(19) (a) Murphy, T. A.; Pawlik, T.; Weidinger, A.; Höhne, M.; Alcala, R.; Spaeth, J.-M. *Phys*. *Rev*. *Lett*. **1996**, *77*, 1075. (b) Suetsuna, T.; Dragoe, N.; Harneit, W.; Weidinger, A.; Shimotani, H.; Ito, S.; Takagi, H.; Kitazawa, K. *Chem*. *Eur*. *J*. **2002**, *8*, 5079. (c) Kanai, M.; Porfyrakis, K.; Briggs, G. A. D.; Dennis, T. J. S. *Chem*. *Commun*. **2004**, 210. (d) Nikawa, H.; Araki, Y.; Slanina, Z.; Tsuchiya, T.; Akasaka, T.; Wada, T.; Ito, O.; Dinse, K.-P.; Ata, M.; Kato, T.; Nagase, S. *Chem*. *Commun*. **2010**, *46*, 631.

(20) (a) Harneit, W. *Phys*. *Rev*. *A* **2002**, *65*, 032322. (b) Suter, D.; Lim, K. *Phys*. *Rev*. *A* **2002**, *65*, 052309. (c) Benjamin, S. C.; Ardavan, A.; Briggs, G. A. D.; Britz, D. A.; Gunlycke, D.; Jefferson, J.; Jones, M. A. G.; Leigh, D. F.; Lovett, B. W.; Khlobystov, A. N.; Lyon, S. A.; Morton, J. J. L.; Porfyrakis, K.; Sambrook, M. R.; Tyryshkin, A. M. *J*. *Phys*.: *Condens*. *Mater*. **2006**, *18*, S867. (d) Morton, J. J. L.; Tyryshkin, A. M.; Ardavan, A.; Benjamin, S. C.; Porfyrakis, K.; Lyon, S. A.; Briggs, A. D. *Nat*. *Phys*. **2006**, *2*, 40.

(21) (a) Huang, H.; Ata, M.; Ramm, M. *Chem*. *Commun*. **2002**, 2076. (b) Ata, M.; Huang, H.; Akasaka, T. *J*. *Phys*. *Chem*. *B* **2004**, *108*, 4640. (c) Miyanaga, S.; Kaneko, T.; Ishida, H.; Hatakeyama, R. *Thin Solid Films* **2010**, *518*, 3509. (d) Akasaka, T.; Nagase, S. *Endofullerenes*: *A New Family of Carbon Clusters*; Kluwer Academic, Dordrecht, **2002**.

(22) (a) Pietzak, B.; Waiblinger, M.; Murphy, T. A.; Weidinger, A.; Höhne, M.; Dietel, E; Hirsch, A. *Chem*. *Phys*. *Lett*. **1997**, *279*, 259. (b) Dietel, E.; Hirsch, A.; Pietzak, B.; Waiblinger, M.; Lips, K.; Weidinger, A.; Gruss, A.; Dinse, K.-P. *J*. *Am*. *Chem*. *Soc*. **1999**,

121, 2432.

(23) Zhao, Y.; Truhlar, D. G. *Theor*. *Chem*. *Acc*. **2008**, *120*, 215.

(24) Hehre, W. J.; Ditchfield, R.; Pople, J. A. *J*. *Chem*. *Phys*. **1972**, *56*, 2257.

(25) Krishnan, R.; Binkley, J. S.; Seeger, R.; Pople, J. A. *J*. *Chem*. *Phys*. **1980**, *72*, 650.

(26) Frisch, M. J. ; Trucks, G. W.; Schlegel, H. B.; Scuseria, G. E.; Robb, M. A.; Cheeseman, J. R.; Scalmani, G.; Barone, V.; Mennucci, B.; Petersson, G. A.; Nakatsuji, H.; Caricato, M.; Li, X.; Hratchian, H. P.; Izmaylov, A. F.; Bloino, J.; Zheng, G.; Sonnenberg, J. L.; Hada, M.; Ehara, M.; Toyota, K.; Fukuda, R.; Hasegawa, J.; Ishida, M.; Nakajima, T.; Honda, Y.; Kitao, O.; Nakai, H.; Vreven, T.; Montgomery, Jr. J. A.; Peralta, J. E.; Ogliaro, F.; Bearpark, M.; Heyd, J. J.; Brothers, E.; Kudin, K. N.; Staroverov, V. N.; Kobayashi, R.; Normand, J.; Raghavachari, K.; Rendell, A.; Burant, J. C.; Iyengar, S. S.; Tomasi, J.; Cossi, M.; Rega, N.; Millam, J. M.; Klene, M.; Knox, J. E.; Cross, J. B.; Bakken, V.; Adamo, C.; Jaramillo, J.; Gomperts, R.; Stratmann, R. E.; Yazyev, O.; Austin, A. J.; Cammi, R.; Pomelli, C.; Ochterski, J. W.; Martin, R. L.; Morokuma, K.; Zakrzewski, V. G.; Voth, G. A.; Salvador, P.; Dannenberg, J. J.; Dapprich, S.; Daniels, A. D.; Farkas, O.; Foresman, J. B.; Ortiz, J. V.; Cioslowski, J.; Fox, D. J.; *GAUSSIAN 09*, Revision A. 02; Gaussian Inc.: Wallingford CT, **2010**.

(27) Møller, C.; Plesset, M. S. *Phys*. *Rev*. **1934**, *46*, 618.

(28) Bader, R. F. W. *Atoms in Molecules: A Quantum Theory*; Oxford University Press, Oxford, U. K., **1990**.

(29) The AIM 2000 program (version 2.0) was employed to analyze and visualize.

(30) The He-N interaction is classified as closed-shell type bonding; the electron density is small (0.025), the Laplacian is positive (0.142), and the total energy is positive (0.005). The same trend was observed at the BCPs on four N-C bond paths; the electron density is small (0.014), the Laplacian is positive (0.054-0.055), and the total energy is positive (0.002).

(31) Krapp, A.; Frenking, G. *Chem*. *Eur*. *J*. **2007**, *13*, 8256.

(32) Cambridge crystallographic database http://www.ccdc.cam.ac.uk/.

(33) Duling, D. R. *J*. *Magn*. *Reson*. *Ser*. *B* **1994**, *104*, 105.

(34) Sheldrick, G. M. *Acta Crystallogr*. *A* **2008**, *64*, 112.

Chapter 4

Modification of the σ-framework of [60]fullerene for Bulk-heterojunction Solar Cells

Abstract: Skeletally-modified fullerenes (SMFs) with different LUMO levels were newly synthesized toward n-type materials for polymer solar cells (PSCs). The PSCs composed of SMF as an acceptor and poly-3-hexylthiophene (P3HT) as a donor were fabricated. As a result, the clear correlation between the LUMO levels of SMFs and the open-circuit voltage (V_{oc}) values in PSCs was observed. Reflecting the higher LUMO level of the SMF than that of the standard acceptor, PCBM, the best P3HT:SMF-based device showed the V_{oc} of 0.74 V, which is 23% higher than that of the PCBM:P3HT-based device (V_{oc} = 0.60 V). Moreover, the best power conversion efficiency (PCE) of the P3HT:SMF-based device (PCE = 3.11%) was comparable to that of PCBM:P3HT-based device (PCE = 3.12%), indicating that ‘‘skeletal modification’’ of fullerenes is a promising approach to provide n-type materials with tunable LUMO levels for PSCs.

Introduction

As mentioned in General Introduction, the development of n-type fullerene materials with a higher LUMO level than that of [6,6]-phenyl-C_{61}-butyric acid methyl ester (PCBM)[1] has been a promising strategy to improve an open-circuit voltage (V_{oc}) in polymer solar cells (PSCs).[2] It is well known that multi-addition of organic groups on the surface of C_{60} causes an elevation of the LUMO level of the molecule.[3] Therefore, a variety of fullerene bisadducts with 56π-electron systems have been synthesized for the application in PSCs: bis-[60]PCBM,[4] indene-based bisadduct (ICBA),[5] dihydronaphthyl-based bisadduct (NCBA),[6] thieno-*o*-quinodimethane-based bisadduct (TOQC),[7] and so on (Figure 1). The PSCs using bisadducts as the n-type materials have been demonstrated to show the higher V_{oc} and power conversion efficiency (PCE) values than those of PCBM-based solar cell, when paired with poly-3-hexylthiophene (P3HT) as the donor material.[8] However, these bisadducts are used as complicated mixtures of regioisomers with the different LUMO levels and are difficult to be purified. Moreover, application of bisadduct ICBA in the PSCs with donor-acceptor (D-A) copolymers having a narrow bandgap has been mostly unsuccessful.[9] This was in part ascribed to the inferior electron transport through the ICBA channels formed in the active layer of the PSC due to the presence of two attached indene groups.[10] Hence, development of new approaches to control the LUMO level of fullerene is strongly desired.

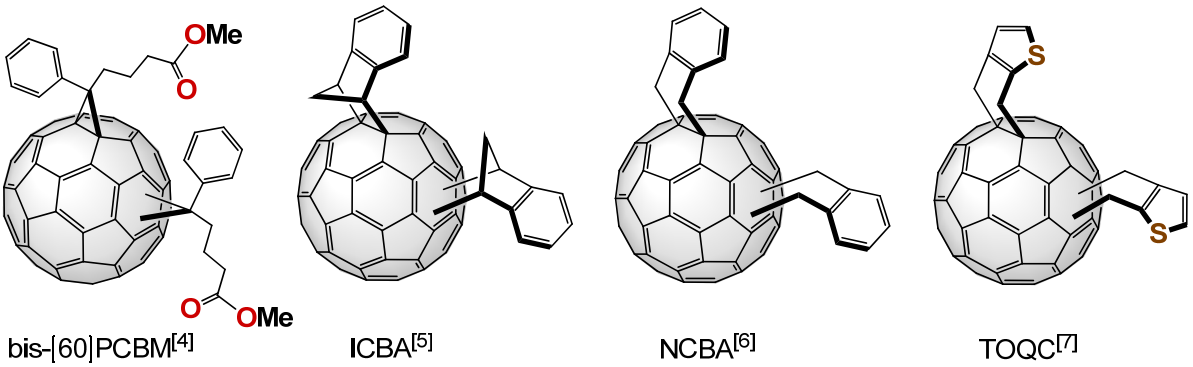

Figure 1. Structures of bisadducts for PSCs.

On the other hand, Komatsu et al. synthesized open-cage C_{60} derivatives **1**-**3** for the purpose of synthesizing endohedral fullerenes (Figure 2).[11] These "skeletally-modified

fullerenes'' (SMFs) **1**-**3** retain 60π-electron system, while the conventional approach using addition reactions accompanies the scission(s) of the π-electron system of the cage. Moreover, according to the results of differential pulse voltammetry (DPV), the distinct values of the first one-electron reduction potential (E_{red}^{1}) were observed as –1.21 V for **1**, –0.97 V for **2**, and –1.15 V for **3**, indicating that the ''skeletal modification'' of fullerenes could be a rational approach to control the LUMO levels. However, studies on the reactions of such SMFs have been so far limited; an oxidation of the sulfide of SMF **3** to the sulfinyl moiety with *m*-chloroperbenzoic acid to give SMF **4**,[12] and a reduction of one of the carbonyl groups of SMF **3** with $NaBH_4$ to give SMF **5** after transannular cyclization of the hydroxyl group with the imine moiety (Figure 3).[13] In addition, because the materials for PSCs are required to have good solubilities in organic solvents to obtain solution processability, the poor solubility of SMF **3** is not suitable for device fabrication. To improve the solubility, installation of long alkyl chains would be effective. For such a purpose, the author decided to use new pyridazine derivative **6** for the synthesis of highly soluble SMFs **7**, **8**, and **9** (Figure 4). In addition, the ''skeletal modification'' of SMF **9** was conducted to obtain fullerene material with a higher LUMO level than that of PCBM for efficient PSCs. In this chapter, the synthesis and photovoltaic properties of such SMFs are described. The PSCs composed of P3HT and SMF as the donor and the acceptor materials, respectively, show clear correlation between the V_{oc} and the LUMO levels of SMFs, indicating that the SMFs are promising materials with tunable LUMO levels.

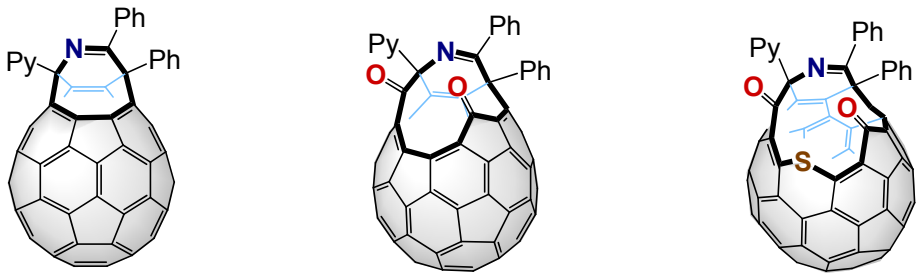

1 (Py = 2-pyridyl) **2** **3**

E_{red}^{1} (V) –1.21 –0.97 –1.15

Figure 2. The structures of open-cage C_{60} deribvatives **1**-**3** and their E_{red}^{1} values obtained from the DPV measurements: V vs. Fc/Fc^{+}, 1 mM sample, 0.05 M Bu_4NBF_4 in ODCB, scan rate 20 mVs^{-1}.[11]

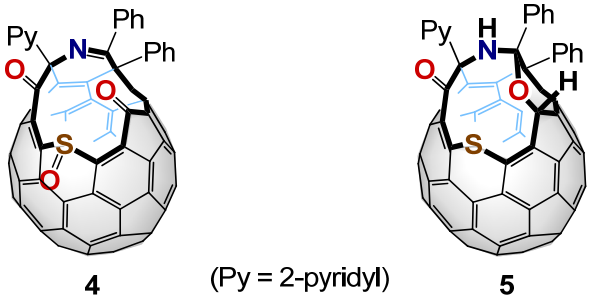

Figure 3. Structures of SMFs **4**[12] and **5**.[13]

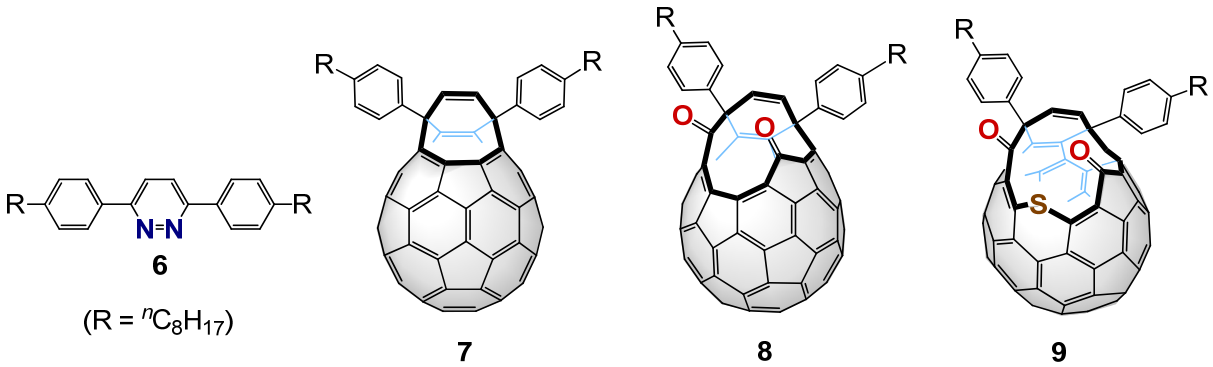

Figure 4. Structures of pyridazine derivative **6** and highly soluble SMFs **7**, **8**, and **9**.

Results and Discussion

The 1-chloronaphthalene (1-ClNp) solution containing pyridazine derivative **6** and C_{60} was refluxed at 255 ºC for 40 h to generate SMF **7** with two *n*-octyl chains, via [4+2] reaction, extrusion of N_2, formal [4+4] reaction, and retro [4+2] reaction (Scheme 1). After cooling to room temperature, the resulting solution was diluted with CS_2 and bubbled with O_2 gas for 30 min. Then, the solution was irradiated with visible light by a Xe lamp to afford SMF **8** in 37% yield. As shown in Scheme 2, by heating a mixture of SMF **8**, elemental sulfur, and tetrakis(dimethylamino)ethylene (TDAE) in *o*-dichlorobenzene (ODCB), the sulfur-insertion onto the rim of the opening[11] of SMF **8** was achieved to give SMF **9** in 93% yield. As expected, SMFs **8** and **9** have excellent solubility in common organic solvents such as chloroform and THF.

Scheme 1. Synthesis of the highly soluble SMF **8**

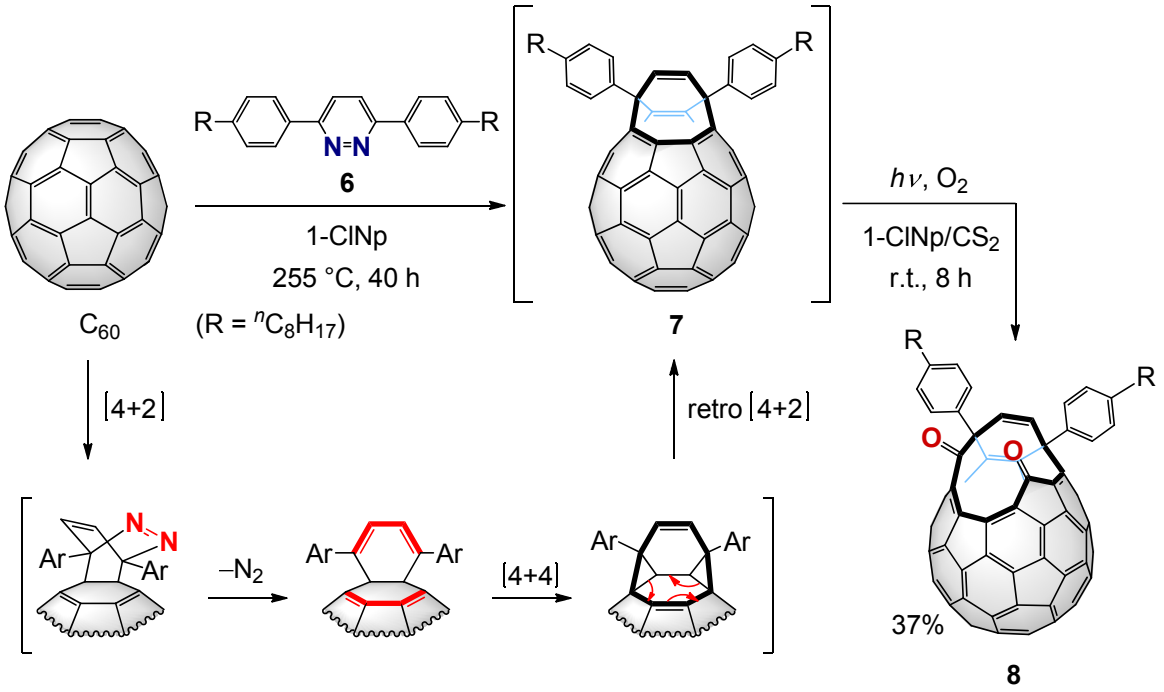

Scheme 2. Sulfur-insertion onto the rim of the opening of SMF **8**

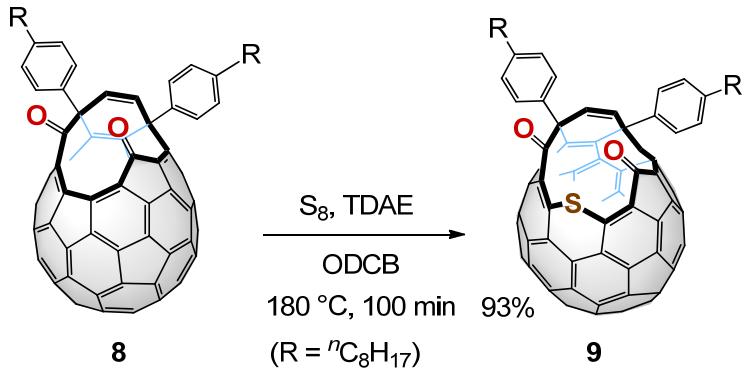

Next, the author conducted additions of organometallic nucleophiles such as methyl and allyl Grignard reagents to SMF **9**. It should be mentioned that a reaction of RMgBr (R = Et, ^{i}Pr, ^{t}Bu, $^{n}C_8H_{17}$, CH=CHCH$_2$CH$_3$, and Ph) or Me$_3$SiCH$_2$MgCl with pristine C_{60} was reported to give a monoadduct R-C_{60}-H or Me$_3$SiCH$_2$-C_{60}-H.[14] As shown in Figure 5, the DFT calculations[15] for model compound **9'**, in which the two *n*-octyl chains are replaced by methyl

groups, indicated that the LUMO is delocalized over the fullerene cage and not over the two carbonyl groups on the rim of opening. This result makes it difficult to predict the reaction course toward nucleophiles such as Grignard reagents. However, it was found that the reaction of MeMgCl takes place selectively at one of the carbonyl groups of SMF **9**.

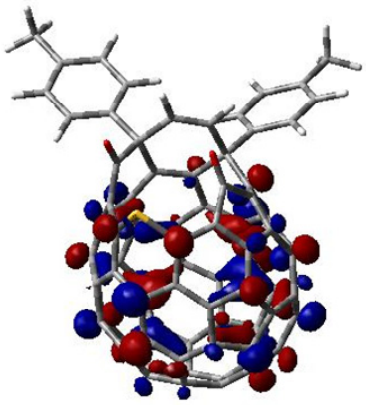

Figure 5. LUMO of **9'** calculated at the B3LYP/6-31G(d) level. The *n*-octyl groups were replaced by methyl groups.

Upon treatment of SMF **9** with MeMgCl (5.0 equiv.) in THF at –20 ºC, the color of the solution immediately changed from dark red to dark brown. After 70 min the mixture was quenched with trifluoroacetic acid and subjected to a chromatographic purification over SiO_2 to give SMF **10** as a dark brown solid in 46% yield (Scheme 3). As shown in Figure 6, the ^{1}H NMR of SMF **10** exhibited a singlet for the hydroxyl group (δ = 5.04) and the ^{13}C NMR showed one carbonyl carbon signal (δ = 199.4) together with a deshielded sp^3 carbon signal (δ = 92.53) in accordance with the 1,2-addition of MeMgCl to one of the carbonyl groups of SMF **9**. The addition of MeMgCl to the SMF **9** in the presence of $CeCl_3$[16] gave the same product SMF **10**, albeit in a lower yield (39%). Allyl magnesium chloride also reacted with SMF **9** in a manner similar to MeMgCl to afford SMF **11** in 9% yield, while no carbonyl addition was observed when EtMgCl or Me_3SiCH_2MgCl was employed. The addition of methyl or allyl Grignard reagents to the other carbonyl group in SMF **9** to give SMF **12** or SMF **13** did not occur presumably due to the effect of steric hindrance by the adjacent phenyl group as judged by the results of DFT calculations; SMF **10'** was shown to be more stable than SMF **12'** by 9.5 kcal mol^{-1}, in which the two octyl groups of **10** and **12** are replaced by

methyl groups.

Scheme 3. Additions of the Grignard reagents to SMF **9**

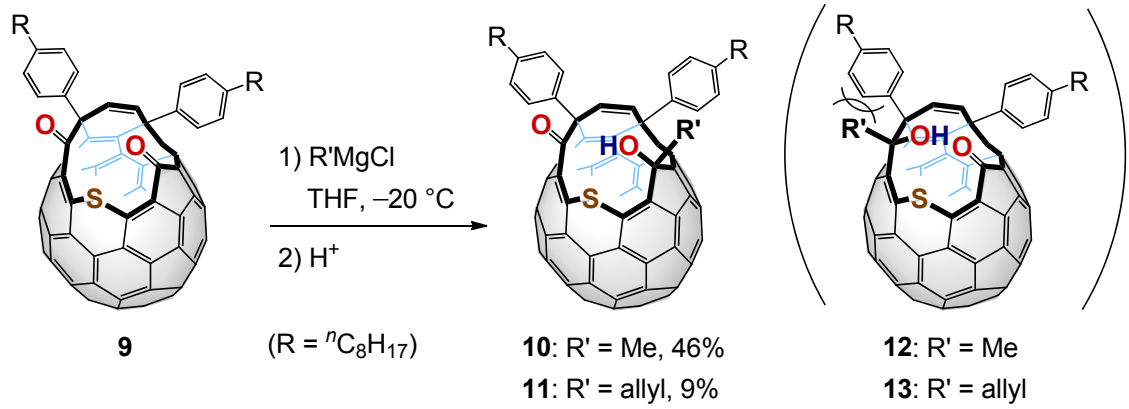

9 (R = $^{n}C_8H_{17}$)

10: R' = Me, 46%
11: R' = allyl, 9%

12: R' = Me
13: R' = allyl

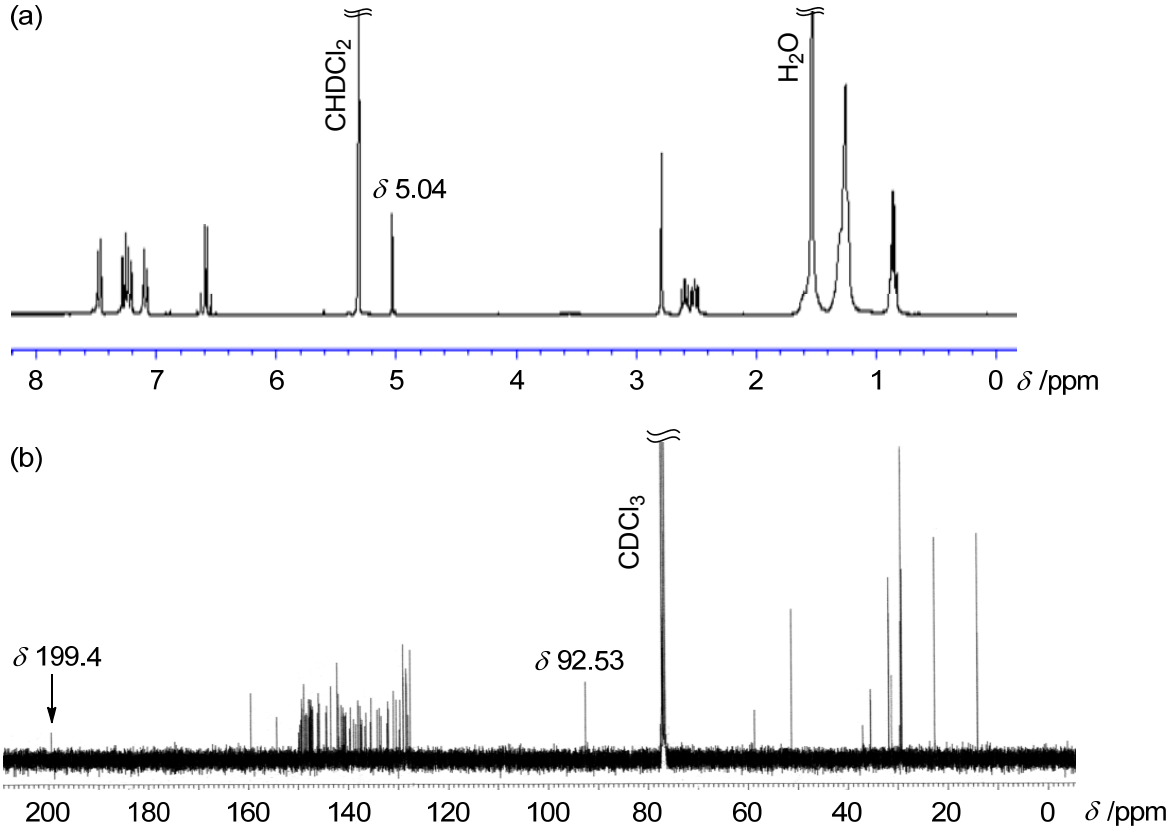

Figure 6. (a) ^{1}H NMR (300 MHz, CD_2Cl_2) and (b) ^{13}C NMR (100 MHz, $CDCl_3$) spectra of SMF **10**.

Although SMF **10** is stable under ambient conditions, there is a possibility that the active hydrogen of the hydroxyl group of SMF **10** negatively influences the device performance of PSCs.[17] To transform the SMF **10** into a more stable compound a transannular cyclization was conducted by heating a solution of SMF **10** in refluxing toluene in the presence of *p*-TsOH (2.9 equiv.) for 12 h (Scheme 4). Chromatographic purification over SiO_2 afforded SMF **14** in 75% yield as a brown solid. It should be mentioned that the similar transannular cyclization was conducted through the reaction of SMF **3** with $NaBH_4$ to give SMF **5** (Figure 3).[13] Although the DFT calculations (B3LYP/6-31G(d)) showed that both transformations of SMF **10'** to SMF **14'** and SMF **15'** are highly exothermic (ΔE = –29.3 and –22.7 kcal mol^{-1}, respectively), only SMF **14** was obtained as a single product presumably because of its lower energy than SMF **15** ($\Delta\Delta E$ = –6.6 kcal mol^{-1} for SMF **15'** from SMF **14'**).

Scheme 4. Transannular cyclization of SMF **10**

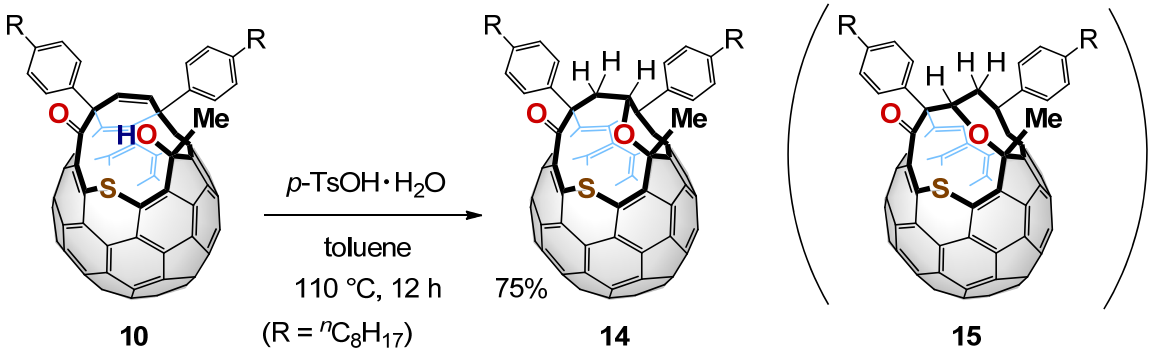

Electrochemical reduction potentials of C_{60}, SMFs **8**, **9**, **14**, and PCBM were measured by cyclic voltammetry (CV) (Figure 7), and the results are summarized in Table 1 together with the calculated LUMO energy levels. All SMFs **8**, **9**, and **14** exhibited pseudo-reversible first to third reduction waves in the same manner as those for C_{60} and PCBM. It is worth nothing that the E_{red}^1 of SMFs **9** and **14** markedly shifted to negative upon the simple modifications from SMF **8**. The sulfur-insertion caused the negative shift by ΔE_{red}^1 = 120 mV and the functionalization of the carbonyl group resulted in the further negative shift by ΔE_{red}^1 = 110 mV, as supported by the results of DFT calculations. Thus, the "skeletal modification" of fullerenes provides a useful way to control the LUMO energy level of

fullerene derivatives without causing significant loss of the native π-conjugation. Since the V_{oc} has an association with the energy difference between acceptor's LUMO and donor's HOMO,[2] the higher LUMO energy level of SMF **14** than that of PCBM should contribute to improve V_{oc} of the device when SMF **14** is combined with a donor polymer having an adequately high LUMO level. On the other hand, UV-vis absorption spectra showed slightly enhanced absorption bands in a range of 300-500 nm for SMF **8**, **9**, and **14** with reference to PCBM, which are advantageous for efficient light harvest in PSCs (Figure 8).

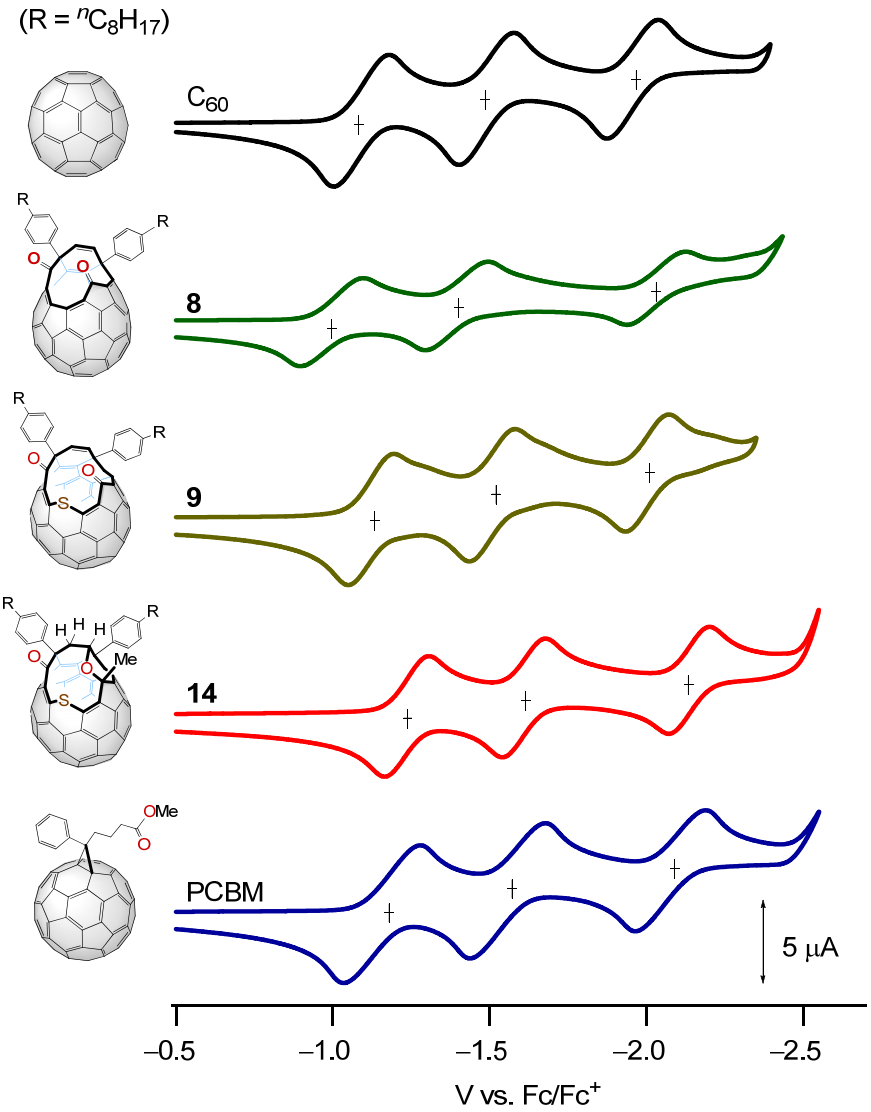

Figure 7. The cyclic voltammograms of C_{60}, SMFs **8**, **9**, **14**, and PCBM; 0.1 M Bu_4NBF_4 in ODCB, scan rate 20 mVs^{-1}.

Table 1. Electrochemical reduction potentials[a] and calculated LUMO levels[b]

Compound	E_{red}^1 (V)	E_{red}^2 (V)	E_{red}^3 (V)	LUMO (eV)
C_{60}	–1.09	–1.49	–1.95	–3.23
8	–1.00	–1.40	–2.03	–3.32
9	–1.12	–1.52	–2.01	–3.18
14	–1.23	–1.62	–2.14	–3.00
PCBM	–1.17	–1.57	–2.09	–3.09

[a] Values for 0.5 ($E_{pa} + E_{pc}$) in V vs. Fc/Fc^+; in ODCB with 0.1 M Bu_4NBF_4 as a supporting electrolyte; Pt wire as a counter electrode and glassy carbon as a working electrode; scan rate of 20 mVs^{-1}.
[b] Calculated at the B3LYP/6-31G(d) level of theory with replacement of the *n*-octyl groups by methyl groups.

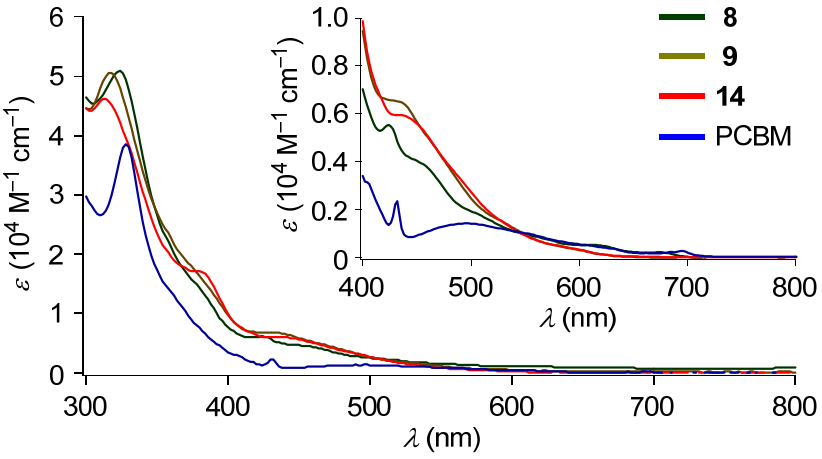

Figure 8. UV-vis absorption spectra of SMFs **8**, **9**, **14** and PCBM in cyclohexane.

In order to observe the effects of the controlled LUMO levels of SMFs on the V_{oc}, PSCs were fabricated using SMFs **8**, **9**, and **14** as the acceptor materials in a combination with P3HT as the donor material, by basically following the procedure established for a P3HT:PCBM-based standard device.[18] The devices with a layered structure of glass/ITO/PEDOT:PSS/P3HT:SMF/TiO_x/Al were prepared as follows. The chlorobenzene solutions containing P3HT and SMF derivative at a weight ratio of 1.6 : 1 were spin-coated

onto the indium tin oxide (ITO)/glass substrate covered with a PEDOT:PSS layer under argon, and the resulting films were annealed at 150 ºC for 6 min to induce phase separation. Then, a TiO_x layer was coated on the active layers in air and subsequently an aluminium electrode was thermally deposited under vaccum. The optimum thickness of the active layer was approximately 80 nm. The surface morphologies of the active layers of P3HT:**8**, P3HT:**9**, P3HT:**14**, and P3HT:PCBM as the standard reference were observed by the use of atomic force microscopy (AFM) (Figure 9). All films using SMFs showed fine features similar to that using PCBM. The root mean square (rms) roughness values were 1.0 nm for P3HT:**8**, 0.9 nm for P3HT:**9**, 1.1 nm for P3HT:**14**, and 1.0 nm for P3HT:PCBM, respectively, suggesting that the domain size of all blend films was almost identical regardless of the ‘‘skeletal modifications’’ of C_{60} and the introduction of the *n*-octyl chains.

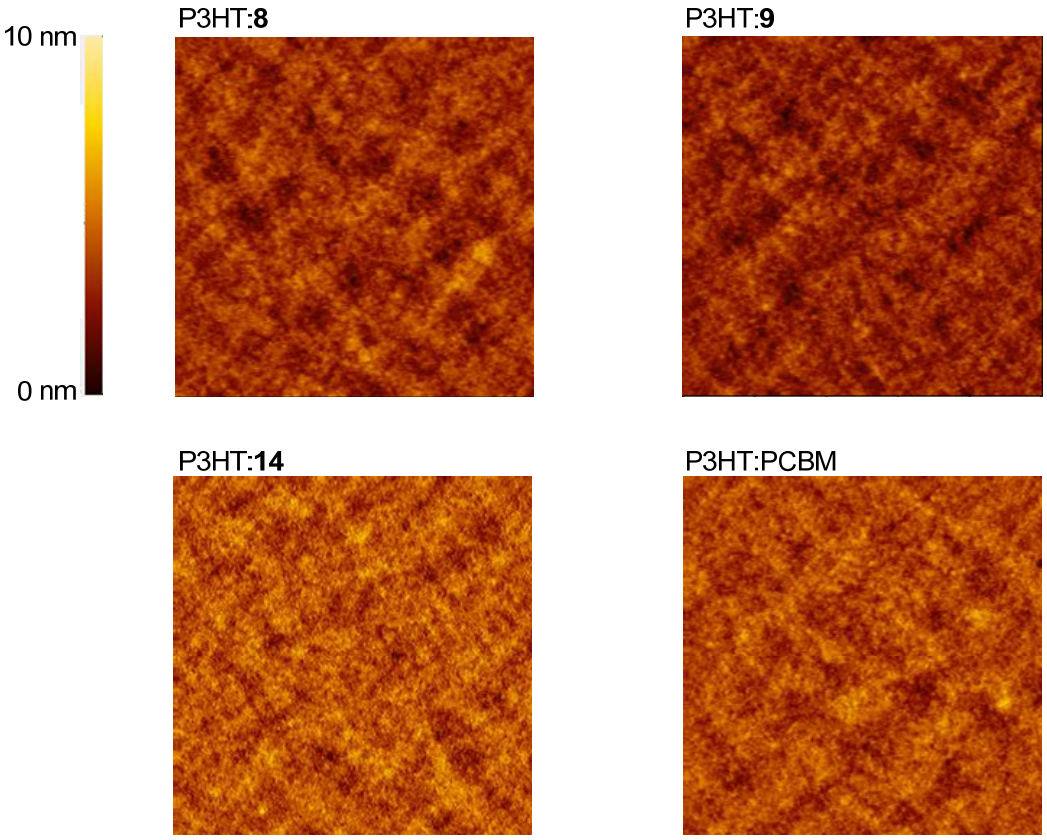

Figure 9. Tapping mode AFM images (10×10 μm) of blend films measured after annealing.

The typical current density-voltage (*J*-*V*) curves for the PSCs under AM 1.5G conditions of 100 mW cm^{-2} are shown in Figure 10 and the device performances are summarized in Table 2. Actually, as expected, the P3HT:**8**-based device marked a low V_{oc} value (0.49 V), reflecting the relatively low-lying LUMO energy level of the acceptor, SMF **8**. This value was clearly improved to V_{oc} = 0.62 V for the P3HT:**9**-based device and further to V_{oc} = 0.74 V for the P3HT:**14**-based device. As shown in Figure 11, the linear regression indicated the clear correlation (r^2 = 1.0) between the LUMO energy levels of the SMF derivatives and the V_{oc} values of the devices, although the point for P3HT:PCBM appears to deviate downward. It is worth noting that the V_{oc} of the P3HT:**14**-based device was superior to that of the P3HT:PCBM-based device (V_{oc} = 0.60 V) by ΔV_{oc} = 140 mV. This ΔV_{oc} is much larger than the value achieved by the introduction of electron-donating groups on the phenyl ring of PCBM (ΔV_{oc} = ~ 30 mV).[19] These data demonstrated that the SMF derivatives are potential *n*-type materials with tunable LUMO levels for PSCs.

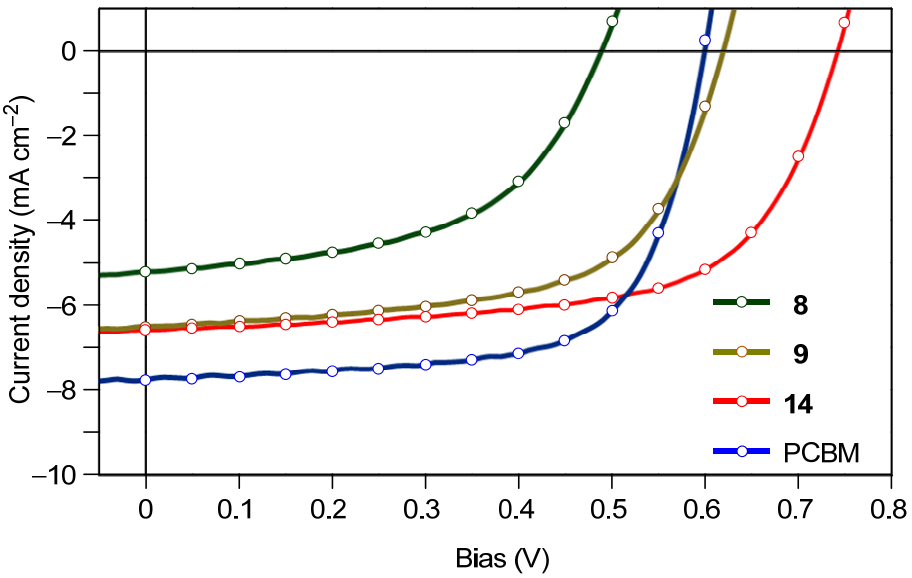

Figure 10. Current density-voltage (*J*-*V*) characteristics of PSCs based on the active layers of P3HT:SMF and P3HT:PCBM under AM 1.5G illumination from a calibrated solar simulator.

Table 2. Characteristics of PSCs[a]

Active layer	V_{oc} (V)	J_{sc} (mA cm^{-2})	FF	PCE (%)
P3HT:**8**	0.49	5.20	0.53	1.35
P3HT:**9**	0.62	6.49	0.62	2.49
P3HT:**14**	0.74	6.57	0.64	3.11
P3HT:PCBM	0.60	7.76	0.67	3.12

[a] The active area of the device is 5.2 mm^2.

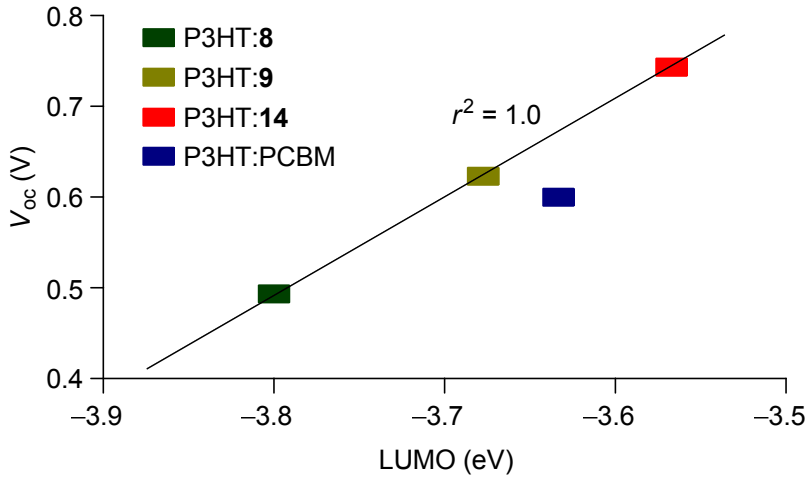

Figure 11. The open-circuit voltage (V_{oc}) of PSCs using SMFs and PCBM as the acceptor materials in a combination with P3HT as the donor material, plotted against LUMO levels of the acceptor materials estimated based on the first reduction potentials (E_{red}^1, V vs. Fc/Fc$^+$) on CV with the equation: LUMO level = –(E_{red}^1 + 4.8).[14d] Linear regression was carried out with the data for P3HT:SMF.

On the other hand, the short-circuit current density (J_{sc}) of P3HT:**9**-based and P3HT:**14**-based devices (J_{sc} = 6.49 and 6.57 mA cm^{-2}, respectively) were found to be slightly lower than that of the P3HT:PCBM-based device (J_{sc} = 7.76 mA cm^{-2}), while the fill factor (FF) were almost identical. One possible reason would be that the presence of two *n*-octyl chains prevented the effective intermolecular π-π interaction between the C_{60} cages and hence decreased the charge mobility.[20] As a result, in a combination with P3HT, the device using

14 provided the best PCE (PCE = 3.11%), which is comparable to that of the benchmark P3HT:PCBM-based device (PCE = 3.12%). The notably low values of J_{sc} (5.20 mA cm^{-2}) and FF (0.53) obtained for the P3HT:**8**-based device probably resulted from the increased charge recombination in BHJ film. As shown in Figure 12, the shape of the LUMO of SMF **8'** was relatively localized at the opening and the absolute values of the coefficients of LUMO at the conjugated butadiene part were 0.18 ~ 0.26. Thus, the almost completely delocalized LUMOs of SMF **9'** and **14'** as well as PCBM are considered to contribute to their improved J_{sc} and FF.

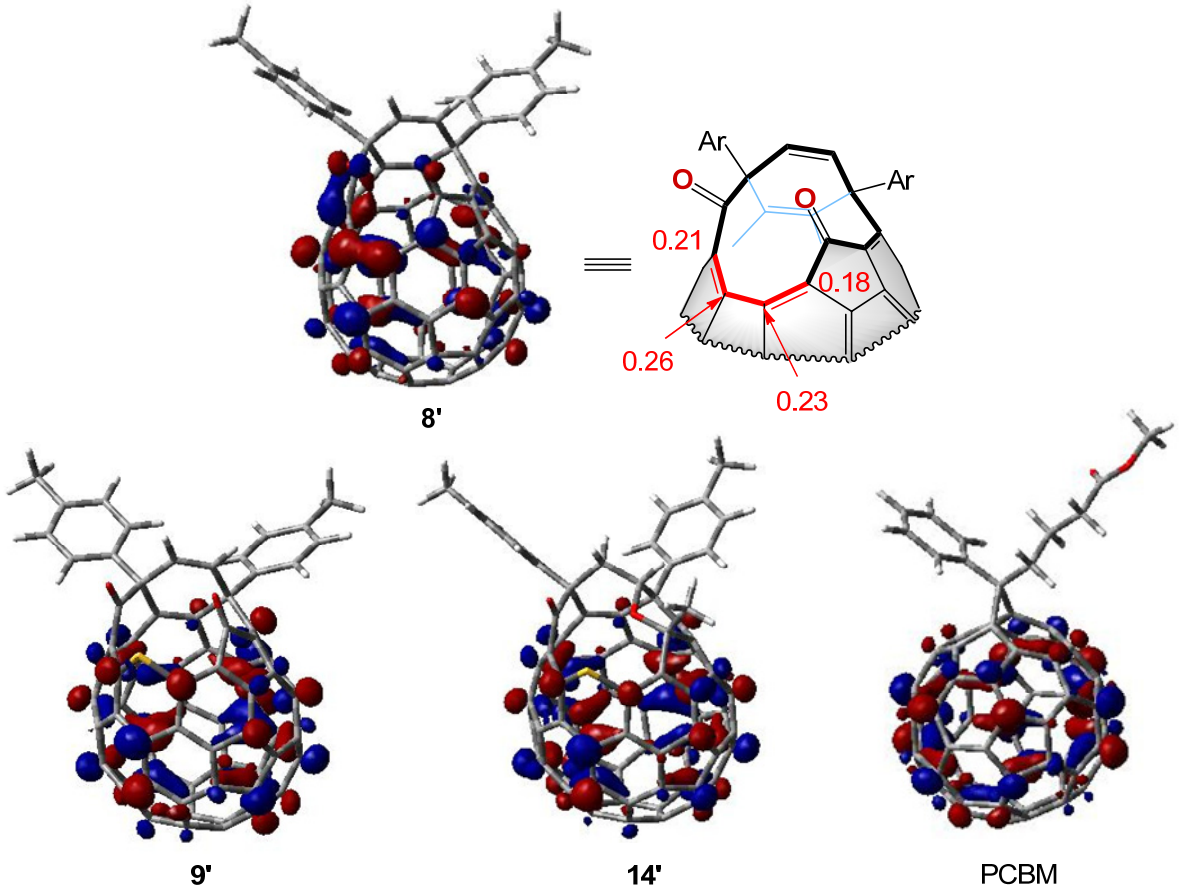

Figure 12. LUMO of SMFs **8'**, **9'**, **14'** and PCBM calculated at the B3LYP/6-31G(d) level. The *n*-octyl groups were replaced by methyl groups. The molecular orbital coefficients of the selected atoms were obtained by an equation: $C = (C_{2px}^2 + C_{2py}^2 + C_{2pz}^2)^{0.5}$. The average coefficients for 60 sp^2 carbons of SMFs were 0.12.

Conclusion

In summary, skeletally-modified fullerenes (SMFs) **8**, **9**, and **14** were newly synthesized for the acceptor materials of PSCs. The reaction of pyridazine derivative **6** with two *n*-octyl chains and C_{60} gave highly soluble SMF **7**, which was subsequently transformed into SMF **8** by photochemical oxidation. The sulfur-insertion onto the rim of the opening of SMF **8** was conducted to give SMF **9**. Although the theoretical calculation showed that the coefficients of the LUMO of SMF **9** is mainly delocalized over fullerene cage, the selective 1,2-addition of MeMgCl took place at the carbonyl group on the rim of the opening of SMF **9** to afford SMF **10**. The transannular cyclization of SMF **10** was conducted by heating of the toluene solution containing SMF **10** and *p*-TsOH·H_2O to give SMF **14**. The cyclic voltammetry showed the distinct values of the first one-electron reduction potential (E_{red}^1) of SMFs, indicating that the ‘‘skeletal modification’’ of fullerenes should be the promising approach for tuning the LUMO levels of fullerenes with retention of their native 60π-system. The photovoltaic characteristics of SMFs were studied through the fabrication of PSCs using SMFs in a combination with P3HT. As a result, the clear correlation was observed between the open-circuit voltage (V_{oc}) and the LUMO level of SMFs, indicating the potential of SMFs as n-type acceptor materials for PSCs. Moreover, the P3HT:**14**-based device showed the higher V_{oc} of 0.74 V than that of P3HT:PCBM-based device (V_{oc} = 0.60 V) and achieved the power conversion efficiency (PCE) of 3.11%.

Experimental Section

General. The ^{1}H and ^{13}C NMR measurements were carried out with a Varian Mercury 300 instrument and a JEOL AL-400 instrument. The NMR chemical shifts are reported in ppm with reference to residual protons and carbons of $CDCl_3$ (δ 7.26 ppm in ^{1}H NMR, δ 77.0 ppm in ^{13}C NMR) and CD_2Cl_2 (δ 5.32 ppm in ^{1}H NMR, δ 54.0 ppm in ^{13}C NMR). IR spectra were taken with a Shimadzu FTIR-8600 spectrometer. FAB mass spectra were recorded on a JEOL MStation JMS-700. The melting points were determined on a Yanaco MP-500D apparatus. The high-pressure liquid chromatography (HPLC) was performed with the use of a Cosmosil Buckyprep column (250 mm length, 4.6 mm inner diameter) for analytical purpose, and the same column (two directly connected columns; 250 mm length, 10

mm inner diameter) for preparative purpose. Cyclic voltammetry and differential pulse voltammetry were conducted on a BAS Electrochemical Analyzer ALS 620C using a three-electrode cell with a glassy carbon working electrode, a platinum wire counter electrode, and a $Ag/AgNO_3$ reference electrode. The measurements were carried out in 1.0 mM solutions of substrate using tetrabutylammonium tetrafluoroborate (Bu_4NBF_4) as a supporting electrolyte (0.1 M), and the potentials were calibrated with ferrocene used as an internal standard which was added after each measurement. Fullerene C_{60} was purchased from SES Research Co. Methyl and allylmagnesium chloride (3.0 M and 2.0 M in THF, respectively), *o*-Dichlorobenzene-d_4 (ODCB-d_4), and poly-3-hexylthiophene (P3HT) were purchased from Aldrich Co. Carbon disulfide (CS_2), tetrahydrofuran (THF), and titanium tetraisopropoxide were purchased from Wako Pure Chemical Industries, Ltd. THF was distilled from sodium benzophenone ketyl under argon before use. The glass substrates covered with indium tin oxide (ITO) (5 Ω sq^{-1}) were purchased from GEOMATEC Co., Ltd. Poly(3,4-ethylenedioxythiophene):poly(styrenesulfonic acid) (PEDOT:PSS) (Denatron PT-100) was purchased from Nagase ChemteX Co. [6,6]-Phenyl-C_{61}-butyric acid methyl ester (PCBM) was purchased from Nano-C, Inc. The ITO/glass substrate was cleaned with a UV/ozone cleaner (UV-253) (Filgen, Inc.). Photocurrent-voltage characteristics were measured by using a CEP 2000 (BUNKOUKEIKI Co., Ltd.). The light intensity of the illumination source was adjusted by using a standard silicon photodiode (BS520) (BUNKOUKEIKI Co., Ltd.). The thicknesses of the films were determined with an Alpha-Step IQ Surface Profiler (KLA-Tencor Co.)

Computational Method. All calculations were conducted with Gaussian 09 packages. The structures were fully optimized with the B3LYP hybrid functional and 6-31G(d) basis set without any symmetry assumptions. Frequency calculations at the optimized structures produced no imaginary frequencies in all cases.

Synthesis of pyridazine derivative 6. To a vigorously stirred suspension of magnesium (powder, 1.105 g, 45.46 mmol) in THF (25 mL) was added dropwise 4-*n*-octyl-1-bromobenzene (10.75 mL, 45.12 mmol) under argon at room temperature and the mixture was kept stirring for 30 min. Then, zinc (II) chloride (6.150 g, 45.12 mmol) and

THF (150 mL) was added to the solution. After stirring for 2 h, 3,6-dichloropyridazine (2.235 g, 15.00 mmol) and tetrakis(triphenylphosphine)palladium(0) (440.0 mg, 0.381 mmol) were added and the mixture was stirred for 24 h at 50 ºC. The mixture was treated with aqueous solution of $NaHCO_3$ (saturated, 200 mL) at ambient temperature for 30 min. The organic layer was separated and the aqueous layer was extracted with $CHCl_3$ (150 mL × 3). The organic layers were combined, dried over Na_2SO_4, and evaporated under reduced pressure. The residue was recrystallized from CH_2Cl_2-hexane (1:1) to give product **6** (5.791 g, 85%) as a colorless solid.

6: mp = 209-210 ºC; ^{1}H NMR (300 MHz, $CDCl_3$) δ 8.08 (d, J = 8.3 Hz, 4H, phenyl), 7.89 (s, 2H, pyridazine), 7.35 (d, J = 8.4 Hz, 4H, phenyl), 2.69 (t, J = 7.7 Hz, 4H, CH_2), 1.67 (quintet, J = 7.4 Hz, 4H, CH_2), 1.28–1.33 (m, 20H, CH_2), 0.88 (t, J = 6.7 Hz, 6H, Me); ^{13}C NMR (100 MHz, $CDCl_3$) δ 157.37, 145.21, 133.57, 129.13, 126.77, 123.89, 35.82, 31.89, 31.36, 29.49, 29.33, 29.27, 22.68, 14.13; HRMS (+EI), calcd for $C_{32}H_{44}N_2$ (M^+) 456.3504, found 456.3506.

Synthesis of SMF 8. A solution of **6** (952.0 mg, 2.084 mmol) and C_{60} (1.000 g, 1.390 mmol) in 1-chloronaphthalene (50 mL) was refluxed for 40 h. After cooling to room temperature, the solution was diluted with CS_2 (50 mL). The solution was bubbled with O_2 gas for 30 min and irradiated with visible light by a Xe lamp for 8 h. The solvents were evaporated under reduced pressure and the residue was purified by flash column chromatography over silica gel with toluene-hexane (1:1) as an eluent to give a crude product. To a solution of the crude product in toluene (3 mL) was added acetonitrile (15 mL) under vigorous stirring and the precipitate was collected by centrifuge. The solid was dried under reduced pressure to give product **8** (613.4 mg, 0.519 mmol, 37%) as a brown solid.

8: mp = 151-153 ºC; IR (KBr) ν = 1688, 1746 cm^{-1} (C=O); ^{1}H NMR (300 MHz, $CDCl_3$) δ 7.48 (d, J = 8.3 Hz, 2H, phenyl), 7.46 (d, J = 8.3 Hz, 2H, phenyl), 7.22 (d, J = 7.9 Hz, 4H, phenyl), 6.84 (dd, J = 15.71 Hz, 9.91 Hz, vinyl), 2.59 (t, J = 7.0 Hz, 4H, CH_2), 1.56-1.64 (m, 4H, CH_2), 1.26–1.33 (m, 20H, CH_2), 0.87 (t, J = 6.6 Hz, 6H, CH_3); ^{13}C NMR (100 MHz, $CDCl_3$) δ 200.73, 191.60, 154.52, 149.93, 148.71, 147.95, 147.84, 147.76, 147.74, 147.33, 147.16, 146.84, 146.49, 146.27, 146.16, 146.05, 145.95, 145.85, 145.75, 145.71, 145.63, 145.60, 145.50, 145.25, 144.98, 144.77, 144.68, 144.54, 144.22, 144.10, 143.78,

142.89, 142.56, 142.55, 142.44, 142.32, 142.26, 142.00, 141.88, 141.81, 141.50, 141.02, 140.78, 140.31, 140.00, 139.93, 139.87, 139.85, 139.68, 139.58, 139.32, 139.03, 138.82, 137.62, 137.25, 136.40, 136.16, 136.10, 135.54, 133.61, 132.93, 132.19, 132.06, 131.34, 131.29, 130.72, 129.12, 128.79, 128.56, 127.17, 58.29, 51.83, 35.57, 35.50, 31.85, 31.31, 31.28, 29.43, 29.37, 29.21, 22.64, 14.11; HRMS (+FAB), calcd for $C_{92}H_{44}O_2$ (M+1) 1181.3420, found 1181.3418.

Synthesis of SMF 9. To a stirred suspension of SMF **8** (1.00 g, 0.847 mmol) and elemental sulfur (crystal, 2.17 g, 8.46 mmol) in dry 1,2-dichlorobenzene (ODCB) (12 mL) was added tetrakis(dimethylamino)ethylene (TDAE) (215 μL, 187 mg, 0.934 mmol) at 180 ºC under argon. After stirring for 100 min, the mixture was cooled to room temperature. Then the resulting mixture was subjected to flash column chromatography over silica gel. Elution with toluene-hexane (1:4) gave SMF **9** (954 mg, 0.787 mmol, 93%) as a dark red solid.

9: mp = 170-171 ºC; IR (KBr) ν = 1695, 1749 cm^{-1} (C=O); ^1H NMR (300 MHz, CD_2Cl_2) δ 7.52 (d, J = 8.7 Hz, 2H), 7.24 (d, J = 8.4 Hz, 2H), 7.21 (d, J = 8.4 Hz, 2H), 7.11 (d, J = 8.7 Hz, 2H), 6.91 (d, J = 10.2 Hz, 1H), 6.65 (d, J = 10.2 Hz, 1H), 2.61 (t, J = 7.7 Hz, 2H), 2.52 (t, J = 7.8 Hz, 2H), 1.64-1.42 (m, 4H), 1.32-1.20 (m, 20H), 0.87 (t, J = 6.6 Hz, 3H), 0.85 (t, J = 6.9 Hz, 3H) (the signals at the range of δ 1.52 ~ 1.60 were overlapped with the signal of H_2O); ^{13}C NMR (100 MHz, $CDCl_3$) δ 197.45, 187.66, 153.22, 150.49, 149.82, 149.71, 149.16, 148.99, 148.99, 148.70, 148.59, 148.37, 148.16, 148.16, 147.95, 147.92, 147.72, 147.71, 147.68, 147.59, 147.56, 147.56, 147.11, 147.07, 146.95, 146.85, 146.09, 146.07, 144.06, 146.04, 142.63, 142.56, 141.86, 141.74, 141.74, 141.55, 141.36, 141.11, 140.93, 140.87, 140.29, 140.24, 139.95, 139.45, 138.79, 138.70, 138.60, 138.59, 138.30, 138.15, 137.93, 137.67, 137.43, 135.53, 135.49, 134.99, 133.60, 132.45, 132.42, 132.29, 130.94, 130.72, 130.14, 130.00, 129.16, 129.02, 128.69, 128.16, 127.39, 127.11, 125.49, 57.71, 51.50, 35.55, 35.49, 31.88, 31.83, 31.29, 31.21, 29.46, 29.42, 29.42, 29.40, 29.22, 29.18, 22.66, 22.62, 14.11, 14.09; HRMS (+FAB), calcd for $C_{92}H_{44}O_2S$ (M^+) 1212.3062, found 1212.3082.

Synthesis of SMF 10. To a stirred solution of SMF **9** (300.0 mg, 0.247 mmol) in dry THF (15 mL) was added a THF solution of methylmagnesium chloride (3.0 M, 410 μL, 1.24 mmol) at –20 ºC under argon. The color of the solution immediately changed from dark red

to dark brown. After stirring for 70 min, trifluoroacetic acid (0.2 mL) was added to the solution. The volatile components in the mixture were removed *in vacuo* to give a residual brown solid. The resulting solid was dissolved in *o*-dichlorobenzene (3 mL) and subjected to flash column chromatography over silica gel. Elution with toluene-hexane (1:4) gave SMF **10** (141.1 mg, 0.115 mmol, 46%) as a dark brown solid.

10: mp = 172-173 ºC; IR (KBr) ν = 1692 cm^{-1} (C=O); ^{1}H NMR (300 MHz, CD_2Cl_2) δ 7.48 (d, J = 8.7 Hz, 2H), 7.28 (d, J = 8.7 Hz, 2H), 7.23 (d, J = 8.1 Hz, 2H), 7.10 (d, J = 8.1 Hz, 2H), 6.62 (d, J = 10.2 Hz, 1H), 6.57 (d, J = 10.2 Hz, 1H), 5.04 (s, 1H), 2.80 (s, 3H), 2.60 (t, J = 7.8 Hz, 2H), 2.52 (t, J = 7.8 Hz, 2H), 1.66-1.42 (m, 4H), 1.36-1.20 (m, 20H), 0.87 (t, J = 6.6 Hz, 3H), 0.86 (t, J = 6.6 Hz, 3H) (the signals at the range of δ 1.52 ~ 1.60 were overlapped with the signal of H_2O); ^{13}C NMR (100 MHz, $CDCl_3$) δ 199.42, 159.53, 154.30, 149.94, 149.72, 149.47, 149.35, 149.23, 148.86, 148.68, 148.67, 148.64, 148.37, 148.30, 147.95, 147.92, 147.87, 147.76, 147.69, 147.61, 147.52, 147.44, 147.27, 147.13, 147.09, 146.18, 146.00, 145.78, 144.46, 144.38, 143.50, 142.26, 141.96, 141.46, 141.38, 141.10, 140.96, 140.72, 140.62, 140.48, 139.76, 139.60, 138.94, 138.49, 138.08, 137.97, 137.66, 137.61, 137.44, 137.30, 136.71, 136.51, 135.59, 135.47, 134.22, 133.78, 133.45, 132.27, 132.08, 132.00, 130.96, 130.42, 129.91, 129.66, 129.03, 128.41, 128.41, 128.10, 127.61, 92.53, 58.78, 51.36, 37.03, 35.51, 35.47, 31.88, 31.85, 31.29, 31.26, 29.69, 29.46, 29.42, 29.42, 29.23, 29.20, 22.66, 22.64, 14.11, 14.09; HRMS (+FAB), calcd for $C_{93}H_{48}O_2S$ (MH^+) 1229.3453, found 1229.3452.

Synthesis of SMF 11. To a stirred solution of SMF **9** (100.0 mg, 0.082 mmol) in dry THF (20 mL) was added a THF solution of allylmagnesium chloride (0.83 M, 149 μL, 0.124 mmol) at –20 ºC under argon. The color of the solution immediately changed from dark red to dark brown. After stirring for 1 h, trifluoroacetic acid (0.1 mL) was added to the solution. Then the mixture was diluted with $CHCl_3$ (20 mL) and the resulting solution was washed with aqueous solution of NH_4Cl (saturated, 40 mL). The organic layer was dried over $MgSO_4$ and evaporated under reduced pressure to give a residual brown solid. The solid was dissolved in toluene (5 mL) and subjected to recycling HPLC using Buckyprep column with toluene as an eluent. SMF **11** (9.4 mg, 0.007 mmol, 9%) was obtained as a dark brown solid.

11: mp = 175 - 176 ºC; IR (KBr) ν = 1744 cm^{-1} (C=O); ^{1}H NMR (400 MHz, CD_2Cl_2) δ

7.47 (d, J = 8.7 Hz, 2H), 7.26 (d, J = 8.7 Hz, 2H), 7.22 (d, J = 8.7 Hz, 2H), 7.10 (d, J = 8.7 Hz, 2H), 6.59 (d, J = 9.9 Hz, 1H), 6.56 (d, J = 9.9 Hz, 1H), 6.38 (m, 1H), 5.65-5.58 (m, 2H), 5.06 (s, 1H), 3.78-3.65 (m, 2H), 2.60 (t, J = 7.9 Hz, 2H), 2.52 (t, J = 7.9 Hz, 2H), 1.70-1.50 (m, 4H), 1.40-1.20 (m, 20H), 0.87 (t, J = 6.8 Hz, 3H), 0.86 (t, J = 7.0 Hz, 3H) (the signals at the range of δ 1.52 ~ 1.60 were overlapped with the signal of H_2O); ^{13}C NMR (100 MHz, $CDCl_3$) δ 199.15, 158.42, 153.04, 150.58, 149.96, 149.75, 149.48, 149.23, 148.96, 148.71, 148.67, 148.67, 148.37, 148.30, 147.92, 147.86, 147.78, 147.69, 147.63, 147.54, 147.43, 147.26, 147.12, 147.11, 146.25, 146.24, 145.77, 145.77, 144.42, 144.26, 143.48, 142.23, 141.94, 141.52, 141.38, 141.38, 141.09, 140.92, 140.65, 140.58, 140.49, 139.73, 139.62, 138.92, 138.41, 138.18, 137.94, 137.66, 137.61, 137.41, 137.41, 137.36, 136.78, 136.00, 135.46, 135.46, 134.25, 133.71, 133.48, 133.35, 132.24, 132.07, 131.99, 130.96, 130.40, 129.93, 129.63, 129.00, 128.43, 127.86, 127.59, 121.86, 94.31, 58.65, 52.91, 51.31, 35.50, 35.46, 31.88, 31.84, 31.28, 31.25, 29.46, 29.42, 29.42, 29.40, 29.22, 29.19, 22.65, 22.64, 14.10, 14.10; HRMS (+FAB), calcd for $C_{95}H_{50}O_2S$ (M^+) 1254.3532, found 1254.3516.

Synthesis of SMF 14. A stirred solution of SMF **10** (120.0 mg, 0.098 mmol) and *p*-TsOH·H_2O (53.8 mg, 0.283 mmol) in dry toluene (10.0 mL) was refluxed for 12 h. After cooling to ambient temperature, the resulting brown suspension was diluted with $CHCl_3$ (10 mL). Then the solution was washed with aqueous solution of NH_4Cl (saturated, 20 mL). The organic layer was dried over $MgSO_4$ and the solvent was evaporated under reduced pressure to give a residual brown solid. The solid was dissolved in CS_2 (3 mL) and subjected to flash column chromatography over silica gel. Elution with toluene-hexane (1:1) gave SMF **14** (90.4 mg, 0.074 mmol, 75%) as a brown solid.

14: mp = 157-158 ºC; IR (KBr) ν = 1697 cm^{-1} (C=O); ^{1}H NMR (400 MHz, CD_2Cl_2) δ 7.49 (d, J = 8.3 Hz, 2H), 7.46 (d, J = 8.3 Hz, 2H), 7.23 (d, J = 8.3 Hz, 2H), 7.19 (d, J = 8.3 Hz, 2H), 5.15 (dd, J = 3.2, 1.3 Hz, 1H), 3.73 (dd, J = 9.5, 4.7 Hz, 1H), 2.81 (s, 3H), 2.60 (t, J = 1.6 Hz, 2H), 2.56 (dd, J = 12.3, 1.6 Hz, 1H), 2.56 (t, J = 1.6 Hz, 2H), 1.64-1.51 (m, 4H), 1.32-1.24 (m, 20H), 0.87 (t, J = 6.9 Hz, 3H), 0.85 (t, J = 6.9 Hz, 3H) (the signals at the range of δ 1.52 ~ 1.60 were overlapped with the signal of H_2O); ^{13}C NMR (100 MHz, CD_2Cl_2) δ 197.33, 160.36, 153.29, 151.78, 150.78, 150.04, 149.89, 149.15, 148.94, 148.77, 148.72, 148.46, 148.45, 148.38, 148.23, 148.17, 148.11, 148.01, 147.91, 147.90, 147.73, 147.59,

147.54, 147.35, 146.81, 146.06, 143.95, 143.22, 142.95, 142.75, 142.69, 142.00, 141.98, 141.69, 141.30, 141.24, 141.16, 140.91, 140.64, 140.43, 139.95, 139.74, 139.31, 139.10, 138.75, 138.57, 138.06, 137.91, 137.33, 136.63, 136.25, 135.98, 133.43, 133.41, 132.92, 132.19, 131.69, 130.59, 129.64, 129.62, 129.51, 129.46, 129.42, 129.17, 127.67, 92.17, 76.71, 55.96, 48.24, 36.00, 35.78, 35.72, 32.25, 32.21, 31.76, 31.72, 29.82, 29.78, 29.76, 29.72, 29.61, 29.56, 26.15, 23.04, 23.00, 14.24, 14.22; HRMS (+FAB), calcd for $C_{93}H_{48}O_2S$ (MH^+) 1229.3453, found 1229.3452.

Procedure for fabrication of the PSCs. The photovoltaic devices with a layered structure of glass/ITO/PEDOT:PSS/1:P3HT/TiO_x/Al were fabricated as follows. The ITO-coated glass substrate (5 Ω sq^{-1}, 2.5 cm × 2.5 cm) was washed carefully under ultrasonic irradiation using water, acetone, and ethanol. The substrate was further cleaned with a UV/ozone cleaner. A thin layer (~40 nm) of PEDOT:PSS was prepared onto the ITO surface by spin-coating the solution (Denatron PT-100) at 5000 rpm for 1 min. The resulting substrate was heated at 200 ºC for 10 min under ambient conditions. Then, an active layer (77 nm) was prepared onto the PEDOT:PSS layer by spin-coating a solution (50 μL) containing P3HT and SMF **8** (weight ratio of 1.6 : 1) in dry chlorobenzene with a concentration of 24 mg/mL at 1000 rpm for 40 seconds under argon. The substrate was annealed at 150 ºC for 6 min under argon. After cooling to room temperature, a thin layer (~10 nm) of TiO_x was immediately prepared on the active layer by spin-coating a solution of titanium tetraisopropoxide in ethanol (50 μL) at 4000 rpm for ~20 seconds followed by being hydrolyzed for 20 min under ambient conditions. Finally, aluminum electrodes were thermally deposited under vacuum (3.8×10^{-5} Torr).

The devices based on SMF **9**, **14**, and PCBM were prepared in a manner similar to that described above. The thicknesses of the active layers of P3HT:**9** and P3HT:**14** were 84 nm and 95 nm, respectively.

References

(1) Hummelen, J. C.; Knight, B. W.; LePeq, F.; Wudl, F. *J*. *Org*. *Chem*. **1995**, *60*, 532.

(2) (a) Vandewal, K.; Tvingstedt, K.; Gadisa, A.; Inganäs, O.; Manca, J. V. *Nat*. *Mater*. **2009**, *8*. 904. (b) Brabec, C. J.; Cravino, A.; Meissner, D.; Sariciftci, N. S.; Fromherz, T.; Rispens, M. T.; Sanchez, L.; Hummelen, J. C. *Adv*. *Funct*. *Mater*. **2001**, *11*, 374.

(3) (a) Gardullo, F.; Isaacs, L.; Diederich, F.; Gisselbrecht, J.-P.; Boudon, C.; Gross, M. *Chem*. *Commun*. **1996**, 797. (b) Gardullo, F.; Seiler, P.; Isaacs, L.; Nierengarten, J.-F.; Haldimann, R. F.; Diederich, F. Mordasini-Denti, T.; Thiel, W.; Boudon, C.; Gisselbrecht, J.-P.; Gross, M. *Hev*. *Chim*. *Acta*. **1997**, *80*, 343.

(4) Lenes, M.; Wetzelaer, G.-J. A. H.; Kooistra, F. B.; Veenstra, S. C.; Hummelen, J. C.; Blom, P. W. M. *Adv*. *Mater*. **2008**, *20*, 2116.

(5) (a) He, Y.; Chen, H.-Y.; Hou, J.; Li, Y. *J*. *Am*. *Chem*. *Soc*. **2010**, *132*, 1377. (b) Zhao, G.; He, Y.; Li, Y. *Adv*. *Mater*. **2010**, *22*, 4355.

(6) (a) Meng, X.; Zhang, W.; Tan, Z.; Du, C.; Li, C.; Bo, Z.; Li, Y.; Yang, X.; Zhen, M.; Jiang, F.; Zheng, J.; Wang, T.; Jiang, L.; Shu, C.; Wang, C. *Chem*. *Commun*. **2012**, *48*, 425. (b) Kim, K.-H.; Kang, H.; Nam, S. Y.; Jung, J.; Kim, P. S.; Cho, C.-H.; Lee, C.; Yoon, S. C.; Kim, B. J. *Chem*. *Mater*. **2011**, *23*, 5090.

(7) Zhang, C.; Chen, S.; Xiao, Z.; Zuo, Q.; Ding, L. *Org*. *Lett*. **2012**, *14*, 1508.

(8) (a) Chen, T.-A.; Rieke, R. D. *J*. *Am*. *Chem*. *Soc*. **1992**, *114*, 10087. (b) McCullough, R. D.; Lowe, R. D. *J*. *Chem*. *Soc*., *Chem*. *Commun*. **1992**, 70. (c) Chen, T.-A.; Wu, X.; Rieke, R. D. *J*. *Am*. *Chem*. *Soc*. **1995**, *117*, 233. (d) Wang, T.; Takita, R.; Kikuzaki, Y.; Ozawa, F. *J*. *Am*. *Chem*. *Soc*. **2010**, *132*, 11420.

(9) Guo, X.; Zhang, M.; Huo, L.; Cui, C.; Wu, Y.; Hou, J.; Li, Y. *Macromolecules* **2012**, *45*, 6930.

(10) Miller, N. C.; Sweetnam, S.; Hoke, E. T.; Gysel, R.; Miller, C. E.; Bartelt, J. A.; Xie, X.; Toney, M. F.; McGehee, M. D. *Nano Lett*. **2012**, *12*, 1566.

(11) Murata, Y.; Murata, M.; Komatsu, K. *Chem*. *Eur*. *J*. **2003**, *9*, 1600.

(12) (a) Komatsu, K.; Murata, M.; Murata, Y. *Science* **2005**, *307*, 238. (b) Murata, M.; Murata, Y.; Komatsu, K. *J*. *Am*. *Chem*. *Soc*. **2006**, *128*, 8024.

(13) Chuang, S.-C.; Murata, Y.; Murata, M.; Komatsu, K. *Chem*. *Commun*. **2007**, 1751.

(14) (a) Hirsch, A.; Soi, A.; Karfunkel, H. R. *Angew*. *Chem*. *Int*. *Ed*. *Engl*. **1992**, *31*, 766.

(b) Hirsch, A.; Grösser, T.; Skiebe, A.; Soi, A. *Chem*. *Ber*. **1993**, *126*, 1061. (c) Nagashima, H.; Terasaki, H.; Kimura, E.; Nakajima, K.; Itoh, K. *J*. *Org*. *Chem*. **1994**, *59*, 1246. (d) Matsuo, Y.; Iwashita, A.; Abe, Y.; Li, C.-Z.; Matsuo, K.; Hashiguchi, M.; Nakamura, E. *J*. *Am*. *Chem*. *Soc*. **2008**, *130*, 15429.

(15) Frisch, M. J. ; Trucks, G. W.; Schlegel, H. B.; Scuseria, G. E.; Robb, M. A.; Cheeseman, J. R.; Scalmani, G.; Barone, V.; Mennucci, B.; Petersson, G. A.; Nakatsuji, H.; Caricato, M.; Li, X.; Hratchian, H. P.; Izmaylov, A. F.; Bloino, J.; Zheng, G.; Sonnenberg, J. L.; Hada, M.; Ehara, M.; Toyota, K.; Fukuda, R.; Hasegawa, J.; Ishida, M.; Nakajima, T.; Honda, Y.; Kitao, O.; Nakai, H.; Vreven, T.; Montgomery, Jr. J. A.; Peralta, J. E.; Ogliaro, F.; Bearpark, M.; Heyd, J. J.; Brothers, E.; Kudin, K. N.; Staroverov, V. N.; Kobayashi, R.; Normand, J.; Raghavachari, K.; Rendell, A.; Burant, J. C.; Iyengar, S. S.; Tomasi, J.; Cossi, M.; Rega, N.; Millam, J. M.; Klene, M.; Knox, J. E.; Cross, J. B.; Bakken, V.; Adamo, C.; Jaramillo, J.; Gomperts, R.; Stratmann, R. E.; Yazyev, O.; Austin, A. J.; Cammi, R.; Pomelli, C.; Ochterski, J. W.; Martin, R. L.; Morokuma, K.; Zakrzewski, V. G.; Voth, G. A.; Salvador, P.; Dannenberg, J. J.; Dapprich, S.; Daniels, A. D.; Farkas, O.; Foresman, J. B.; Ortiz, J. V.; Cioslowski, J.; Fox, D. J.; *GAUSSIAN 09*, Revision B. 01; Gaussian Inc.: Wallingford CT, **2010**.

(16) (a) Imamoto, T.; Kusumoto, T.; Tawarayama, Y.; Sugiura, Y.; Mita, T.; Hatanaka, Y.; Yokoyama, M. *J*. *Org*. *Chem*. **1984**, *49*, 3904. (b) Imamoto, T.; Takiyama, N.; Nakamura, K.; Hatajima, T.; Kamiya, Y. *J*. *Am*. *Chem*. *Soc*. **1989**, *111*, 4392.

(17) Niinomi, T.; Matsuo, Y.; Hashiguchi, M.; Sato, Y.; Nakamura, E. *J*. *Mater*. *Chem*. **2009**, *19*, 5804.

(18) Hayakawa, A.; Yoshikawa, O.; Fujieda, T.; Uehara, K.; Yoshikawa, S. *Appl*. *Phys*. *Lett*. **2007**, *90*, 163517.

(19) Kooistra, F. B.; Knol, J.; Kastenberg, F.; Popescu, L. M.; Verhees, W. J. H.; Kroon, J. M.; Hummelen, J. C. *Org*. *Lett*. **2007**, *9*, 551.

(20) Piliego, C.; Holcombe, T. W.; Douglas, J. D.; Woo, C. H.; Beaujuge, P. M.; Fréchet, J. M. J. *J*. *Am*. *Chem*. *Soc*. **2010**, *132*, 7595.

Chapter 5

Synthesis and Photovoltaic Properties of Bulky Acceptor Materials Based on the Dimerization of Fullerene C_{60} for Efficient Polymer Solar Cells

Abstract: Bulky acceptor materials were synthesized by connecting two fullerenes in close proximity and the performances of these dimeric fullerenes in the polymer solar cells as acceptor materials are studied. It is demonstrated that one of the dimeric fullerenes works as an excellent n-type material comparable to benchmark PCBM. In a combination with representative donor-acceptor copolymer PTB7, the best dimeric fullerene-based device showed the power conversion efficiency of 6.14% which is comparable to that of PCBM-based device (6.24%). The data demonstrated that the dimeric fullerene can be added as a new entry of n-type materials toward the development of efficient solar cells.

Introduction

As mentioned in General Introduction, the key of the polymer solar cells (PSCs) is the active layer composed of a mixture of a hole-transporting polymer and an electron-transporting fullerene with an interpenetrating network, so called bulk-heterojunction (BHJ) structures, where the large interfacial area induces efficient charge separation. The BHJ solar cells composed of regioregular poly-3-hexylthiophene (P3HT)[1] and [6,6]-phenyl-C_{61}-butyric acid methyl ester (PCBM),[2] used as the donor and the acceptor materials, respectively, have been well-studied (Figure 1).[3] By following guidelines for the efficient PSCs,[4] a variety of donor-acceptor (D-A) copolymers with narrow bandgap have been reported during the last few years,[5] and actually high power conversion efficiency (PCE) values have been achieved in a combination with PCBM or its C_{70} analogue, $PC_{71}BM$.[6] Among them, the PTB7:$PC_{71}BM$-based device[7] (PCE = 9.2%) is one of the most successful PSCs (Figure 1).[8]

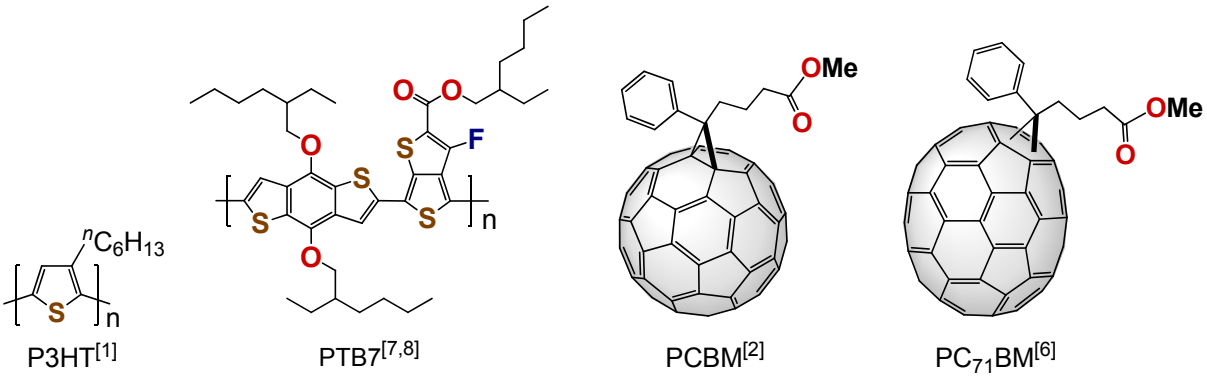

Figure 1. Structures of P3HT, PTB7, and PCBMs.

In contrast to the rapid progress in the development of the donor polymers, a repertoire of the fullerene derivatives have been rather limited. Although a number of fullerene derivatives with various functional group(s) have been studied in a combination with P3HT, only a few derivatives were shown to work as efficient acceptor materials: PCBM, ICBA,[9] and SIMEF,[10] etc. Among them, application of ICBA to PSCs in a combination with most

D-A copolymers is known to be unsuccessful.[11] This was ascribed to lower crystallinity and higher LUMO level of ICBA than that of PCBM. In addition, recent observation by the specular XRD patterns demonstrated that PCBM and ICBA tend to intercalate between the side-alkyl chains of amorphous or semicrystalline polymers, when there is enough space between the side chains; the possible arrangement of the ICBA in the PBTTT:ICBA bimolecular crystal is shown in Figure 2.[12] The suppressed electron transport in the polymer domain, due to the two attached indene groups, was considered to reduce the photocurrent generation critically as compared to PCBM.[12] Such intercalation should be prevented by developing bulky acceptor materials, which would result in a desirable phase separation into relatively pure polymer and pure fullerene domains.

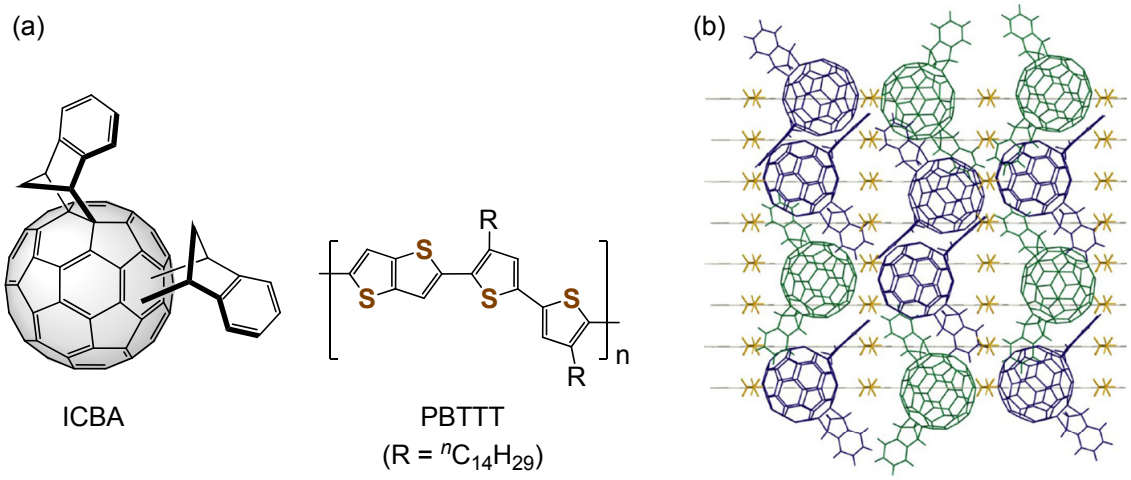

Figure 2. (a) Structures of ICBA and PBTTT. (b) A top-down representation showing a possible arrangement of the ICBA fullerenes in the PBTTT:ICBA bimolecular crystal. The polymer side chains and polymer backbones are shown in yellow and grey, respectively. Note that this figure is only for illustration and is not meant to depict the exact molecular packing in PBTTT:ICBA bimolecular crystals.[12b]

Recently, the photovoltaic performances of dimeric fullerene derivatives in a combination with P3HT were reported by several groups. As shown in Figure 3, Martín et al.

synthesized fullerene dimer **1** albeit showing rather low performance (PCE = <1%).[13] Qin et al. also synthesized dimer **2**, where C_{60} units were chained with long and flexible aliphatic spacer(s).[14] In the present study, the author provides new tightly linked PCBM dimers, PDB and MDB (abbreviations of Para-substituted DumBbell-shaped dimer and its Meta- analogue, respectively) (Figure 4), which showed excellent performance in PSCs in a combination with both P3HT and representative D-A copolymer PTB7. In this Chapter, synthesis, and photovoltaic properties of dimeric fullerenes are described.

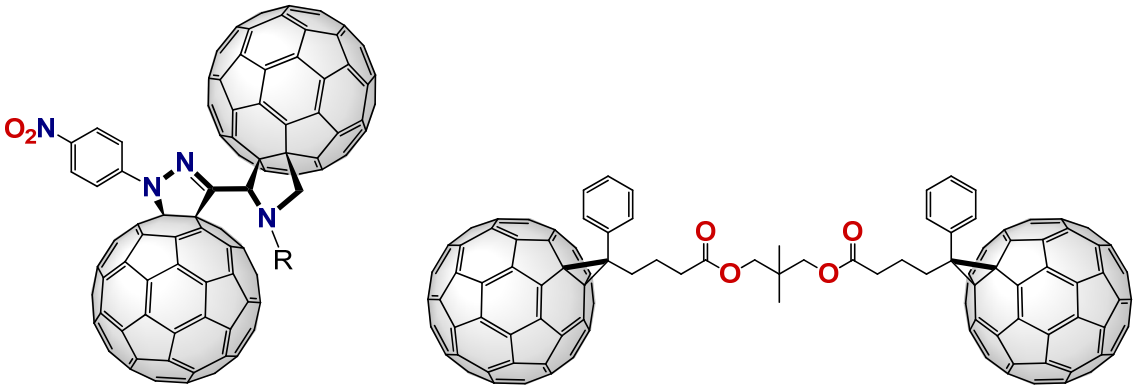

1[13] (R = $^{n}C_8H_{17}$) **2**[14]

Figure 3. Structures of dimeric fullerenes.

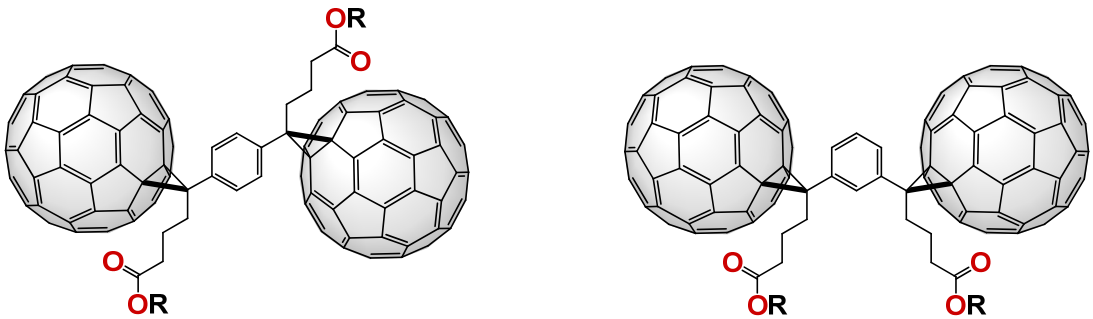

PDB (R = ^{n}Bu) MDB

Figure 4. Structures of PDB and MDB.

Results and Discussion

In the design of PDB and MDB, the author decided to use the advantage of the structure of benchmark PCBM, as it is generally considered that structure of addend(s) on the C_{60} cage considerably affects the photovoltaic performance.[15] In light of the close distance and rigidity of the linker, compared to other reported dimers,[13,14] these dimers are regarded as bulky acceptor materials having doubly expanded molecular volume and π-system. The synthesis was carried out by basically following the procedure reported for PCBM,[2] though the author prepared new precursors for diazo compounds possessing two tosylhydrazone units as shown in Scheme 1. The precursors **7a,b** were prepared as follows. First, the reactions of phthalaldehydes **3a,b** with 2-amino-3-picoline afforded diimines **4a,b** in good yields. Then, hydroacylation of **4a,b** with methyl 3-butenoate in the presence of Wilkinson's catalyst and subsequent acid hydrolysis afforded tetracarbonyl compounds **5a,b**.[16] To overcome low solubility of dimers transesterification of **5a,b** with ^{n}BuOH was conducted by the use of pentafluorophenylammonium triflate (PFPAT) as a catalyst[17] to afford **6a,b**. The phenyl ketone moieties of **6a,b** were quantitatively transformed into tosylhydrazones **7a,b**. Finally, diazo compounds were generated by treatment of **7a,b** with NaH and were trapped *in situ* by C_{60} to afford PDB and MDB in 23% and 37%, respectively. PDB and MDB (R = ^{n}Bu) showed high solubility similar to that of PCBM, while corresponding dimers with shorter alkyl chains (R = Me, Et, and ^{n}Pr) were hardly soluble in common organic solvents.

Scheme 1. Synthesis of PDB and MDB

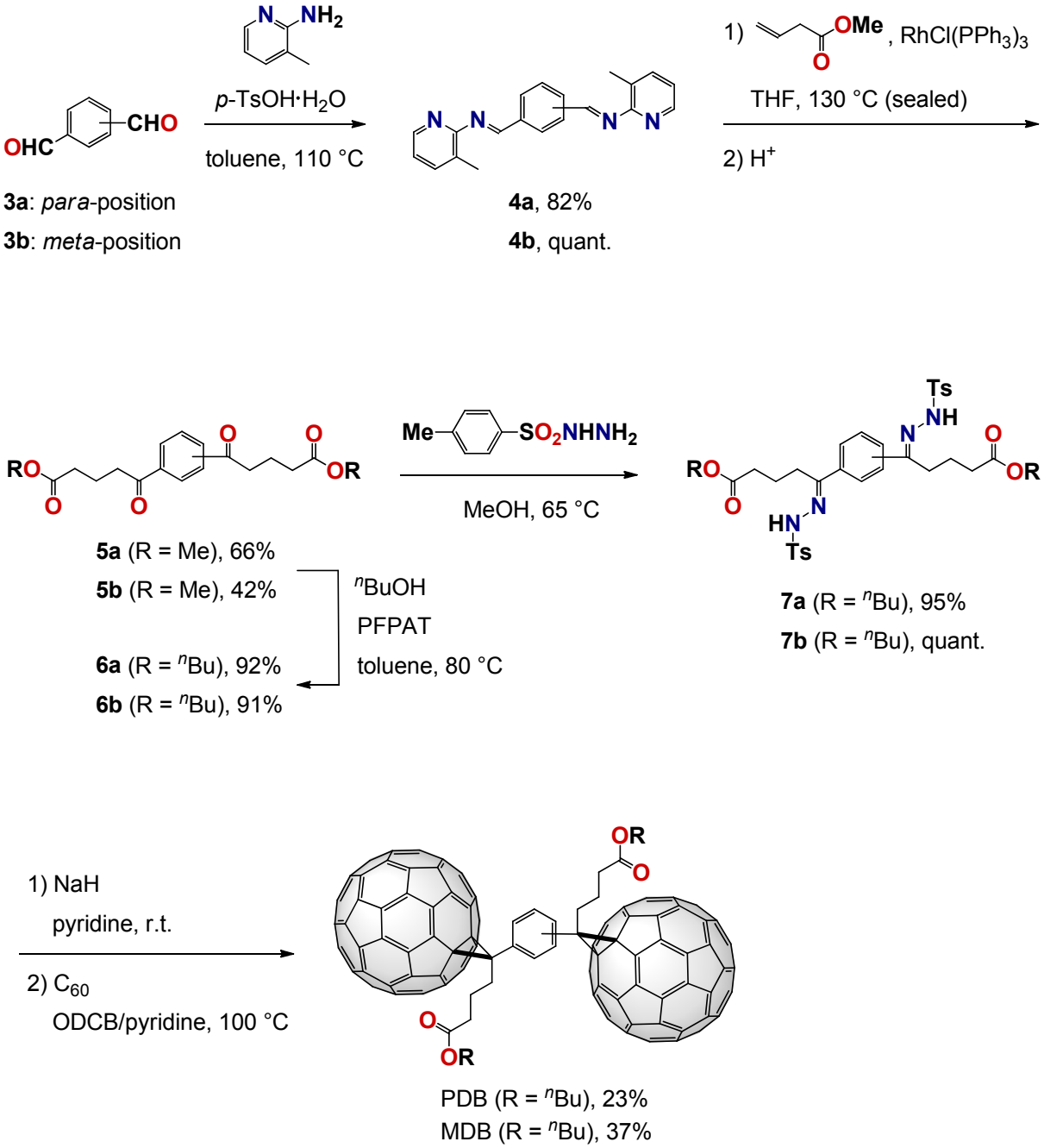

The UV-vis absorption spectra of PDB, MDB, and PCBM in cyclohexane are shown in Figure 5. The small peaks at 430 nm observed in all cases indicate their [6,6] methanofullerene structures. The absorption coefficients of PDB and MDB are doubled with respect to that of PCBM, reflecting little interaction between the two C_{60} moieties.

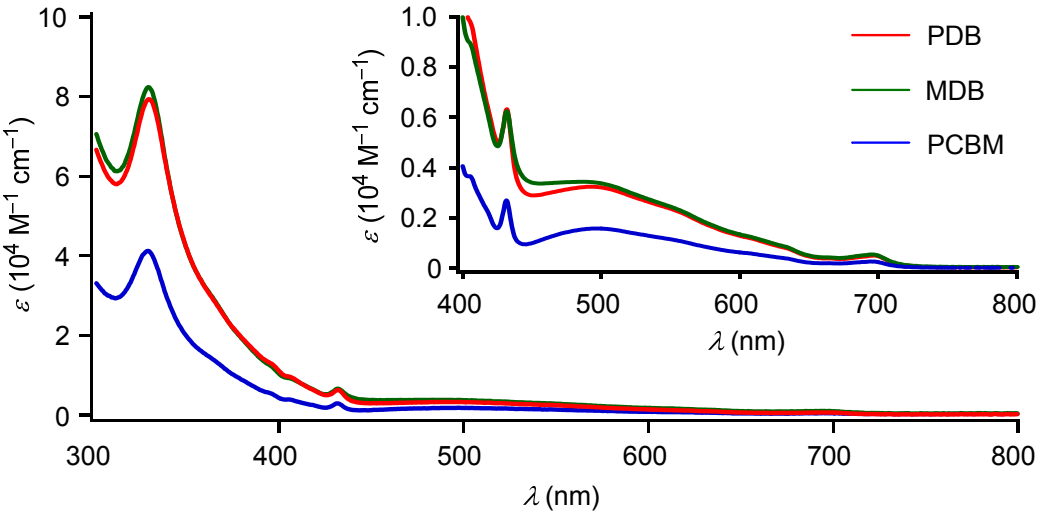

Figure 5. UV-vis absorption spectra of PDB, MDB, and PCBM in cyclohexane.

As shown in Figure 6, the electrochemical properties of PDB and MDB were investigated by cyclic voltammetry (CV) and the results are summarized in Table 1. Both dimers exhibited three sets of pseudo-reversible two-electron reduction waves, indicating that there is little electronic communication between closely linked two cages. In addition, the reduction waves appeared at almost the same potentials as those of PCBM, indicating that the LUMO levels are almost identical.

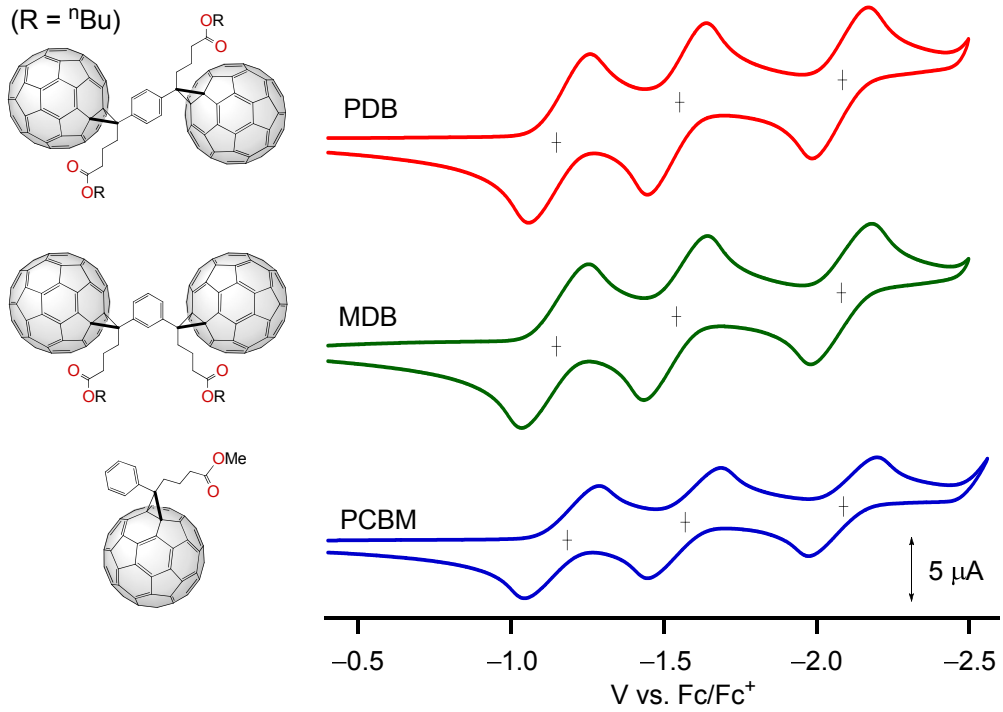

Figure 6. The measurement of CV of PDB, MDB, and PCBM; 0.1 M Bu_4NBF_4 in ODCB, scan rate 20 mVs^{-1}.

Table 1. Electrochemical reduction potentials[a] and LUMO levels[b]

Compound	E_{red}^1 (V)	E_{red}^2 (V)	E_{red}^3 (V)	LUMO (eV)
PDB	–1.15	–1.55	–2.09	–3.65
MDB	–1.15	–1.54	–2.08	–3.65
PCBM	–1.17	–1.57	–2.09	–3.63

[a] Values for 0.5 ($E_{pa} + E_{pc}$) in V vs. Fc/Fc^+; 1 mM samples in ODCB with 0.1 M Bu_4NBF_4 as a supporting electrolyte; Pt wire as a counter electrode and glassy carbon as a working electrode; scan rate of 20 mVs^{-1}.
[b] Values from the following equation; LUMO level = $-(E_{red}^1 + 4.8)$.[18]

Following the procedure described in Chapter 4, the author fabricated the PSCs based on the glass/ITO/PEDOT:PSS/polymer:fullerene/TiO_x/Al configuration.[19] The author first optimized fabrication conditions of the active layer composed of P3HT and dimeric fullerenes

PDB and MDB. The optimal donor/acceptor weight ratios and annealing time of the active layers were found to be almost identical to those of P3HT:PCBM-based standard cell. Thus, the active layer (thickness ca. 110 nm) was prepared by spin-coating technique from the chlorobenzene (PhCl) solution of P3HT and dimeric fullerene at a 1.6 : 1 weight ratio. Subsequently thermal annealing was conducted at 150 ºC for 6 min. Next, as to the active layers composed of PTB7 and dimeric fullerenes, we found that *o*-dichlorobenzene (ODCB) is suitable as the solvent for the spin-coating method rather than PhCl. Thus, the solutions containing PTB7 and dimeric fullerenes at a 1 : 1 weight ratio was spin-coated to form the active layer (thickness ca. 90 nm). Again these optimized conditions were almost identical to those optimized for the PTB7:PCBM-based cell.

The current density-voltage (*J*-*V*) curves measured under AM 1.5G illumination are shown in Figure 7, and the corresponding photovoltaic performances are summarized in Table 2. When the author compares the performances of P3HT-based cells, the cell using PDB as the acceptor material showed a decent PCE of 3.32%, which is comparable to PCBM-based cell (PCE = 3.27%), while MDB-based cell showed inferior performance (PCE = 2.75%). In spite of the similar LUMO levels, the V_{oc} and J_{sc} for P3HT:MDB-based cell decreased as compared to those for PDB- and PCBM-based cells. Although the reason for this decrease is not clear, similar data were often reported when morphology of active layer is not suitable.[20] After phase segregation of the active layer, P3HT is considered to form relatively pure domains; PCBM does not intercalate between the alkyl chains inside the crystalline P3HT domain.[12] This would be a reason for the comparable performance of PDB-based cell against PCBM-based cell. More importantly, when D-A copolymer PTB7 was used as the donor materials, PDB-based cell again marked good performance (PCE = 6.14%), which is comparable to that of PCBM-based cell (PCE = 6.24%). In a similar manner to the above-mentioned P3HT-based cell, PTB7:MDB-based cell showed inferior performance (PCE = 5.69%). This is due to the slight decrease in the J_{sc} and FF values while the V_{oc} value is almost the same as that of PDB. These results obtained from both P3HT- and PTB7-based cells suggest that the molecular structure of the dimers is very important to achieve high J_{sc} and FF values. Such a small difference in structures might affect on the film morphology and/or the electron mobility in fullerene-rich domains.[21] Considering most structural modification of PCBM have led to inferior performance,[15] it is interesting that

dimeric fullerenes marked high photovoltaic characteristics and showed applicability even to PTB7 in spite of the difference in the molecular volume. To the best of our knowledge, PDB and MDB are the first dimeric fullerenes applicable to PTB7-based cell.

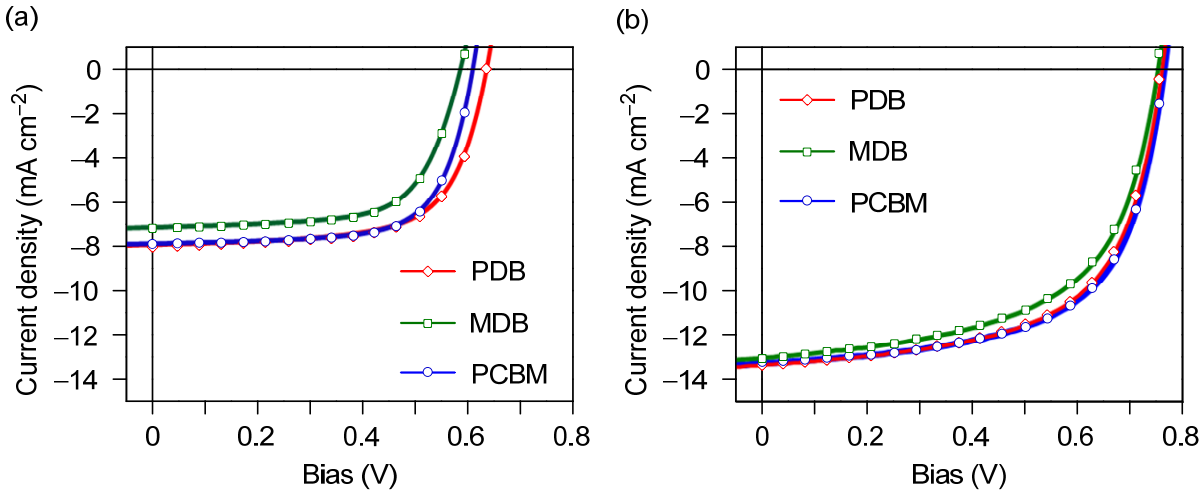

Figure 7. Current density-voltage (*J*-*V*) curves of (a) P3HT-based solar cells, and (b) PTB7-based solar cells under AM 1.5G illumination from a calibrated solar simulator.

Table 2. Photovoltaic data of PSCs based on P3HT and PTB7

Active layer	V_{oc} (V)	J_{sc} (mA cm^{-2})	FF	PCE (%)
P3HT:PDB[a]	0.63	7.89	0.66	3.32
P3HT:MDB[a]	0.58	7.12	0.66	2.75
P3HT:PCBM[a]	0.61	7.84	0.69	3.27
PTB7:PDB[b]	0.76	13.37	0.61	6.14
PTB7:MDB[b]	0.75	13.03	0.58	5.69
PTB7:PCBM[b]	0.76	13.28	0.62	6.24

[a] Cast from PhCl solution. [b] Cast from ODCB solution.

The external quantum efficiency (EQE) spectra of the PSCs are shown in Figure 8. When P3HT was used as the donor material, PDB-based cell gave a curve with a maximum of 58% at 520 nm, which is almost overlapped with that of PCBM-based cell, while MDB-based cell showed apparently decreased EQE values. In the case of PSCs using PTB7 as the donor material, the EQE curves for the dimeric fullerenes and PCBM-based cells appeared to be almost overlapped but slightly inferior for MDB-based cell. A maximum EQE values were 67% for PDB- and MDB-based cells and 69% for PCBM-based cell at 630 nm.

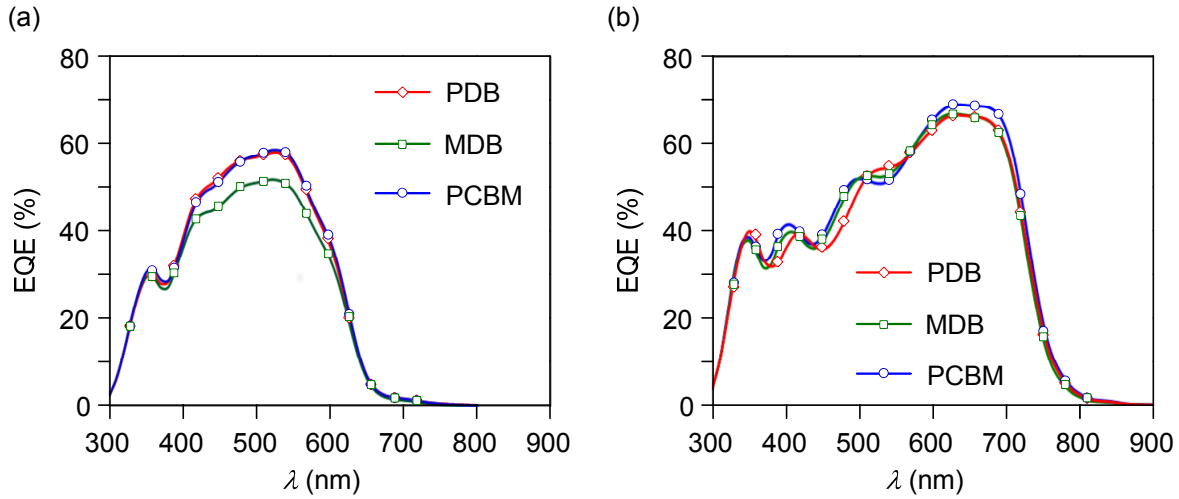

Figure 8. External quantum efficiency (EQE) spectra of (a) P3HT-based solar cells, and (b) PTB7-based solar cells.

The author used the atomic force microscopy (AFM) to obtain information about morphology of the active layers (Figure 9). All of the P3HT- and PTB7-based active layers showed similar root mean square (rms) roughness: 1.1 nm for P3HT:PDB, 1.3 nm for P3HT:MDB, 1.1 nm for P3HT:PCBM, 1.3 nm for PTB7:PDB, 1.6 nm for PTB7:MDB, and 1.5 nm for PTB7:PCBM, respectively. Although clear difference was not observed in the rms roughness, the image of PTB7:MDB blend film appeared to show more detailed texture compared with those of PTB7:PDB and PTB7:PCBM blend films. The author considered that fine phase separation can be ascribed to the inferior performance of MDB-based cell, due to the insufficient formation of MDB channel for the electron transport.

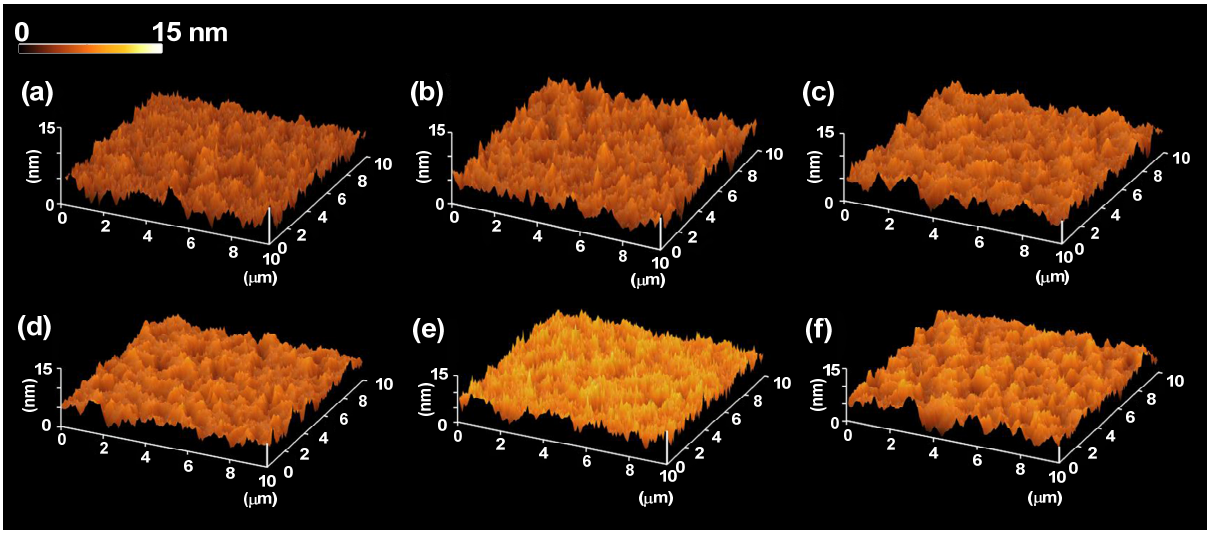

Figure 9. AFM height images of blend films showing a 10×10 μm surface area (tapping mode). The compositions of blend films are (a) P3HT:PDB, (b) P3HT:MDB, (c) P3HT:PCBM, (d) PTB7:PDB, (e) PTB7:MDB, and (f) PTB7:PCBM. P3HT-based blend films were annealed at 150 °C for 6 min.

Conclusion

In summary, dumbbell-shaped C_{60} derivatives PDB and MDB, where two cages are rigidly linked in close proximity, were synthesized and their photovoltaic properties were investigated in both P3HT- and PTB7-based solar cells. These dimeric fullerenes were shown to work as excellent acceptor materials comparable to benchmark PCBM. The data demonstrated that these bulky dimeric fullerenes can be added as a new entry of the acceptor materials for PSCs. It was shown that the difference of the position of the linked C_{60} moieties influenced their photovoltaic performances. This finding would provide the possibility of controlling the morphology in the active layers, which is significant in the design of acceptor materials.

Experimental Section

General. The ^{1}H and ^{13}C NMR measurements were carried out with a Varian Mercury

300 instrument and a Bruker AVANCE III 600 instrument. The NMR chemical shifts are reported in ppm with reference to residual protons and carbons of $CDCl_3$ (δ 7.26 ppm in ^{1}H NMR, δ 77.0 ppm in ^{13}C NMR), and *o*-dichlorobenzene-d_4 (ODCB-d_4) (δ 7.20 ppm in ^{1}H NMR, δ 132.35 ppm in ^{13}C NMR). High-resolution (HR) mass spectra were recorded on a JEOL MStation JMS-700 and a Bruker micrOTOF-QII. The high-pressure liquid chromatography (HPLC) was performed with the use of Cosmosil Buckyprep columns (two directly connected columns; 250 mm length, 20 mm inner diameter) for preparative purpose. Preparative GPC was performed on JAI LC-9130 system equipped with RI-700 next detector, JAIGEL-1H-40 columns (two directly connected columns; 600 mm length, 40 mm inner diameter), and FC-3310 fraction collector using chloroform as eluent (flow rate: 14.0 mL/min).

Photocurrent-voltage characteristics were measured by using a SMO-250III (BUNKOUKEIKI Co., Ltd.). The light intensity of the illumination source was adjusted by using standard silicon photodiodes: BS520 (BUNKOUKEIKI Co., Ltd.) for *J-V* characteristics and SiPD S1337-1010BQ (BUNKOUKEIKI Co., Ltd.) for EQE measurement. The thicknesses of the films were determined with an Alpha-Step IQ Surface Profiler (KLA-Tencor Co.).

Terephthalaldehyde, 2-amino-3-picoline, and $RhCl(PPh_3)_3$ were purchased from Tokyo Chemical Industry Co., LTD. Isophthalaldehyde, ^{n}BuOH, *p*-toluenesulfonylhydrazide, *p*-TsOH·H_2O, and titanium tetraisopropoxide were purchased from Wako Pure Chemical Industries, Ltd. Methyl 3-butenoate, ODCB-d_4, and poly(3-hexylthiophene) (P3HT) were purchased from Sigma-Aldrich Co. [6,6]-Phenyl C_{61}-butyric acid methyl ester (PCBM) was purchased from Nano-C, Inc. Poly(3,4-ethylenedioxythiophene):poly(styrenesulfonic acid) (PEDOT:PSS) (Denatron PT-100) was purchased from Nagase ChemteX Co. The glass substrates covered with indium tin oxide (ITO) (5 Ω sq^{-1}) were purchased from GEOMATEC Co., Ltd. The ITO/glass substrate was cleaned with a UV/ozone cleaner (UV-253) (Filgen, Inc.). Pentafluorophenylammonium triflate (PFPAT)[17] and PTB7[7,22] were prepared by following the literature.

Synthesis of 4a. A solution of terephthalaldehyde **3a** (7.38 g, 55.0 mmol), 2-amino-3-picoline (12.5 g, 116 mmol), and *p*-toluenesulfonic acid monohydrate (523 mg,

2.75 mmol) in toluene (100 mL) was refluxed for 5.5 h in a Dean-Stark apparatus. The resulting yellow solution was washed with aqueous solution of $NaHCO_3$ (saturated, 100 mL) and distilled water (100 mL × 3) to remove excess amine. The organic layer was evaporated under vacuum. The residue was purified by recrystallization ($CHCl_3$-hexane) to give **4a** (14.1 g, 44.9 mmol, 82%) as yellow needles. Compound **4a** was characterized with reference to the reported data.[16]

Synthesis of 5a. To an orange solution containing **4a** (523.3 mg, 1.67 mmol) and $RhCl(PPh_3)_3$ (306.2 mg, 0.33 mmol) in THF (5.0 mL) was added methyl 3-butenoate (1.1 mL, 10.03 mmol) at room temperature, and the solution was heated at 130 ºC in a Young-valve flask. After 6 h the resulting red solution was diluted with EtOAc (ca. 20 mL) and treated with 1 M aqueous HCl. The organic layer was washed with saturated aqueous $NaHCO_3$ and brine. After dried with Na_2SO_4 the organic layer was concentrated under reduced pressure and the residue was subjected to silica gel column chromatography (eluent: CH_2Cl_2) to give **5a** (367.5 mg, 66%, TLC; R_f = 0.35) as a colorless solid.

5a: ^{1}H NMR (300 MHz, $CDCl_3$) δ 8.03 (s, 4H), 3.69 (s, 6H), 3.08 (t, J = 7.2 Hz, 4H), 2.46 (t, J = 7.2 Hz, 4H), 2.08 (quintet, J = 6.9 Hz, 4H); ^{13}C NMR (75 MHz, $CDCl_3$) δ 199.03, 173.84, 140.07, 128.46, 51.87, 38.04, 33.17, 19.34; HRMS (EI): m/z calcd for $C_{18}H_{22}O_6$ (M^+), 334.1416; found, 334.1416.

Synthesis of 6a. A solution containing **5a** (503.2 mg, 1.50 mmol), butanol (1.35 mL, 14.75 mmol), and PFPAT (50.1 mg, 0.15 mmol) in toluene (3.0 mL) was heated at 80 ºC. After 24 h the solution was directly subjected to silica gel column chromatography (eluent: CH_2Cl_2-EtOAc (10:1)) to give **6a** (581.3 mg, 92%, TLC; R_f = 0.52) as a colorless solid.

6a: ^{1}H NMR (300 MHz, $CDCl_3$) δ 8.02 (s, 4H), 4.07 (t, J = 6.6 Hz, 4H), 3.07 (t, J = 7.2 Hz, 4H), 2.43 (t, J = 7.2 Hz, 4H), 2.06 (quintet, J = 7.2 Hz, 4H), 1.60 (quintet , J = 6.6 Hz, 4H), 1.35 (sextet, J = 7.2 Hz, 4H), 0.91 (t, J = 7.5 Hz, 6H); ^{13}C NMR (75 MHz, $CDCl_3$) δ 199.06, 173.46, 140.06, 128.42, 64.55, 38.05, 33.42, 30.82, 19.40, 19.32, 13.89; HRMS (EI): m/z calcd for $C_{24}H_{34}O_6$ (M^+), 418.2355; found, 418.2357.

Synthesis of 7a. A solution containing **6a** (418.3 mg, 1.00 mmol) and

p-toluenesulfonylhydrazide (447.0 mg, 2.40 mmol) in methanol (10.0 mL) was refluxed for 7 h. The solution was cooled in refrigerator for 13 h to form pale yellow precipitates. The solid was collected by filtration and washed with cold methanol to give **7a** (714.6 mg, 95%) as pale yellow powder.

7a: ^{1}H NMR (300 MHz, $CDCl_3$) δ 9.39 (s, 2H), 7.90 (d, J = 7.8 Hz, 4H), 7.62 (s, 4H), 7.30 (d, J = 7.8 Hz, 2H), 4.21 (t, J = 6.6 Hz, 4H), 2.61 (t, J = 8.4 Hz, 4H), 2.41 (s, 6H), 2.30 (t, J = 6.6 Hz, 4H), 1.70–1.60 (m, 8H), 1.40 (sextet, J = 7.5 Hz, 4H), 0.96 (t, J = 7.5 Hz, 6H); ^{13}C NMR (75 MHz, $CDCl_3$) δ 174.84, 152.89, 143.99, 137.22, 136.20, 129.72, 128.11, 126.43, 65.57, 32.43, 30.80, 25.94, 21.81, 21.14, 19.31, 13.94; HRMS (FAB): *m*/*z* calcd for $C_{38}H_{51}N_4O_8S_2$ ($[M+H]^+$), 755.3148; found, 755.3152.

Synthesis of PDB. To a solution of **7a** (92.1 mg, 0.13 mmol) in pyridine (1.3 mL) was added NaH (9.47 mg, 0.39 mmol) and the resulting suspension was stirred at room temperature for 15 min. Small bubbles and white precipitates were formed. To the solution was added a solution of C_{60} (378.3 mg, 0.53 mmol) in ODCB (38.0 mL) and the mixture was heated at 100 ºC for 50 h. The color of the solution changed from purple to brown. The resulting solution was concentrated and subjected to silica gel column chromatography (eluent: toluene-EtOAc (10:1)). The resulting solid was further purified with preparative HPLC (BuckyPrep, eluent: toluene) to give PDB (56.0 mg, 23%) as a brown solid.

PDB: ^{1}H NMR (600 MHz, 80 ºC, ODCB-d_4) δ 8.39 (s, 4H), 4.35 (t, J = 6.8 Hz, 4H), 3.36–3.33 (m, 4H), 2.80 (t, J = 7.2 Hz, 4H), 2.69–2.64 (m, 4H), 1.84 (quintet, J = 7.1 Hz, 4H), 1.60 (sextet, J = 7.4 Hz, 4H), 1.15 (t, J = 7.4 Hz, 6H); ^{13}C NMR (150 MHz, 80 ºC, ODCB-d_4) δ 171.89, 148.81, 147.47, 145.58, 144.89, 144.82, 144.75, 144.53, 144.46, 144.34, 144.22, 144.19, 143.81, 143.49, 143.48, 142.80, 142.69, 142.67, 142.63, 142.62, 142.58, 142.06, 142.04, 141.85, 141.81, 140.80, 140.52, 138.04, 137.43, 137.13, 132.37 (overlapped with the signal of ODCB-d_4 as confirmed by DEPT-135), 79.86, 64.01, 51.88, 33.90, 33.19, 30.85, 22.66, 19.19, 13.50; HRMS (FAB): *m*/*z* calcd for $C_{144}H_{34}O_4$ (M^+), 1826.2457; found, 1826.2461.

Synthesis of 4b. A solution of isophthalaldehyde **3b** (2.37 g, 17.7 mmol), 2-amino-3-picoline (5.13 g, 47.5 mmol), and *p*-toluenesulfonic acid monohydrate (8.8 mg,

0.05 mmol) in toluene (30.0 mL) was refluxed for 17 h in a Dean-Stark apparatus. The resulting yellow solution was washed with distilled water (50 mL × 4 times) to remove excess amine. The organic layer was evaporated under vacuum. The residue was subjected to preparative GPC (eluent: $CHCl_3$) to give **4b** (19.9 g, quant.) as yellow oil.

4b: ^{1}H NMR (300 MHz, $CDCl_3$) δ 9.17 (s, 2H), 8.59 (t, J = 1.5 Hz, 1H), 8.32 (dd, J = 1.5 Hz, 4.8 Hz, 2H), 8.17 (dd, J = 1.8 Hz, 7.8 Hz, 2H), 7.62–7.57 (m, 3H), 7.11 (dd, J =4.8 Hz, 7.5 Hz, 2H), 2.49 (s, 6H); ^{13}C NMR (75 MHz, $CDCl_3$) δ 161.06, 159.38, 146.39, 139.18, 137.06, 132.23, 131.04, 129.35, 129.25, 122.29, 17.63; HRMS (EI): m/z calcd for $C_{20}H_{18}N_4$ (M^+), 314.1531; found, 314.1530.

Synthesis of 5b. To an orange solution containing **4b** (947.2 mg, 3.01 mmol) and $RhCl(PPh_3)_3$ (552.6 mg, 0.60 mmol) in THF (10.0 mL) was added methyl 3-butenoate (1.9 mL, 17.82 mmol) and the mixture was heated at 130 ºC in a Young-valve flask. After 5 h the resulting red solution was diluted with EtOAc (ca. 40 mL) and treated with 1 M aqueous HCl. The organic layer was washed with saturated aqueous $NaHCO_3$ and brine. After dried with Na_2SO_4 the organic layer was concentrated under reduced pressure and subjected to silica gel column chromatography (eluent: CH_2Cl_2-EtOAc (10:1)) to give **5b** (420.4 mg, 42%, TLC; R_f = 0.53) as yellow oil.

5b: ^{1}H NMR (300 MHz, $CDCl_3$) δ 8.52 (t, J = 1.5 Hz, 1H), 8.14 (dd, J = 1.5 Hz, 7.8 Hz, 2H), 7.57 (t, J = 7.8 Hz, 1H), 3.68 (s, 6H), 3.10 (t, J = 7.2 Hz, 4H), 2.46 (t, J = 6.9 Hz, 4H), 2.08 (quintet, J = 6.9 Hz, 4H); ^{13}C NMR (75 MHz, $CDCl_3$) δ 198.87, 173.82, 137.30, 132.45, 129.30, 127.70, 51.83, 37.84, 33.18, 19.39; HRMS (EI): m/z calcd for $C_{18}H_{22}O_6$ (M^+), 334.1416; found, 334.1416.

Synthesis of 6b. A solution containing **5b** (335.6 mg, 1.00 mmol), butanol (0.9 mL, 9.84 mmol), and PFPAT (33.2 mg, 0.10 mmol) in toluene (2.0 mL) was heated at 80 ºC. After 24 h the solution was subjected to silica gel column chromatography (eluent: CH_2Cl_2-EtOAc (10:1)) to give **6b** (380.9 mg, 91%, TLC; R_f = 0.51) as yellow oil.

6b: ^{1}H NMR (300 MHz, $CDCl_3$) δ 8.52 (t, J = 1.8 Hz, 1H), 8.15 (dd, J = 1.8 Hz, 7.8 Hz, 2H), 7.57 (t, J = 7.8 Hz, 1H), 4.08 (t, J = 6.6 Hz, 4H), 3.10 (t, J = 6.6 Hz, 4H), 2.44 (t, J = 7.2 Hz, 4H), 2.08 (quintet, J = 7.2 Hz, 4H), 1.60 (quintet, J = 7.2 Hz, 4H), 1.36 (sextet, J = 7.2 Hz,

4H), 0.94 (t, *J* = 7.2 Hz, 6H); ^{13}C NMR (75 MHz, $CDCl_3$) δ 198.93, 173.49, 137.34, 132.45, 129.30, 127.70, 64.58, 37.88, 33.46, 30.85, 19.47, 19.34, 13.91; HRMS (EI): *m*/*z* calcd for $C_{24}H_{34}O_6$ (M^+), 418.2355; found, 418.2357.

Synthesis of 7b. A solution containing **6b** (333.5 mg, 0.80 mmol) and *p*-toluenesulfonylhydrazide (358.5 mg, 1.93 mmol) in methanol (10.0 mL) was refluxed for 6 h. The solution was cooled in refrigerator for 13 h to form pale yellow co-crystals (needle) with methanol. The crystals were collected by filtration and washed with cold methanol. The crystals were dissolved in $CHCl_3$ and the solvent was evaporated under vacuum to give **7b** (600.1 mg, 99.7%) as pale yellow powder.

7b: ^{1}H NMR (300 MHz, $CDCl_3$) δ 9.40 (s, 2H), 8.01 (s, 1H), 7.90 (dd, *J* = 2.1 Hz, 6.6 Hz, 4H), 7.60 (dd, *J* = 1.8 Hz, 7.8 Hz, 2H), 7.33–7.27 (m, 5H), 4.22 (t, *J* = 6.6 Hz, 4H), 2.63 (t, *J* = 8.4 Hz, 4H), 2.39 (s, 6H), 2.31 (t, *J* = 6.6 Hz, 4H), 1.70–1.61 (m, 8H), 1.40 (sextet, *J* = 7.5 Hz, 4H), 0.96 (t, *J* = 7.5 Hz, 6H) ; ^{13}C NMR (75 MHz, $CDCl_3$) δ 174.86, 153.22, 144.00, 136.62, 136.20, 129.76, 128.77, 128.07, 127.35, 124.06, 65.55, 32.35, 30.79, 26.02, 21.79, 21.13, 19.31, 13.93; HRMS (FAB): *m*/*z* calcd for $C_{38}H_{51}N_4O_8S_2$ ($[M+H]^+$), 755.3147; found, 755.3152.

Synthesis of MDB. To a solution of **7b** (113.8 mg, 0.15 mmol) in pyridine (1.5 mL) was added NaH (10.91 mg, 0.45 mmol) and the resulting suspension was stirred at room temperature for 15 min. Small bubbles and white precipitates were formed. To the solution was added a solution of C_{60} (438.0 mg, 0.61 mmol) in ODCB (44.0 mL) and the mixture was heated at 100 ºC for 50 h. The color of the solution changed from purple to brown. The resulting solution was concentrated and subjected to silica gel column chromatography (eluent: ODCB-EtOAc (10:1)). The resulting solid was further purified with preparative HPLC (BuckyPrep, eluent: toluene) to give MDB (102.3 mg, 37%) as a brown solid.

MDB: ^{1}H NMR (600 MHz, 100 ºC, ODCB-d_4) δ 8.87 (t, *J* = 1.8 Hz, 1H), 8.32 (dd, *J* = 1.8 Hz, 7.7 Hz, 2H), 7.87 (t, *J* = 7.7 Hz, 1H), 4.37 (t, *J* = 6.7 Hz, 4H), 3.40–3.37 (m, 4H), 2.86 (t, *J* = 7.1 Hz, 4H), 2.67–2.62 (m, 4H), 1.85 (quintet, *J* = 7.1 Hz, 4H), 1.61 (sextet, 7.4 Hz, 4H), 1.15 (t, *J* = 7.4 Hz, 6H); ^{13}C NMR (150 MHz, 100 ºC, ODCB-d_4) δ 171.88, 148.46, 147.41, 145.56, 144.86, 144.85, 144.83, 144.79, 144.75, 144.48, 144.44, 144.34, 144.32,

144.14, 144.13, 143.90, 143.42, 143.36, 142.78, 142.70, 142.63, 142.60, 141.99, 141.95, 141.81, 141.79, 140.73, 140.66, 137.95, 137.46, 137.42, 135.85, 131.64, 128.45, 80.07, 63.98, 51.75, 33.82, 33.78, 30.83, 22.58, 19.10, 13.35; APCI-HRMS (–): *m*/*z* calcd for $C_{144}H_{34}O_4$ (M^-), 1826.2463; found, 1826.2539.

Procedure for fabrication of the PSCs. The ITO-coated glass substrate (GEOMATEC, 5 Ω/sq, 2.5 cm × 2.5 cm) was washed carefully under ultrasonic irradiation using acetone (15 min), and ethanol (15 min). The substrate was further cleaned with a Filgen UV230 UV/ozone cleaner. A thin layer of PEDOT:PSS (Nagase ChemteX, Denatron PT-100) was prepared onto the ITO surface by the spin-coating method at 5000 rpm for 1 min. The resulting substrate was heated at 200 ºC for 10 min under ambient conditions.

P3HT-based solar cells. A solution for the active layer was prepared by dissolving P3HT and fullerene derivative at a 1.6 : 1 weight ratio in chlorobenzene (24 mg mL^{-1}) followed by heating at 100 ºC for 2 h under ambient conditions. The resulting solution was spin-coated onto the PEDOT:PSS layer at 1000 rpm for 40 s. Then, the substrate was annealed at 150 ºC for 6 min in an argon-filled glove box. After cooling to room temperature the substrate was transferred into another glove box where the humidity was controlled around 15% by flowing nitrogen gas. Then, a thin layer (ca. 5 nm) of TiO_x was prepared on the active layer by spin-coating a dehydrated ethanol solution of titanium tetraisopropoxide at 4000 rpm for ca. 20 s followed by being hydrolyzed for 20 min under ambient conditions. Finally, aluminum (Nilaco) was thermally deposited under vacuum (1.1×10^{-4} Torr).

PTB7-based solar cells. The solution for the active layer was prepared by dissolving PTB7 and fullerene derivative at a 1 : 1 weight ratio in *o*-dichlorobenzene solution (24 mg mL^{-1}) followed by heating at 165 ºC for 3 h in an argon-filled glove box. The resulting solution was spin-coated onto the PEDOT:PSS layer at 800 rpm for 1 min. Then, the substrate was transferred into another glove box where the humidity was controlled around 15% by flowing nitrogen gas. Then, a thin layer (ca. 5 nm) of TiO_x was prepared on the active layer by spin-coating a dehydrated ethanol solution of titanium tetraisopropoxide at

4000 rpm for ca. 20 s followed by being hydrolyzed for 20 min under ambient conditions. Finally, aluminum (Nilaco) was thermally deposited under vacuum (6.8×10^{-5} Torr).

References

(1) (a) Chen, T.-A.; Rieke, R. D. *J. Am. Chem. Soc.* **1992**, *114*, 10087. (b) McCullough, R. D.; Lowe, R. D. *J. Chem. Soc., Chem. Commun.* **1992**, 70. (c) Chen, T.-A.; Wu, X.; Rieke, R. D. *J. Am. Chem. Soc.* **1995**, *117*, 233. (d) Wang, T.; Takita, R.; Kikuzaki, Y.; Ozawa, F. *J. Am. Chem. Soc.* **2010**, *132*, 11420.

(2) Hummelen, J. C.; Knight, B. W.; LePeq, F.; Wudl, F. *J. Org. Chem.* **1995**, *60*, 532.

(3) (a) Ma, W.; Yang, C.; Gong, X.; Lee, K.; Heeger, A. J. *Adv. Funct. Mater.* **2005**, *15*, 1617. (b) Reyes-Reyes, M.; Kim, K.; Carroll, D. L. *Appl. Phys. Lett.* **2005**, *87*, 083506. (c) Lee, S.-H.; Kim, D.-H.; Kim, J.-H.; Lee, G.-S.; Park, J.-G. *J. Phys. Chem. C* **2009**, *113*, 21915.

(4) (a) Scharber, M. C.; Mühlbacher, D.; Koppe, M.; Denk, P.; Waldauf, C.; Heeger, A. J.; Brabec, C. J. *Adv. Mater.* **2006**, *18*, 789. (b) Blouin, N.; Michaud, A.; Gendron, D.; Wakim, S.; Blair, E.; Neagu-Plesu, R.; Belletête, M.; Durocher, G.; Tao, Y.; Leclerc, M. *J. Am. Chem. Soc.* **2008**, *130*, 732. (c) Zhou, H.; Yang, L.; You, W. *Macromolecules* **2012**, *45*, 607.

(5) (a) Mühlbacher, D.; Scharber, M.; Morana, M.; Zhu, Z.; Waller, D.; Gaudiana, R.; Brabec, C. *Adv. Mater.* **2006**, *18*, 2884. (b) Chen, H.-Y.; Hou, J.; Zhang, S.; Liang, Y.; Yang, G.; Yang, Y.; Yu, L.; Wu, Y.; Li, G. *Nat. Photon.* **2009**, *3*, 649. (c) Qin, R.; Li, W.; Li, C.; Du, C.; Veit, C.; Schleiermacher, H.-F.; Andersson, M.; Bo, Z.; Liu, Z.; Inganäs, O.; Wuerfel, U.; Zhang, F. *J. Am. Chem. Soc.* **2009**, *131*, 14612. (d) Huo, L.; Hou, J.; Zhang, S.; Chen, H.-Y.; Yang, Y. *Angew. Chem. Int. Ed.* **2010**, *49*, 1500. (e) Zhou, H.; Yang, L.; Price, S. C.; Knight, K. J.; You, W. *Angew. Chem. Int. Ed.* **2010**, *49*, 7992. (f) Li, Z.; Ding, J.; Song, N.; Lu, J.; Tao, Y. *J. Am. Chem. Soc.* **2010**, *132*, 13160. (g) Yiu, A. T.; Beaujuge, P. M.; Lee, O. P.; Woo, C. H.; Toney, M. F.; Fréchet, J. M. J. *J. Am. Chem. Soc.* **2012**, *134*, 2180. (h) Osaka, I.; Shimawaki, M.; Mori, H.; Doi, I.; Miyazaki, E.; Koganezawa, T.; Takimiya, K. *J. Am. Chem. Soc.* **2012**, *134*, 3498.

(6) Wienk, M. M.; Kroon, J. M.; Verhees, W. J. H.; Knol, J.; Hummelen, J. C.; Hal, P. A.;

Janssen, R. A. J. *Angew*. *Chem*. *Int*. *Ed*. **2003**, *42*, 3371.

(7) Liang, Y.; Xu, Z.; Xia, J.; Tsai, S.-T.; Wu, Y.; Li, G.; Ray, C.; Yu, L. *Adv*. *Mater*. **2010**, *22*, E135.

(8) He, Z.; Zhong, C.; Su, S.; Xu, M.; Wu, H.; Cao, Y. *Nat. Photon*. **2012**, *6*, 591.

(9) (a) He, Y.; Chen, H.-Y.; Hou, J.; Li, Y. *J*. *Am*. *Chem*. *Soc*. **2010**, *132*, 1377. (b) Zhao, G.; He, Y.; Li, Y. *Adv*. *Mater*. **2010**, *22*, 4355.

(10) Matsuo, Y.; Sato, Y.; Niinomi, T.; Soga, I.; Tanaka, H.; Nakamura, E. *J*. *Am*. *Chem*. *Soc*. **2009**, *131*, 16048.

(11) (a) Guo, X.; Zhang, M.; Huo, L.; Cui, C.; Wu, Y.; Hou, J.; Li, Y. *Macromolecules* **2012**, *45*, 6930. (b) Xin, H.; Subramaniyan, S.; Kwon, T.-W.; Shoaee, S.; Durrant, J. R.; Jenekhe, S. A. *Chem*. *Mater*. **2012**, *24*, 1995. (c) Zhang, Z.-G.; Zhang, S.; Min, J.; Chui, C.; Zhang, J.; Zhang, M.; Li, Y. *Macromolecules* **2012**, *45*, 113. (d) Zhang, Z.-G.; Zhang, S.; Min, J.; Cui, C.; Geng, H.; Shuai, Z.; Li, Y. *Macromolecules* **2012**, *45*, 2312. (e) He, Y.; You, J.; Dou, L.; Chen, C.-C.; Richard, E.; Cha, K. C.; Wu, Y.; Li, G.; Yang, Y. *Chem*. *Commun*. **2012**, *48*, 7616.

(12) (a) Mayer, A. C.; Toney, M. F.; Scully, S. R.; Rivnay, J.; Brabec, C. J.; Scharber, M.; Koppe, M.; Heeney, M.; McCulloch, I.; McGehee, M. D. *Adv*. *Funct*. *Mater*. **2009**, *19*, 1173. (b) Miller, N. C.; Sweetnam, S.; Hoke, E. T.; Gysel, R.; Miller, C. E.; Bartelt, J. A.; Xie, X.; Toney, M. F.; McGehee, M. D. *Nano Lett*. **2012**, *12*, 1566.

(13) Delgado, J. L.; Espíldora, E.; Liedtke, M.; Sperlich, A.; Rauh, D.; Baumann, A.; Deibel, C.; Dyakonov, V.; Marín, N. *Chem*. *Eur*. *J*. **2009**, *15*, 13474.

(14) (a) Liu, J.; Guo, X.; Qin, Y.; Liang, S.; Guo, Z.-X.; Li, Y. *J*. *Mater*. *Chem*. **2012**, *22*, 1758. (b) Ge, J.; Liu, J.; Guo, X.; Qin, Y.; Luo, H.; Guo, Z.-X.; Li, Y. *Chem*. *Phys*. *Lett*. **2012**, *535*, 100.

(15) (a) Troshin, P. A.; Hoppe, H.; Renz, J.; Egginger, M.; Mayorova, J. Y.; Goryachev, A. E.; Peregudov, A. S.; Lyubovskaya, R. N.; Gobsch, G.; Sariciftci, N. S.; Razumov, V. F. *Adv*. *Funct*. *Mater*. **2009**, *19*, 779. (b) Zhao, G.; He, Y; Xu, Z.; Hou, J.; Zhang, M.; Min, J.; Chen, H.-Y.; Ye, M.; Hong, Z.; Yang, Y.; Li, Y. *Adv*. *Funct*. *Mater*. **2010**, *20*, 1480. (c) Kooistra, F. B.; Knol, J.; Kastenberg, F.; Popescu, L. M.; Verhees, W. J. H.; Kroon, J. M.; Hummelen, J. C. *Org*. *Lett*. **2007**, *9*, 551.

(16) Willis, M. C.; Sapmaz, S. *Chem*. *Commun*. **2001**, 2558.

(17) Funatomi, T.; Wakasugi, K.; Misaki, T.; Tanabe, Y. *Green Chem*. **2006**, *8*, 1022.

(18) Matsuo, Y.; Iwashita, A.; Abe, Y.; Li, C.-Z.; Matsuo, K.; Hashiguchi, M.; Nakamura, E. *J*. *Am*. *Chem*. *Soc*. **2008**, *130*, 15429.

(19) Murata, M.; Morinaka, Y.; Murata, Y.; Yoshikawa, O.; Sagawa, T.; Yoshikawa, S. *Chem*. *Commun*. **2011**, *47*, 7335.

(20) Kim, J.; Yun, M. H.; Lee, J.; Kim, J. Y.; Wudl, F.; Yang, C. *Chem*. *Commun*. **2011**, *47*, 3078.

(21) (a) Yang, C.; Kim, J. Y.; Cho, S.; Lee, J. K.; Heeger, A. J.; Wudl, F. *J*. *Am*. *Chem*. *Soc*. **2008**, *130*, 6444. (b) Zhang, Y.; Yip, H.-L.; Acton, O.; Hau, S. K.; Huang, F.; Jen, A. K.-Y. *Chem*. *Mater*. **2009**, *21*, 2598.

(22) Liang, Y.; Feng, D.; Wu, Y.; Tsai, S.-T.; Li, G.; Ray, C.; Yu, L. *J*. *Am*. *Chem*. *Soc*. **2009**, *131*, 7792.

List of Publications

Chapter 1 Murata, M.; Maeda, S.; Morinaka, Y.; Murata, Y.; Komatsu, K. ‘‘Synthesis and Reaction of Fullerene C_{70} Encapsulating Two Molecules of H_2’’ *J*. *Am*. *Chem*. *Soc*. **2008**, *130*, 15800-15801.

Chapter 2 Morinaka, Y.; Tanabe, F.; Murata, M.; Murata, Y.; Komatsu, K. ‘‘Rational Synthesis, Enrichment, and ^{13}C NMR Spectra of Endohedral C_{60} and C_{70} Encapsulating a Helium Atom’’ *Chem*. *Commun*. **2010**, *46*, 4532-4534.

Chapter 3 Morinaka, Y.; Sato, S.; Wakamiya, A.; Nikawa, H.; Mizorogi, N.; Tanabe, F.; Murata, M.; Komatsu, K.; Furukawa, K.; Kato, T.; Nagase, S.; Akasaka, T.; Murata, Y. ‘‘X-ray Observation of a Helium Atom and Placing a Nitrogen Atom inside He@C_{60} and He@C_{70}’’ *Nat*. *Commun*. **2013**, *4*, 1554/1-1554/5.

Chapter 4 Murata, M.; Morinaka, Y.; Kurotobi, K.; Komatsu, K.; Murata, Y. ‘‘Reaction of Cage-opened Fullerene Derivative with Grignard Reagents and Subsequent Transannular Cyclization’’ *Chem*. *Lett*. **2010**, *39*, 298-299.

Murata, M.; Morinaka, Y.; Murata, Y.; Yoshikawa, O.; Sagawa, T.; Yoshikawa, S. ‘‘Modification of the σ-framework of [60]fullerene for Bulk-heterojunction Solar Cells’’ *Chem*. *Commun*. **2011**, *47*, 7335-7337.

Chapter 5 Morinaka, Y.; Nobori, M.; Murata, M.; Wakamiya, A.; Murata, Y.; Sagawa, T.; Yoshikawa, S. ‘‘Synthesis and Photovoltaic Properties of Acceptor Materials Based on the Dimerization of Fullerene C_{60} for Use in Efficient Polymer Solar Cells’’ *Chem*. *Commun*. **2013**, *49*, 3670-3672.

Acknowledgment

The study presented in this thesis has been carried out under the direction of Professor Yasujiro Murata at Institute for Chemical Research, Kyoto University during the period of April 2008 to March 2013.

The author wishes to express his sincerest gratitude to Professor Yasujiro Murata for his kind guidance, valuable suggestions, and hearty encouragement throughout this work. The author would like to express his deep appreciation to Dr. Michihisa Murata for his intense teaching, technical assistance, and kind encouragement. The author is grateful to Professor Atsushi Wakamiya for continuous advice, helpful discussions, and exhortation. The author is also grateful to Professor Koichi Komatsu for his kind encouragement and helpful comments on his articles.

The author wishes to appreciate Professor Takeshi Akasaka, Dr. Satoru Sato, Dr. Hidefumi Nikawa, and Dr. Naomi Mizorogi at Life Science Center of Tsukuba Advanced Research Alliance, University of Tsukuba, and Professor Tatsuhisa Kato at Institute for the Promotion of Excellence in Higher Education, Kyoto University, and Dr. Ko Furukawa at Institute for Molecular Science, and Professor Shigeru Nagase at Fukui Institute for Fundamental Chemistry, Kyoto University for their valuable collaboration in the nitrogen-frequency methods, ESR measurements, and theoretical calculations.

The author is deeply grateful to Professor Susumu Yoshikawa, Professor Takashi Sagawa, Dr. Osamu Yoshikawa, and Mr. Yueh-Tsung Tsai at Institute for Advanced Energy, Kyoto University for their kind guidance on fabrication of organic photovoltaic devices and the photo-CELIV technique.

The author is grateful to Professor Yoshinobu Tsujii, Dr. Keita Sakakibara, and Dr. Akihiro Nomura at Institute for Chemical Research, Kyoto University for their kind guidance on AFM measurements.

The author is grateful to Dr. Seiki Baba, Dr. Nobuhiro Mizuno, and Dr. Keiko Miura at Japan Synchrotron Radiation Research Institute (JASRI), and Professor Takahiro Sasamori and Professor Hikaru Takaya at Institute for Chemical Research, Kyoto University for the support of synchrotron X-ray measurements.

The author grateful to Ms. Kyoko Ohmine and Ms. Akiko Fujihashi at Institute for Chemical Research, Kyoto University for their work of NMR spectra and mass spectra, respectively.

The author is grateful to the experimental contribution of Mr. Shuhei Maeda, Mr. Fumiyuki Tanabe, Dr. Kei Kurotobi, and Mr. Masahiro Nobori to the results shown in Chapter 1, 2-3, 4, and 5, respectively. The author also thanks the former and present group members:

Murata lab.

Dr. Takuhiro Taniguchi	Mr. Hidetaka Nishimura	Dr. Hiroki Sugiura
Dr. Masaru Endo	Mr. Haruki Mori	Ms. Akiko Watanabe
Dr. Yumi Nakaike	Ms. Yuko Sakurai	Ms. Tomoko Nishida
Mr. Keisuke Kato	Mr. Hiroyuki Shimogawa	Ms. Naoko Ikeda
Mr. Yuya Hirose	Mr. Tsukasa Futagoishi	(Secretary)
Mr. Hidefumi Yasui	Mr. Zhang Rui	Ms. Hidemi Teramoto
Mr. Satoshi Katsuya	Mr. Yasunori Sugano	(Experimental Support)
	Mr. Kensuke Uchinaga	Mr. Nobuhiko Nishitani

The author would like to appreciate Professor Kouichi Ohe and Professor Masaharu Nakamura for careful reviewing of this thesis and fruitful comments.

The author deeply wishes to appreciate to Professor Tetsuo Ohta at Doshisha University for introducing him to organic chemistry and kind encouragement.

The author is thankful to all members of Professor Yoshikawa's group, Professor Nakamura's group, Professor Ozawa's group, and Professor Tokitoh's group at Kyoto University. The author also thanks all members of Professor Akasaka's group at Tsukuba University and Professor Itami's group at Nagoya University.

The author thanks to the Japan Society for the Promotion of Science (JSPS) for the Research Fellowship for Young Scientists (DC2).

Finally, the author would like to express his sincerest appreciation to his family: Dr. Hideo Morinaka, Ms. Junko Morinaka, Mr. Tatsuya Morinaka, and Mr. Yosuke Morinaka, and his grandparents: Ms. Kiyoshi Morinaka, Ms. Tsuneko Morinaka, Mr. Akira Oda, and Ms. Etsuko Oda for their constant assistance and encouragement.

Yuta Morinaka
Institute for Chemical Research
Kyoto University
2013